RIGA TECHNICAL
UNIVERSITY

1862

Aleksandrs Korņejevs

RESEARCH AND DEVELOPMENT OF SELF-LEARNING NEURAL NETWORK ALGORITHM FOR OPTIMAL ENERGY-EFFICIENT AUTONOMOUS ELECTRICAL UNMANNED VEHICLES MOTION CONTROL

Doctoral Thesis

RIGA TECHNICAL UNIVERSITY

Faculty of Electrical and Environmental Engineering
Institute of Industrial Electronics and Electrical Engineering

Aleksandrs Korņejevs

Doctoral Student of the Study Programme "Computer Control of Electrical Technology"

RESEARCH AND DEVELOPMENT OF SELF-LEARNING NEURAL NETWORK ALGORITHM FOR OPTIMAL ENERGY-EFFICIENT AUTONOMOUS UNMANNED ELECTRICAL VEHICLES MOTION CONTROL

Doctoral thesis

Scientific supevisor
Professor Dr. sc. ing.
MIHAILS GOROBECS

Riga 2023

Published in accordance with the decision of the Promotion Council "P-14" of 4 October 2023, Minutes No. 04030-9.12.2/5.

NATIONAL DEVELOPMENT PLAN 2020

EUROPEAN UNION
European Social Fund

INVESTING IN YOUR FUTURE

DOCTORAL THESIS PROPOSED TO RIGA TECHNICAL UNIVERSITY FOR THE PROMOTION TO THE SCIENTIFIC DEGREE OF DOCTOR OF SCIENCE

To be granted the scientific degree of Doctor of Science (Ph. D.), the present Doctoral Thesis has been submitted for the defence at the open meeting of RTU Promotion Council on 29 December 2023 at 9.30 at the Faculty of Electrical and Environmental Engineering of Riga Technical University, 12/1 Āzenes Street, Room 212.

OFFICIAL REVIEWERS

Professor Dr. sc. ing. Nadežda Kuņicina
Riga Technical University

Researcher Dr. sc. ing. Artjoms Obuševs
Zurich University of Applied Science, Switzerland

Associate Professor Ph. D. Augusto Montisci
Università degli Studi di Cagliari, Italy

DECLARATION OF ACADEMIC INTEGRITY

I hereby declare that the Doctoral Thesis submitted for the review to Riga Technical University for the promotion to the scientific degree of Doctor of Science (Ph. D.) is my own. I confirm that this Doctoral Thesis had not been submitted to any other university for the promotion to a scientific degree.

Aleksandrs Korņejevs ……………………………. (signature)

Date: ………………………

The Doctoral Thesis has been written in English. It consists of an Introduction; 4 Chapters; Conclusion; 84 figures; 8 tables; the total number of pages is 126. The Bibliography contains 92 titles.

ANNOTATION

The main objective of the doctoral thesis is to investigate algorithms for minimizing energy consumption, neural networks, and develop a method for reducing energy consumption in unmanned vehicles.

The doctoral thesis consists of 4 chapters, conclusions, and a list of references.

In the first section of the doctoral thesis, unmanned vehicles are studied, and the control structure of unmanned vehicles is described. The control of unmanned vehicles with the implementation of the developed method into the existing control structure is proposed. The structure of the newly developed self-learning optimization controller with a neural network is described.

The second section of the doctoral thesis describes the spatial models of vehicles, identifies the objective function and energy consumption function. Mathematical models of vehicle motion, neural network, and mechanical model of vehicles are developed.

In the third section, a general algorithm for optimizing the energy consumption of unmanned vehicles is developed. Four minimization algorithms are described, two of which are stochastic and two are deterministic. The neural network training algorithm is also described. A self-learning algorithm for optimal energy consumption with a neural network is developed.

The fourth section of the doctoral thesis presents the results of the research experiments. The developed algorithms are simulated on computer models. Experimental devices are constructed and used to test the investigated algorithms.

Results of the work: The method allows for a 12.93 % reduction in energy consumption by autonomous electric vehicles.

The doctoral thesis consists of 126 pages, including an introduction, 4 chapters, 84 figures, 8 tables, conclusions, and 92 references.

Table of contents

INTRODUCTION

Relevance of the topic

In our time, there is development and an increase in the number of autonomous vehicles, and in the near future, a complete transition to driverless transportation is planned. Transportation consumes 26.6% [55] of the energy consumed worldwide. A significant portion of this energy is fossil fuel-based, which pollutes the atmosphere or causes other harm to the planet. By applying energy consumption optimization methods to autonomous transportation, it is possible to reduce the harmful impact on the atmosphere and also decrease the use of energy resources. This results in environmental and economic benefits.

Furthermore, the use of autonomous driverless transportation reduces the risk of injury or loss of human life during travel or work in hazardous and inaccessible areas.

Advancing technologies allow for the application of compact control systems that include image recognition, which plays an important role in autonomous transportation capable of operating without a driver. Currently, autonomous driverless electric trains, unmanned aerial vehicles, and autonomous vehicles are being used on public roads in some countries.

This work is focused on the research and development of an adaptive control system algorithm, its implementation, and integration into the control system of an existing driverless vehicle.

An additional optimization controller is proposed for energy-efficient control of the movement of a driverless vehicle. The structure based on a neural network expands the adaptive search algorithm, significantly reducing the time required to determine the optimal control signal values and maximizing the energy efficiency of the driverless vehicle.

The proposed algorithm is expected to be universally applicable in any driverless vehicle with varying numbers of traction drives, different or variable masses, and other configuration differences without any initial manual tuning. Any electric autonomous vehicle should operate with maximum energy efficiency using the proposed algorithm.

To understand the feasibility of optimizing energy consumption in electric transport, the author conducted a study on the prospects of using electric transport, which is reflected in the publication "Long-term Energy and Fuel Consumption Forecast in Private and Commercial Transport using Artificial Life Approach," authored by M. Gorobetz, A. Korneyev, and L. Zemite [85].

In the work [23], the prospects of using energy sources for automotive transport are investigated. The development of a model is described, which is intended for dynamic modeling of the country's economic and demographic processes related to the transportation market, vehicles, and fuel consumption. The method is based on a combination of three methods - Monte Carlo, Artificial Life, and Bayesian Trees. The situation with fuel consumption in Latvia is considered. The developing model examines factors influencing the volume of fuel consumption for automobiles. The model takes into account the influence of various factors on fuel consumption, such as population, gross domestic product, the number of vehicles, regional countries, taxes, and economic factors. The subject of developing the model for forecasting gas consumption in automobiles is a set of practical planning and forecasting methods considering

micro and macroeconomic indicators. Since forecasting is a scientific study of specific development prospects based on a system of qualitative and quantitative scientific research aimed at identifying trends in desired indicators, it is necessary to compile statistics on micro and macroeconomics. Data from various areas related to different spheres of human activity have been collected and analyzed. A forecast has been modeled for residents, automotive transport, types of fuel, and others up to the year 2050.

Various forecasting methods are used to predict energy consumption. Forecasts are made for periods ranging from one day to several decades. The use of simple exponential smoothing, double exponential smoothing, linear exponential smoothing for trend suppression, short-term forecasting [26], multi-year results forecasting, average absolute range, normalized error and average sum in MARNE1 (mean absolute normalized error range) = 1.92% and MARNE2 = 3.27% for the first and second day of natural gas forecast [27]. In calculating the gas price forecast, adding to last year's price forecast reduces the error from 15.85% to 14.31% [28]. Artificial neural networks are also used to predict natural gas [29]. When forecasting the monthly nature of the current gas price for a year, the accuracy of the forecast will gradually decline as the forecast period expands. Using the neural multiplication network in the long-term monthly forecast of natural gas prices, the accuracy of the forecast is high, RMSE (standard error) and MAPE (average absolute error) are 0.2677% and 6.39% respectively. Using the ARIMA [30] model, the results showed that the error rate was 2.2% lower than the traditional prediction model [31]. Research methods used include medium-term forecasting of cold, electrical and gas loads in another grid based on the VAR [32] model, GM and Markov chain method of forecasting natural gas demand [33]. Prediction of natural gas consumption in China based on genetic algorithm [34], impact of gas prices on electricity price forecasting through teacher training and random wandering [35]. Also, the importance of prediction the financial impact of energy storage systems for public electric transport is proved in research of Latvian scientists [36]. In this study, the authors propose to use artificial life simulation method to predict the consumption in long-term perspectives. Artificial life [37] approach is used to solve various problems such as pattern recognition [38], energy system planning [39], and emotional mechanism of behaviour [40]. Further provides another modification of artificial life method and description of the developed appropriate mathematical model for long-term forecasting.

A mathematical model has been developed, which is based on the following main:

- Object-oriented modeling of artificial life, including objects from the following classes - residents, automobiles, companies, the automotive transportation market. The initial number of objects roughly corresponds to the population of Latvia, the number of automobiles, and the number of companies. Each class has programmed behavior that can be modified according to the forecast scenario. Modeling the artificial life of objects allows observing the dynamics of changes by operating not with aggregated statistical data, but directly with each object in the system and modeling the behavior and interaction of each object in the system.
- Monte Carlo modeling - all processes are simulated using random numbers, but according to certain probability distributions, which allows for implementing both the stochastic nature of the processes and the existence and dynamics of their parameters within certain limits and proportions.

The following element groups (sets) are defined in the forecasting model for Latvia:
- Regions of Latvia (hereinafter regions):
  R = (r_1 = "RIGA", r_2 = "PIERIGA", r_3 = "VIDZEME", r_4 = "KURZEME", r_5 = "ZEMGALE", r_6 = "LATGALE")
- Types of housing of the population
  H = (h_1 = " Private house", h_2 = " Twin / Townhouse ", h_3 = " Apartment house ", h_4 = " Block of flats ", h_5 = "Other"}
- Type of residence:
  Z = (z_1 ="City", z_2 = " Rural "} -
- Types of vehicles:
  T = (t_1 = " Car ", t_2 = " Truck ", t_3 = "Bus"};
- Vehicle fuel types:
  D = (d_1="Petrol", d_2 =" Diesel fuel ", d_3 ="LPG", d_4 ="LNG/CNG", d_5 = " Electric"};
- Vehicle age category:
  A = (a = "11+Y", a_2 = "6-10Y", a_3 = "2-5Y", a_4 = "0-1Y")

The main task of the model is to generate the initial state for modelling future processes.
As a baseline, use the statistics from which the following breakdowns are derived:
- Population by age and regions
  AR = (ar^1_1, … , ar^v_r, … , ar^{85}_6) , ar^{85}_r is the population of region r aged 85 and over
- Population in the regions
  S = (s_1, …, s_r, … , s_6)
- Number of births in regions
  Dz = (dz_1, …, dz_r, …, dz_6)
- Probability of death depending on age and region:
  M = (m^1_1, … , m^v_r, … , m^{18}_6), where the age is divided into five years –
  v=1 ir 0-5 years, v=2 is 6-10 etc.., v = 18 is 85 and more years
- Percentage distribution of population by region and type of housing
  HR = (hr^1_1, …, hr^h_r, … , hr^5_6), $\forall r \in R$, $\sum_{h=1}^{5} hr^h_r = 1$
- Percentage distribution of housing types in urban and rural areas
  HZ = (hz^1_1, … , hz^5_1, hz^1_2, …, hz^5_2), $\forall z \in Z$, $\sum_{h=1}^{5} hz^h_z = 1$
- Percentage distribution of the population by three income categories k in each region
  RI = (ri^1_1, …, ri^k_r, … , ri^3_6) , $\forall r \in R$, $\sum_{k=1}^{3} ri^k_r = 1$
- Monthly salary limits for each income category:
  IK = (<ik^1_{min}, ik^1_{max}>,…, <ik^k_{min}, ik^k_{max}>)
- Number of vehicles in the regions
  TR = (tr_1, …, tr_r, … , tr_6)
- Number of vehicles by type and region
  TT = (tt^1_1, … , tt^t_r, … , tt^3_6)
- Percentage distribution of vehicle type ownership between natural and legal persons:
  TI = (ti^1_{fiz}, ti^1_{jur}, ti^t_{fiz}, ti^t_{jur}, ti^3_{fiz}, ti^3_{jur})

- Probability of having a vehicle depending on income category

  $PI = (pi^1, pi^k, pi^3)$

- Number of vehicles by fuel type and vehicle type:

  $TD = (td^1_1, \ldots, td^d_t, \ldots, td^5_3)$

- Percentage distribution of vehicle age

  $TV = (tv_1, \ldots, tv_v, \ldots tv_{23})$

- Vehicle fuel consumption by fuel type and vehicle type

  $DP = (dp^1_1, \ldots, dp^d_t, \ldots, dp^5_3)$

- Fuel prices

  $DC = (dc_1, \ldots, dc_d, \ldots, dc_5)$

- Number of filling stations / charging points by fuel type:

  $DUS = (dus_1, \ldots, dus_d, \ldots, dus_5)$

- Car market prices by age category A and fuel D in four price groups – $C = (c_1 = 10L, c_2 = 20L, c_3 = 20D, c_4 = 10D)$.

Price groups are formed by placing all market proposals of cars of a given year of production and fuel type at market price in ascending order. The list is divided into four parts - first 10% (cheapest c_1), between 10% and 20% (cheap c_2), between last 20% and 10% (expensive c_3), last 10% (the most expensive c_4).

An average price has been calculated for each group, which makes up the following breakdown:

$TC_{vieg} = (\ldots, <tc10L^d_a, tc20L^d_a, tc20D^a_a, tc10D^d_a>, \ldots)$,

For trucks, the price breakdown is by age

$TC_{krav} = (\ldots, <tc10L_a, tc20L_a, tc20D_a, tc10D_a>, \ldots)$

Given the small number of buses, only the minimum and maximum market prices are defined for them.

$TC_{bus} = (\ldots, <tcmin_a, tcmax_a>, \ldots)$

- Technical inspection prices by vehicle type and fuel

  $TA = (ta^1_1, \ldots, ta^d_t, \ldots, ta^5_3)$

- Repeated inspection prices by vehicle type and fuel

  $TAA = (taa^1_1, \ldots, taa^d_t, \ldots, taa^5_3)$

  The following element classes are defined for the model

- Market

- Percentage distribution of cars by age category

  $AV = (av_1, \ldots, av_a, \ldots, av_4)$, $\quad \sum_{a=1}^{4} av_a = 1$

- Percentage distribution of cars in each age category by fuel type

  $AD = (ad^1_1, \ldots, ad^d_a, \ldots, ad^5_4)$, $\quad \forall a \in A, \sum_{d=1}^{5} ad^d_a = 1$

- List of cars available on the market

$TMC = (tmc_1, tmc_2, \ldots)$, where tmc_i – is a unique identifier for a model car that is on the market for sale and available for purchase

- Vehicle V

- $id_v \in \mathbb{R}$ – the unique identifier of the vehicle

- $d_v \in D$ – type of fuel

- $c_v \in \mathbb{R}$ – fuel consumption L or kWh to 100 km
- $a_v \in \mathbb{N}$ – age (years)
- $s_v \in \mathbb{N}$ – mileage (km)
- $cc_v \in \mathbb{R}$ – the amount of fuel consumed during the year
- $ac_v \in \mathbb{R}$ – annual total costs
- $bc_v \in \mathbb{R}$ – travel costs
- $mc_v \in \mathbb{R}$ – maintenance costs
- $rc_v \in \mathbb{R}$ – repair costs
- $tc_v \in \mathbb{R}$ – market price
- $ip_v \in \mathbb{R}$ – unique identifier of the owner (person) if the machine belongs to a person or -1 if just imported
- $ipt_v \in (0, 1)$ – owner type – 0 – private, 1 – commercial
- $t_v \in T$ – vehicle type
- $r_v \in R$ – region
- $br_v \in (0, 1)$ – or broken
- $L_v \in (0, 1)$ – is in leasing
- $m_v \in \mathbb{R}$ – gross vehicle weight (kg)
- $N_v \in \mathbb{R}$ – vehicle power (kW)
- $Q_v \in \mathbb{R}$ – engine capacity (cm^3)
- $CO2_v \in \mathbb{R}$ – documented CO2 emissions per km
- $EURO_v \in \mathbb{R}$ – Euro eco-level, if applicable (for diesel lorries and buses)
- ○ sale $\in \mathbb{N}$ – number of years on the market
- Person P
- $id_p \in \mathbb{R}$ – unique identifier of the person
- $r_p \in R$ – region of registration of the person
- $h_p \in H$ – type of housing
- $z_p \in Z$ – in the city or in the rural
- $k_p \in K$ – income category
- $in_p \in \mathbb{R}$ – monthly income
- $v_p \in \mathbb{N}$ – age (years)
- $km_p \in \mathbb{R}$ – average mileage per day
- $dz_p \in (0, 1)$ – is alive
- $vad_p \in \mathbb{N}$ – driving experience (years)
- $BM_p \in \mathbb{N}$ – bonus-malus level
- $Cars_p$ – the object of the list of machines with the identification numbers of the machines owned

The following object sets are defined in the model:
- CIT = (p_1, p_2, … , p_{max}), where $p_i \in P$ – objects of a the Person class
- CAR = (car_1, car_2, …, car_{max}), kur $car_j \in V$ – objects of the Vehicle class
- MARKET – object of the class Market

The model is sufficiently flexible, and if necessary, one can specify the nature of changes in other parameters, such as tax policies or other political decisions, which can have a significant impact on the process.

For the assessment and forecasting of fuel (and gas consumption for transportation) resulting from the modeling, the following output values are estimated for each year:

- Fuel prices
- Total number of vehicles
- Number of vehicles by fuel type
- Total annual fuel consumption
- Population size

Thus, the model allows for evaluating and forecasting important indicators based on different scenarios and changes in parameters, which helps analyze and make decisions regarding energy policy and sustainable development in the transportation sector.

Computer modelling

Using the developed model and algorithms, various changes and development scenarios for the Latvian transport system were modeled. In all scenarios, existing birth and mortality probabilities are used.
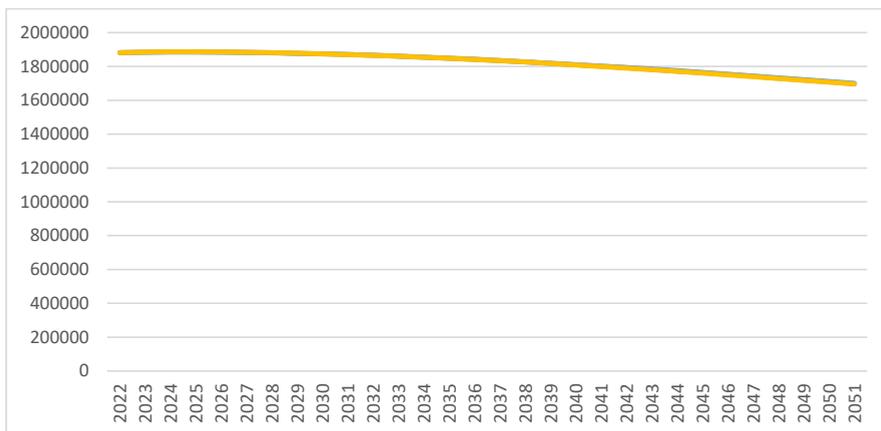
Fig. 1. The population of Latvia was modeled in the scenario.

Description o scenario parameters

In the scenario, the following parameters of change are defined and based on a subjective authors' experience:

– Increase in petrol prices by 10% per year for the first 5 years, then by 1% per year
– The price of diesel fuel (DD) increases by 10% per year for the first 5 years, then by 1% per year.
– The price of liquefied petroleum gas is 0.55 of the prices of petrol
– Natural gas - liquefied/compressed (LNG/CNG) - 5% price increase per year for the first 5 years, then 0.5% per year

– Electricity price increases by 5 % per year for the first 5 years, then by 0.5 % per year

Each year, the income of each resident changes according to a formula that is random:

$$in_p^i = in_p^i + in_p^i \cdot (\xi \cdot \frac{10}{75} - 0.05) \tag{1}$$

This means that the probability of income growth is 0.625 and the probability of decrease is 0.325, which gives an overall statistical increase in average income. The number of LNG/CNG gas fuelling stations dus4 and the number of dus5 fast charging stations are increased as follows:

$$dus_5 = dus_5 \cdot 2^{1/(gads+1)} \tag{2}$$
$$dus_4 = dus_4 \cdot 2^{1/(gads+1)} \tag{3}$$

This means that, of 75 recharge points in 2021, 611 will be recharged in 2050.

– Expected next situation on the road transport market
– Annual number of imported cars does not change (no deficit)
– Vehicles sold for 3 years (after 3 years in the absence of an application, they disappear)
– The breakdown of imported cars over 5 years of age is determined by market demand (number of cars sold on a given fuel relative to total number of cars sold).
– The breakdown of new imported vehicles 0-5 years is as follows:
    o 20 % of the market is petrol cars
    o 10 % of the market is diesel cars
    o LPG cars account for 15 % of the market
    o 20 % of the market is LNG / CNG cars
    o Electric cars account for 35 % of the market.

Scenario forecast results

Monte Carlo modeling is performed with scenario-defined parameters and functional dependencies. Considering the use of random numbers, the numerical results of each modeling iteration may vary slightly, but the trends of change are visible and similar for identical scenario settings.

The scenario predicts the number of vehicles and their percentage distribution.
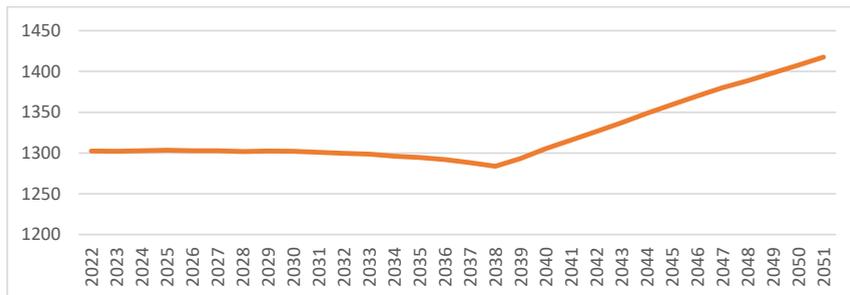
Fig. 2. The average monthly income level of an individual in the scenario.
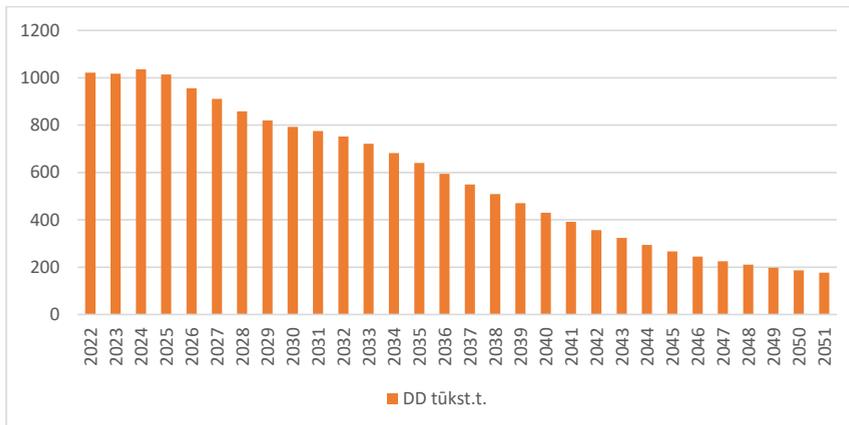
Fig. 3. Projected changes in the volume of diesel fuel sales in the scenario.
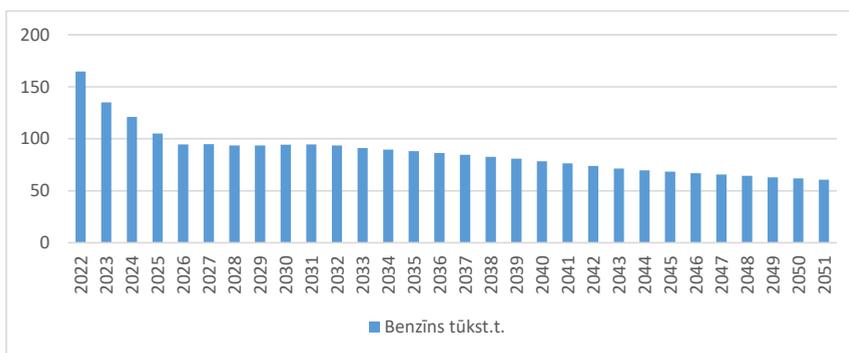
Fig. 4. Projected changes in the volume of gasoline sales in the scenario.
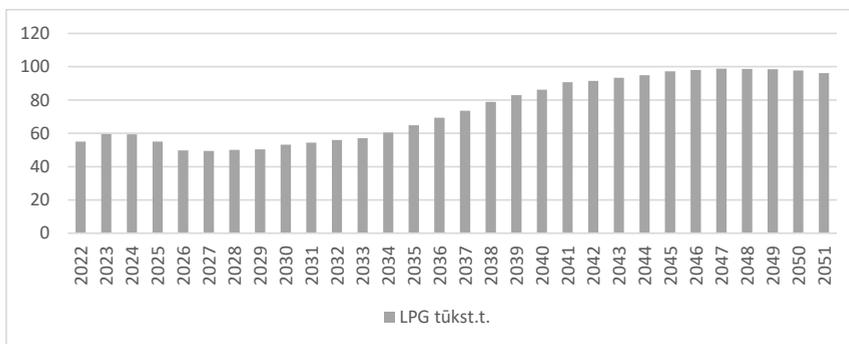
Fig. 5. Projected changes in the volume of LPG (liquefied petroleum gas) sales in the scenario.
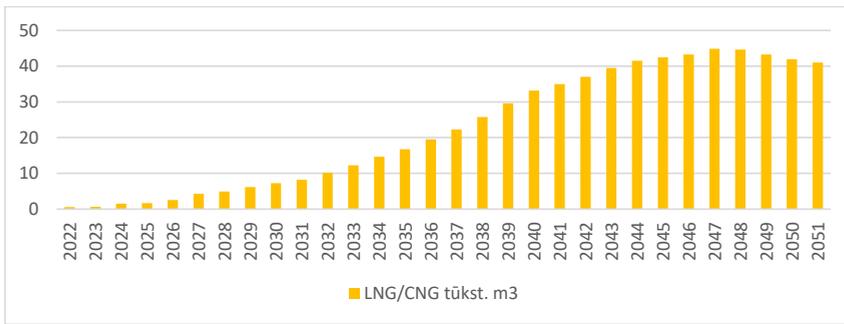
Fig. 6. Projected changes in the volume of natural gas required for LNG/CNG vehicles in the scenario.
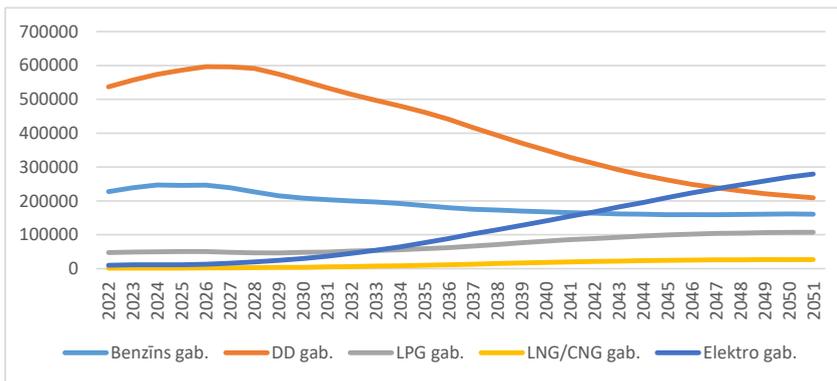
Fig. 7. The projected number of vehicles by fuel type (in units) in the scenario.
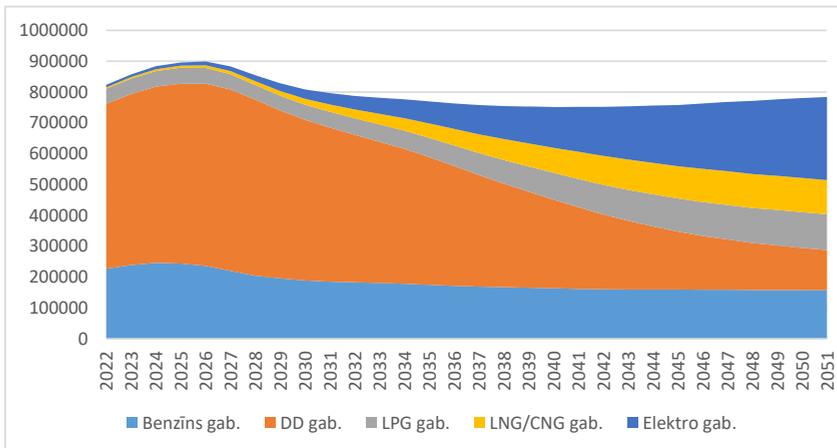
Fig. 8. The projected distribution of the number of vehicles by fuel type in the scenario.
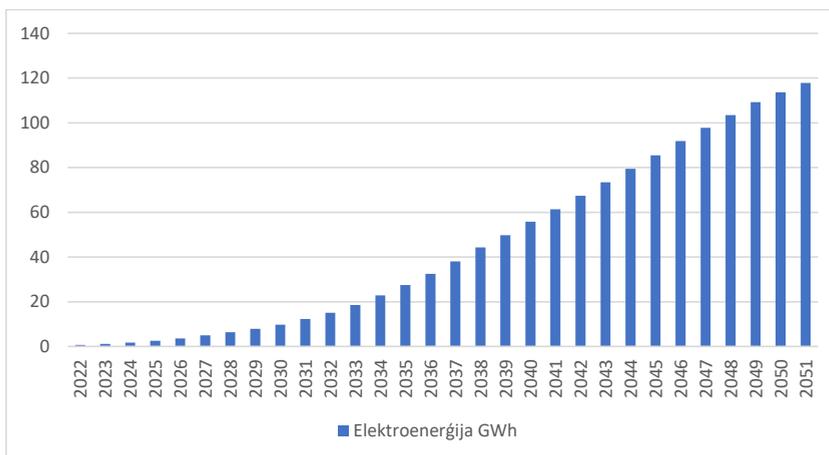
Fig. 9. Projected changes in the volume of electricity required for electric vehicles in the scenario.

By analysing the results of the research and development carried out, it can be concluded that the predictive models work correctly, the predictive scenarios they have created are comparable to the results of the predictions made in other studies. For example, looking at projections of the number of electric vehicles in 2030 published on https://uzladets.lv/, one can see that the data vary depending on the methodology:

- Ministry of Transport – 6000 (0.82 % from the existing)
- AS Latvenergo – 36500 (5.01 %)
- Latvia's national development plan 2027–14570 (2%)
- Exponential curve – 10500 (1.43 %)
- An exponential curve that takes into account data from 2018.g. – 33500 (4.58 %)
- Unchanged 60 % (average of the last 4 quarters) An increase – 116000 (15.94 %)

These data indirectly indicate the reliability of the projected results.

The obtained results indicate that the number of electric vehicles will increase, leading to a growth in electricity consumption. However, the use of autonomous electric vehicles with energy-efficient management will contribute to reducing electricity consumption.

To investigate the advancements in the optimization of electric transportation and specifically autonomous electric vehicles, a study and analysis of scientific publications on this topic have been conducted.

Research has been conducted to examine the progress and developments in the field of optimizing electric transportation, with a particular focus on autonomous electric vehicles. Scientific publications on this subject have been analyzed to gain insights into the current state of research, innovative technologies, and potential solutions. The study aims to understand the existing knowledge, identify emerging trends, and explore opportunities for further improvements in otimizing electric transportation systems, including the integration of autonomous features.

16

Literature review

Energy consumption optimization in electric transportation can be carried out both at the individual vehicle level and within the transportation network [58].

In the paper [1], an electric bus with a supercapacitor and ultra-fast charging is proposed as a public transport solution. Additionally, a combined panel that converts kinetic energy and solar energy into electricity is suggested as an alternative energy source. This panel not only converts and stores energy but also serves as a contactless charging platform and road surface. The integration of these solutions aims to create an energy-efficient urban transportation system.

Another network-based strategy is implemented in the paper [2]. The vehicle (electric car) is connected to the Integrated Command and Control Centre (ICCC) platform, which includes an implementation for energy consumption reduction independent of the vehicle connection, developed for the JOSPEL project. Data from the car's sensors are transmitted to the Information technology architecture (ICT) structure. An energy efficiency assistant informs the driver about the optimal route to a given destination and the most efficient way to manage the vehicle's subsystems. As evident, energy consumption optimization occurs with the assistance of human input.

These studies highlight different approaches to optimizing energy consumption in electric transportation, ranging from innovative energy sources and charging systems to intelligent platforms and driver guidance systems. The aim is to achieve greater energy efficiency, reduce environmental impact, and enhance the overall performance of electric transportation systems.

The main feature emphasized in research [3] is the prediction of preceding vehicle motion. Accurate prediction of the speed of the vehicle ahead in the next time period enables an energy-efficient controller to optimize the speed and torque distribution in the electric vehicle. Energy consumption optimization is achieved through the predictive control method using a nonlinear model. When this method is applied, energy efficiency is higher when the vehicles are integrated into a common network.

In paper [4], a metaheuristic study of energy-efficient routing is conducted. Ant Colony Optimization (ACO) and Particle Swarm Optimization (PSO) methods are considered and compared. Both algorithms have shown productive results. Using the PSO algorithm, a solution for an efficient route was found in less than 400 milliseconds, while ACO required almost 1.8 seconds to analyze the same problem, which can be attributed to the simplicity of the PSO logic.

Energy-efficient management is applied in hybrid vehicles. In a hybrid car, a population-based optimization algorithm was employed [5]. The energy consumption control strategy is implemented using a hybrid energy storage system with hydrogen, a battery, and a supercapacitor as energy sources. The optimization algorithm was used to solve a constrained optimization problem, where the energy consumed by the battery needed to be minimized for a given driving cycle in order to increase the vehicle's range. The developed energy management system addresses the minimization of energy costs while maintaining imposed constraints (energy reserves, etc.), which can extend the lifespan of components.

In paper [6], the authors investigated the optimization of energy consumption in electric vehicles using dynamic programming. Travel routes are generated using an online application,

which allows for the creation of movements considering the optimal route and relevant constraints. The route description provides a control space for dynamic programming. The proposed quasi-static model is optimized for short computation time and provides sufficient accuracy in energy calculations. As a result, the computation time for optimizing the trajectory for a 25 km route is reduced to 14.3 seconds when using a distance step of 10 m and a velocity step of 0.1 m/s.

Optimization can also be carried out at the structural topological level. Paper [7] specifically considers this type of optimization. The authors find a compromise between the materials used in the production of hybrid vehicles, such as copper (used in electric motors) and lithium (used in batteries), and energy consumption based on the Pareto rule. This article demonstrated that the combination of a preselection algorithm and transmission optimization can work with a certain number of components. As the number of components increases, the number of reasonable topologies that need to be optimized will also increase. To calculate the optimal parameters, a multi-objective thermodynamic genetic algorithm is applied, which was extensively described in paper [8] and proved to be suitable for solving these problems.

To improve energy efficiency on roads with variable slopes, an instant optimization strategy for energy consumption in electric vehicles is applied, known as the normalized energy consumption minimization strategy [9]. The method is based on utilizing the vehicle's kinetic energy. The kinetic energy management system can either store energy during regenerative braking [10] or excess energy generated by the motor, or use it for propulsion. The application of this method resulted in energy savings of 5.9 % over a 35 km road segment compared to driving without using this method.

The optimization of energy consumption in electric vehicles with distributed drive using a motion-following controller and torque distribution module is proposed in paper [11]. The optimization method combines a one-iteration sequential quadratic programming algorithm with a one-dimensional search algorithm. The one-dimensional search algorithm operates on the practical assumption that steering and tire slip angles can be neglected under normal driving conditions. The torque distribution results of the proposed algorithm correspond to three different desired acceleration intensities set by the driver. Simulation results of this method compared to an average distribution algorithm show that both algorithms can satisfy the torque and yaw moment requirements. However, the proposed distribution algorithm consumes less energy. Nevertheless, the optimization coefficient decreases from 16 % to 1 % as the acceleration demand increases.

In paper [12] the optimization of energy consumption is applied using torque distribution and dynamic characteristics for a four-wheel-motor electric vehicle. Unlike the previous study, a multi-objective optimization approach is employed, considering three factors: energy consumption, road handling, and driving comfort. To solve this multi-objective optimization problem, an adaptive particle swarm optimization (APSO) algorithm is utilized. The proposed torque distribution algorithm can enhance energy savings, road handling, and driving comfort for the four-wheel-motor electric vehicle compared to a uniform distribution algorithm. The proposed algorithm outperforms the traditional uniform torque distribution method, with vehicle efficiency coefficients (0.5749 and 0.3047, respectively).

In paper [13], various strategies for electric motor actuation are investigated. To maximize energy transmission efficiency, the transmission gear ratios are adjusted to maintain

speed and acceleration constraints of the vehicle, as well as limits on angular velocity and torque of the electric motor. An ecologically friendly speed profile is generated based on smooth speed changes and constraints on maximum speed and acceleration to reduce energy consumption. Additionally, regenerative braking is used to accumulate energy.

In paper [14], fuel consumption reduction through optimization of an existing tourist route is examined. The LINGO [15] software is utilized, which can solve nonlinear programming problems with unlimited linear and nonlinear constraints, as well as an unlimited number of integer, nonlinear, and global variables. A model with multiple constraints is built to search for minimum energy consumption, with the rotational speed of the shaft (rpm) as the decision variable and the total fuel consumption (liters) as the objective function. Factors such as water depth, wind, and traffic flow are not considered in this study, and only the influence of water current on vessel speed is incorporated in the established model. By analyzing and processing these data, regression functions are obtained between the fuel consumption of the main engine and shaft rotational speed, as well as between the vessel's speed relative to the water and shaft rotational speed. Three scenarios are presented in the study, where the best result allows for reducing fuel consumption from 8348.7 liters without optimization to 7143.6 liters with optimization, over a route length of 493 km, while increasing the travel time from 21.5 hours to 28.9 hours.

Paper [16] investigates energy-efficient train operation between consecutive stations with the aim of reducing energy consumption. The optimization task involves determining the optimal switching points between cruise and coasting phases of the train. The authors propose a hybrid algorithm that combines a genetic algorithm and simulated annealing to find the switching points. The algorithm is tested on multiple test tracks of varying lengths, considering real constraints such as punctuality and maximum speed limits. The train motion model is derived from fundamental physical definitions, and the optimization problem is formulated as an energy consumption minimization task. The hybrid algorithm demonstrates superior performance compared to a standalone genetic algorithm in terms of accuracy and execution time. Moreover, the algorithm is approximately 20 % faster than the genetic algorithm alone. The research results indicate that the proposed hybrid algorithm can provide more accurate solutions for energy-efficient train operation compared to a standalone genetic algorithm. The approach has the potential to be applied to more complex problems.

Paper [17] describes a new approach to energy-efficient train control based on dynamic linearization and predictive control methods. The authors of the article address the energy-saving problem in the railway transport system and propose a new cost function related to energy consumption, which is utilized in the predictive controller. The solution algorithm involves replacing the unknown nonlinear train model with a dynamically linearized model. The control action is obtained by solving an optimization problem over a closed finite horizon using a predictive controller. According to the article, the efficiency of train control is directly influenced by the utilization of traction force and braking, leading to significant losses of kinetic energy. The authors suggest using a cost function that accounts for both energy consumption and trip duration. The article also considers constraints related to control saturation, velocity, and movement safety. The results of simulation modeling demonstrated the effectiveness of the proposed approach, as confirmed by graphical and numerical outcomes. Overall, the proposed

approach to energy-efficient train control shows promise and can be applied in real-world railway transport conditions.

Paper [18] investigates the optimal operation strategy of a high-speed train to minimize energy consumption between neighboring stations. The article fully takes into account the characteristics of high-speed trains, including traction and regenerative braking characteristics, as well as the geographical conditions of the railway route in a dynamic model. A new optimal strategy is developed for optimizing the train operation process, consisting of a global optimization process and an additional optimization process based on route analysis discretization. In the global optimization process, a genetic algorithm is applied to search for the optimal speed at each sub-division end within a fixed time. Then, the optimization strategy is further studied to search for a speed sequence to improve the train operation process. To verify the effectiveness of the proposed train operation strategy, simulations were conducted, and the tests showed that the proposed strategy outperformed conventional train operation strategies. The simulation results met the requirements of time, comfort, and energy consumption. Based on the force analysis, dynamic model, energy transmission analysis, global optimization model, and additional energy-saving analysis, the authors concluded that the proposed optimal train operation strategy could reduce energy consumption by 2.35 % compared to the global optimization strategy, using the example of the Chinese high-speed railway route. Thus, the energy-saving train operation strategy proposed in the article can be useful for optimizing the train operation process and reducing energy consumption, thereby reducing the ecological footprint of the railway transportation system.

Paper [19] describes a model for optimizing the operation of high-speed trains considering nergy-saving modes. The article addresses the problem of optimizing train operation by considering speed variations, incline angles, and other factors, including sections without power supply. To achieve optimal train operation, the authors apply the pseudospectral collocation method. The model takes into account speed, power, and time constraints, as well as brake operation constraints. The authors divide the train's trajectory into multiple phases and describe each phase according to the train's operational characteristics. Based on this, they create a model that minimizes train energy consumption. The study was conducted on the Shanghai-Kunming (Hukun) high-speed railway in China. A comparison between optimal train operation and experienced driver operation showed that energy consumption could be reduced by 18.13 % with optimal operation. Thus, the optimization model for high-speed train operation with multiple phases and the pseudospectral collocation method enable the creation of energy-efficient train operation modes, addressing a relevant problem in modern transportation.

Paper [20] presents work on optimizing the energy consumption of urban trains during travel between two stations. The article proposes an online mode switching control algorithm for urban trains based on a mode switching system model. This algorithm can dynamically adjust the sequence of train mode switching based on disturbances and changes in the train's operational state during real-world operation. The article presents a mode switching system model for urban trains that describes the train's movement characteristics between two stations. This model was used to propose an optimization problem that minimizes train energy consumption. An algorithm for optimizing the switching time was utilized to calculate the optimal switching time. By calculating the state transition matrix between neighboring switching times offline, the computational cost was significantly reduced. Numerical

experiments were conducted to verify the effectiveness of the proposed method, based on measured data from an urban railway train. The Yizhuang subway line in Beijing, China, was used as the model for computation. To calculate the optimal mode switching, the authors of the article employed the time-switching optimization algorithm, determining the optimal switching time that can be calculated online using this algorithm. In conclusion, the article explores optimal energy-saving control for urban trains between two stations. The authors propose a time-switching optimization algorithm that can consider disturbances and real-time changes in the train's operational state, and they verify its effectiveness using data from the Yizhuang subway line.

Paper [21] addresses the issue of optimizing energy consumption for a train moving with a fixed time under constraints on traction and braking force, as well as limits on safe speed. One way to save energy is to find an energy-efficient optimal train trajectory, which is a problem of optimal control. The article employs control parameterization methods to solve the optimal train control problem. The objective function aims to minimize energy consumption while penalizing changes in control signals. The train's traction force control is approximated by a linear combination of basis functions, typically a piecewise-constant function, which transforms the original optimal control problem into a specific type of nonlinear optimization problem. Numerical results demonstrate that the proposed method can obtain an optimal train trajectory that reduces energy consumption.

Paper [22] investigates an optimal energy-saving control strategy for a high-speed train using the maximum principle under speed constraints. The study presents two types of transition diagrams, considering variations and jumps in conjugate variable regulations in two cases: with speed constraints and without speed constraints. Based on this, transitions touching the speed limit are classified into four basic cases, and other transitions are derived or combined from these four basic cases. The study discusses the relationship between optimal and maximum work. It also discusses the connection between optimal and maximum work using the example of reducing the optimal work time to the maximum work time.

Conclusions of the literature review

Deep analysis of the research base reveals that currently, the majority of energy-saving solutions are related to route calculation and trajectory planning for unmanned vehicles (UV's), as well as energy-saving algorithms for other equipment unrelated to UV electric propulsion systems. Only a few studies focused on reducing energy consumption explore the mechanical and electrical properties of power devices.

The goal and tasks of the work

The goal of the work

The goal of this work is to develop a method for optimizing the power consumption of any electric unmanned vehicle. This method will enable determining optimal control signals at the beginning of motion for efficient energy management under varying vehicle parameters, without prior calculations or adjustments.

Hypothesis

Using the new method, it is possible to reduce the energy consumption of unmanned vehicles.

The tasks of the work

- Research the mechanical and electrical properties of electric motors for unmanned electric vehicles.
- Develop a mathematical model of unmanned electric vehicles to solve the energy consumption minimization problem.
- Construct mechanical models of electric unmanned vehicles.
- Identify the target function for minimizing energy consumption.
- Explore algorithms for finding minimal energy consumption.
- Research neural networks.
- Research and develop an algorithm for automatically creating a training set.
- Develop an optimization algorithm for a self-learning neural network.
- Design an electrical circuit for the optimization controller.
- Develop electrical circuits for experimental devices.
- Create a computer model of unmanned electric vehicles for experimental energy consumption calculations and investigation of the optimized objective function.
- Experimentally test various traction electric motors for unmanned electric vehicles and collect data on their performance and consumption.
- Test the optimization algorithm of the self-learning neural network.

Research tools and methods

- Inductive method
- Deductive method
- Systems analysis
- Statistical analysis methods
- Neural network theory
- Optimization methods
- Formalization method

Scientific novelty of the work

A new method for energy savings in electric unmanned vehicles has been developed in this work. The method consists of a new algorithm for automatic generation of a training dataset for a neural network, a new algorithm for load characterization, and a minimum search algorithm.

The novelty of the proposed method is in the self-learning neural network and the algorithm for this network to determine the nature of the load and its change.

Practical application of the work

The application of this method enhances energy efficiency and reduces power consumption in electric unmanned vehicles. The developed optimization controller can be utilized in any electric unmanned vehicle.

Work approbation

1. International conference "61st International Scientific Conference on Power and Electrical Engineering of Riga Technical University" referāts "Neural Network Based UAV Optimal Control Algorithm for Energy Efficiency Maximization", A. Korneyev, M. Gorobetz, Latvia, Riga, 5-7 november, 2020
2. International conference "59th International Scientific Conference on Power and Electrical Engineering of Riga Technical University" referāts "Unified Energy Efficient Control Algorithm for Electric Unmanned Aerial Vehicles with Different Traction Drives and Configurations," A. Korneyev, M. Gorobetz, A. Levchenkov, Latvia, Riga, 12-14 november, 2018
3. International conference "60th International Scientific Conference on Power and Electrical Engineering of Riga Technical University" referāts "Analysis and Modelling of UAV Electrical Traction Drive based on Empirical Data for Energy Efficiency Tasks," M. Gorobetz, A. Potapovs, A. Korneyev, Latvia, Riga, 7-9 october, 2019
4. International conference "7th IEEE International Energy Conference" referāts "Long-term Energy and Fuel Consumption Forecast in Private and Commercial Transport using Artificial Life Approach," M. Gorobetz, A. Korneyev, L. Zemite, Latvia, Riga, 9-12 may, 2022
5. International conference "61st International Scientific Conference on Power and Electrical Engineering of Riga Technical University" referāts "Intelligent Algorithm for Using Overall Energy Consumption Statistics," M. Gorobetz, L. Zemite, A. Jasevics, A. Korneyev, Latvia, Riga, 5-7 november, 2020
6. International Doctoral School "11th International Doctoral School of Energy Conversion and Saving Technologies" referāts "Research and development of evolutionary algorithms for optimal energy efficient control of autonomous unmanned electric vehicle systems," Latvia, Klapkalnciems, 27-28 may, 2022

In the work "Neural Network Based UAV Optimal Control Algorithm for Energy Efficiency Maximization" the author developed and studied the structure and parameters of a neural network for the developed algorithm for optimal energy efficient control.

In the work "Unified Energy Efficient Control Algorithm for Electric Unmanned Aerial Vehicles with Different Traction Drives and Configurations," the author analyzed existing solutions, developed an energy-efficient control algorithm for unmanned aerial vehicles, and built an experimental stand. Together with co-authors, experiments were conducted to simulate the flight of a UAV.

In the work "Analysis and Modeling of UAV Electrical Traction Drive based on Empirical Data for Energy Efficiency Tasks," the author analyzed existing solutions, together with his co-authors he built a test bench and conducted experiments.

The work "Long-term Energy and Fuel Consumption Forecast in Private and Commercial Transport using Artificial Life Approach" is devoted in particular to the forecast for the development of electric vehicles in Latvia. The data obtained indicate the development of electric transport, which indicates the feasibility of research in the field of optimizing energy consumption in electric transport. The author analyzed existing solutions, collected statistical data to build a model, and together with co-authors participated in the development of a mathematical forecast model and processing of the data obtained.

In the work "Intelligent Algorithm for Using Overall Energy Consumption Statistics" [86] the author analyzed the hourly statistics of total consumed energy by different consumers and simulated the intelligent method to separate the electricity consumption caused by artificial lighting from the electrical energy consumed by other equipment.

The paper "Research and development of evolutionary algorithms for optimal energy efficient control of autonomous unmanned electric vehicle systems" presents optimization algorithms developed by the author for energy efficient control of electric unmanned vehicles, experiments conducted by the author, neural network research, experiments on experimental devices and computer modeling. And it is the intermediate result of the entire doctoral thesis at the time of presentation.

Author's publications

1. A. Korneyev, M. Gorobetz. Neural Network Based UAV Optimal Control Algorithm for Energy Efficiency Maximization //2020 IEEE 61st International Scientific Conference on Power and Electrical Engineering of Riga Technical University (RTUCON 2020), Latvia, Riga, 5-7 november, 2020. Piscataway: IEEE, 2020, 1-5 p.
2. A. Korneyev, M. Gorobetz, A. Levchenkov. Unified Energy Efficient Control Algorithm for Electric Unmanned Aerial Vehicles with Different Traction Drives and Configurations. //2018 IEEE 59th International Scientific Conference on Power and Electrical Engineering of Riga Technical University (RTUCON 2018), Latvia, Riga, 12-14 november, 2018. Piscataway: IEEE, 2018, 537-542 p.
3. A. Korneyev, M. Gorobetz, I. Alps, L. Ribickis. Adaptive Traction Drive Control Algorithm for Electrical Energy Consumption Minimisation of Autonomous Unmanned Aerial Vehicle //Electrical, Control and Communication Engineering, 2019, Vol. 15, No. 2, 62-70 p.

4. M. Gorobetz, A. Potapovs, A. Korneyev. Analysis and Modelling of UAV Electrical Traction Drive based on Empirical Data for Energy Efficiency Tasks //2019 IEEE 60th International Scientific Conference on Power and Electrical Engineering of Riga Technical University (RTUCON 2019), Latvia, Riga, 7-9 october, 2019. Piscataway: IEEE, 2019, 399-403 p.

5. M. Gorobetz, A. Potapovs, A. Korneyev, I. Alps. Device and Algorithm for Vehicle Detection and Traffic Intensity Analysis //Electrical, Control and Communication Engineering, 2021, Vol. 17, No. 1, 83-92 p.

6. M. Gorobetz, L. Ribickis. A. Beinarovica, A. Kornejevs. Immune Neural Network Machine Learning of Autonomous Drones for Energy Efficiency and Collision Prevention, //Drones - Various Applications, Rijeka, Published: September 18th, 2023, doi:10.5772/intechopen.1002533

7. E. Kamolins, M. Gorobetz, K. Malnaca, A. Korneyev. Analysis of Test Results for Developed Technology of Diesel Bus Conversion into Electric Bus //Reliability and Statistics in Transportation and Communication, Cham: Springer Nature Switzerland AG 2019, 2020. 1.-10 p.

8. M. Gorobetz, A. Korneyev, L. Zemite. Long-term Energy and Fuel Consumption Forecast in Private and Commercial Transport using Artificial Life Approach //ENERGYCON 2022: 7th IEEE International Energy Conference, Latvia, Riga, 9-12 may, 2022. Piscataway: IEEE, 2022, 1-6 p.

9. M. Gorobetz, L. Zemite, A. Jasevics, A. Korneyev. Intelligent Algorithm for Using Overall Energy Consumption Statistics //2020 IEEE 61st International Scientific Conference on Power and Electrical Engineering of Riga Technical University (RTUCON 2020), Latvia, Riga, 5-7 november, 2020. Piscataway: IEEE, 2020, 1-13p.

10. Malnaca, K., Gorobetz, M., Yatskiv (Jackiva), I., Korneyev A. Decision-Making Process for Choosing Technology of Diesel Bus Conversion into Electric Bus. No: Reliability and Statistics in Transportation and Communication: Selected Papers from the 18th International Conference on Reliability and Statistics in Transportation and Communication, RelStat '18. Lecture Notes in Networks and Systems. Vol.68. Cham: Springer Nature, 2019. 91.-102.lpp.

1. CONTROL STRUCTURE AND DESCRIPTION OF ELEMENTS

1.1. Description of the situation

In the first chapter, various types of transportation are examined in terms of degrees of freedom and modes of movement to determine control signals for optimizing energy consumption. To control the optimization process, an optimization controller is proposed, and its scheme is developed and discussed in this chapter.

The possibility of integrating this controller into an existing structure for unmanned vehicles control is also considered. The functional blocks for energy-efficient control are examined within the structure of the optimization controller.

1.2. Definition of unmanned vehicles

Types of transportation based on the mode of movement for example:

- *Water-based*: Surface vessels, submarines.
- *Air-based*: Airplanes, helicopters, multicopters (multirotor aircraft with three or more rotor blades).
- *Land-based*: Trains, automobiles.

All of these types of vehicles can be unmanned (autonomous) and equipped with electric propulsion.

Types of transportation based on degrees of freedom:

- *Train:* One degree of freedom, controlled by adjusting the engine power or using brakes.
- *Automobile:* Two degrees of freedom, controlled by adjusting engine power, using brakes, and steering the wheel.
- *Airplane:* Four degrees of freedom, controlled by adjusting speed (throttle, airbrakes), pitch (elevator), roll (ailerons), and yaw (rudder). However, it is not capable of moving and being controlled in two directions perpendicular to its longitudinal axis.
- *Helicopter (Rotorcraft):* Six degrees of freedom, but in normal flight, the helicopter's pitch and roll movements are related to lateral and longitudinal velocities. Hence, in ideal circumstances, a helicopter has four control surfaces similar to an airplane. It should be noted that this viewpoint is not universally accepted, and some experts consider throttle and collective pitch as separate control surfaces.

The definitions of unmanned or autonomous transportation can vary. For example, it can correspond to the following criteria:

- Vehicles that move using an autopilot (automatic flight controller):
    - Predefined route with initial, intermediate, and final waypoints and trajectory.
    - Predefined route with initial, intermediate, and final waypoints, and the autopilot selects the trajectory.

In such cases, the command to engage the autopilot can be given by a person either outside or inside the vehicle. The vehicle may also have remote or manual control for managing emergencies or in case of autopilot failure.

In the context of this work, an **unmanned vehicle (UV)** corresponds to an **autonomous electrical vehicle** that includes an autopilot in its control structure, enabling control of the vehicle to reach predetermined coordinates.

1.3. Detection of control signals for optimizing transportation vehicles

To identify control signals for optimizing transportation vehicles, let's consider existing types of vehicles based on degrees of freedom and the control signals they employ, assuming that all of them can be unmanned.

Water-based, air-based and land-based types of vehicles can be unmanned (autonomous) and equipped with electric propulsion.

Types of transportation based on degrees of freedom:

- **Train**: one degree of freedom, controlled by adjusting the engine power or using brakes.
- **Automobile**: two degrees of freedom, controlled by adjusting the engine power, using brakes, and steering the wheel.
- **Airplane**: four degrees of freedom, controlled by adjusting speed (throttle, air brakes), pitch (elevator), roll (ailerons), and yaw (rudder). However, it is unable to move and be controlled in two directions perpendicular to its longitudinal axis.
- **Helicopter (Rotorcraft)**: six degrees of freedom, but in normal flight, the movements of the helicopter's roll and pitch are linked to lateral and longitudinal speeds. Thus, ideally, a helicopter has four control surfaces similar to an airplane. It is worth noting that this position is not accepted by all experts, and some argue that throttle and collective pitch should be considered separate control surfaces.

The train will have the minimum number of control signals:
- o   a throttle control signal level.

The maximum number of control signals will be found in a multirotor rotorcraft (multicopter) with wings:
- o   a roll (aileron) control signal;
- o   a pitch (elevator) control signal;
- o   a throttle control signal;
- o   a yaw (rudder) control signal.

The minimum number of control signals will be present in a train - one control signal. The maximum number of control signals will be found in a multirotor rotorcraft with wings - four control signals.

Thus, for controlling any transportation vehicle, the maximum number of control signals will be four:
- o c_1 – a roll (aileron) control signal;

- c_2 – a pitch (elevator) control signal;
- c_3 – a throttle control signal;
- c_4 – a yaw (rudder) control signal.

1.4. Overview of existing types of electric UV's

There are various types of electric unmanned vehicles currently in existence. Here are a few examples:

Electric Drones: Drones are unmanned aerial vehicles (UAV's) that are powered by electric motors and use batteries for their energy source. They have a wide range of applications, including aerial photography, videography, package delivery, surveying, and even recreational use.

Autonomous Cars: Electric autonomous cars, also known as self-driving cars, use electric propulsion systems and are equipped with sensors, cameras, and AI algorithms to navigate and make decisions on the road. Companies like Tesla, Waymo, and Uber are actively developing autonomous electric vehicle technologies.

Electric Unmanned Surface Vehicles (USV's): USV's are unmanned boats or watercraft that operate on the surface of the water. They can be used for various purposes, such as oceanographic research, environmental monitoring, offshore inspections, and defense applications. Electric USVs offer a more sustainable and quieter alternative to traditional fuel-powered vessels.

Electric Unmanned Underwater Vehicles (UUV's): UUV's are autonomous or remotely operated underwater vehicles. They are commonly used for marine exploration, underwater surveys, oil and gas inspections, scientific research, and military operations. Electric UUVs use electric propulsion systems and are capable of operating underwater for extended periods.

Electric Unmanned Ground Vehicles (UGV's): UGVs are autonomous or remotely operated vehicles designed for various applications on land. They can be used in agriculture, mining, surveillance, search and rescue operations, and military applications. Electric UGV's offer advantages such as reduced noise, lower operating costs, and environmental friendliness. Electric Unmanned Aerial Taxis: Also known as air taxis or flying cars, these vehicles are being developed as a means of urban transportation. Electric vertical takeoff and landing aircraft are designed to transport passengers autonomously or with minimal human intervention. Several companies are working on prototypes and concepts for electric aerial taxis.

These are just a few examples of electric unmanned vehicles currently available or under development. The field of unmanned vehicles is rapidly evolving, and new innovations are continuously being introduced.

1.5. Existing and proposed structure of UV's control

The existing control structure [63], [66] of UV, as depicted in Fig. 1.1.
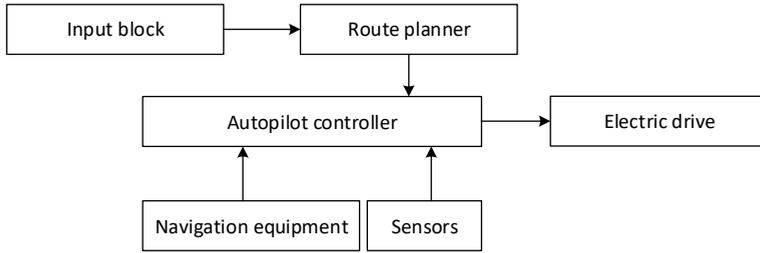
Fig. 1.1. Existing control structure of UV.

The structure of UV's control system consists of an input block, route planner, navigation equipment, sensors, autopilot controller, and electric drive [57]. The input block is used for entering destination points and driving modes. The route planner constructs the movement route from the starting point to the specified coordinates. The navigation equipment determines the vehicle's location. Sensors transmit values of current, voltage, and distance to obstacles along the path. The autopilot analyzes all input data and generates control signals for the electric drive based on a predetermined algorithm [49], [50].

To achieve energy-efficient control, it is proposed to integrate a self-learning optimization controller [61], as investigated in this study, into the existing structure of unmanned transportation control system, between the autopilot controller and the electric drive [41], [48]. The proposed scheme for incorporating the self-learning optimization controller into the existing structure of unmanned transportation control system is depicted in Fig. 1.2. To adapt control signals, an encoder and decoder for control signals may be required.
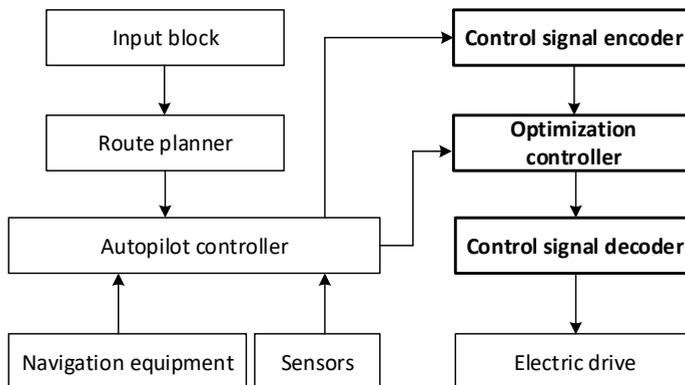
Fig. 1.2. The proposed scheme for integrating the self-learning optimization controller into the existing structure of UVs control system.

Thus, the author proposes to integrate new optimization controller and control signal encoder and decoder into the existing control structure of unmanned vehicles. The existing control structure in general consists of an electric drive, sensors, navigation equipment, input data block, a route planner and an autopilot controller.

Encoder and decoder for control signals components are not considered in this work.

1.6. Structure of the self-learning optimization controller

The structural diagram of the self-learning [64], [67] optimization controller (OC) [70], as depicted in Fig. 1.3.
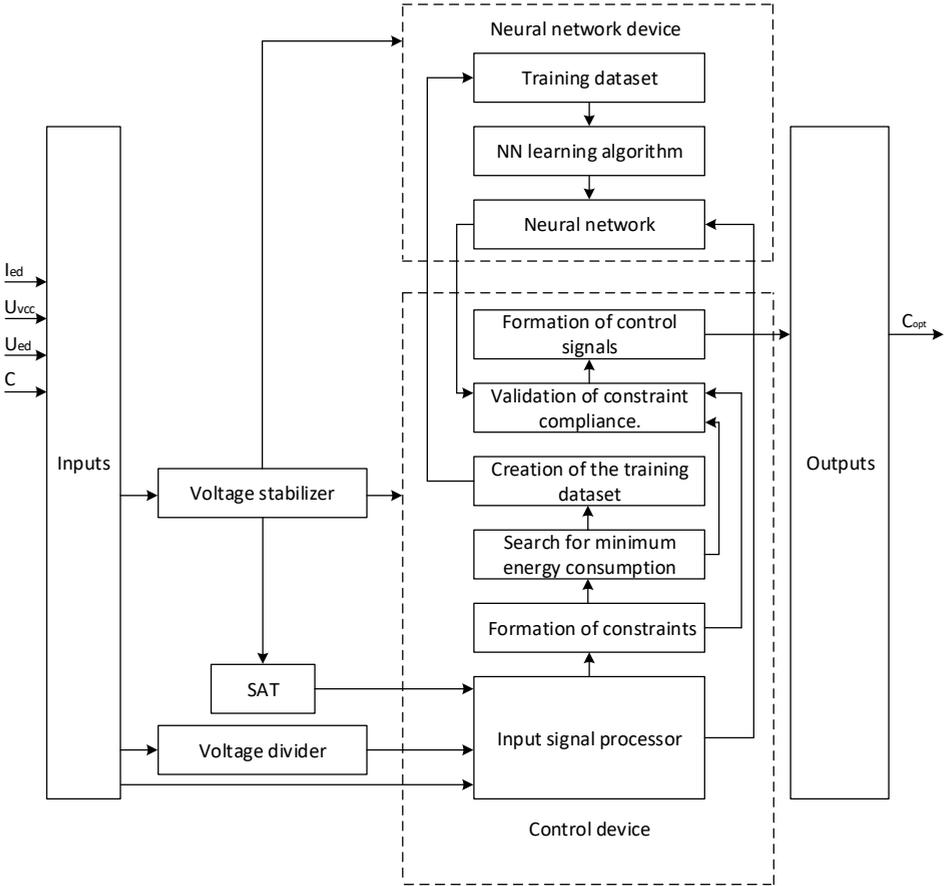
Fig. 1.3. Structural diagram of the self-learning optimization controller.

The structure of the optimization controller consists of inputs, voltage stabilizer, voltage divider, satellite navigation module, neural network (NN) device, control device and outputs. The voltage and current values of the electric drive and control signals are supplied to the input of the optimization microcontroller [56], [57]. The voltage stabilizer powers the neural network device [51] and the control device. The neural network device [78] implements the neural network and the known neural network training algorithm (for example backpropagation

algorithm) and also stores the training dataset. The developed algorithm [79] of the control device includes the algorithm for minimum energy consumption search. For this search known algorithms (for example, uniform search algorithm) may be applied. Additionally the new developed algorithm creates a training data set and generates control signals. The control signals are formed taking into account constraints imposed by safety and other criteria. The optimized control signals are provided at the outputs.

The blocks related to constraints are not considered in this work.

1.7. Influence of the developed method on UV's parameters

In the proposed optimization algorithm, energy efficiency is ensured by finding the minimum energy consumption of the vehicle's electric drive when traveling a given path. Since the engine is an element that converts electrical energy into mechanical energy, in this case the movement of transport, the optimization algorithm has a direct impact on the speed of movement and, as a result, on the travel time. Torque and acceleration change accordingly. Also, with sharp increases in the control signal, there may be current surges in the power circuit. When control signals change, acceleration can change either smoothly or abruptly, which can negatively affect the life of the vehicle's engine or transmission.

Thus, the operation of the optimization algorithm affects the following parameters:

- $M_{e.d.}$ - torque of the electric drive,
- V_{UV} - speed of an unmanned vehicle,
- t_r - travel time,
- a_{UV} - acceleration,
- $I_{e.d.}$ - current in the electric drive circuit.

May influence:

- Motor life
- Transmission resource

If people are being transported, this may affect the comfort of passengers in the vehicle. Therefore, in real conditions, when using an optimization algorithm in vehicles, restrictions on changes in control signals can be introduced to improve safety and reliability.

Some of the parameter limitations for the operation of the optimization controller in real conditions:

- amount of change in control signals per unit of time
- speed limit
- limitation of accelerations.

The developed structure of self-learning optimization controller described in previous chapter has two blocks – formation of constraints and validation of constraints compliance that are responsible to perform this check and do not allow to use control signal out of constraints.

1.8. Electrical diagram of the self-learning optimization controller

Developed electrical diagram [72] of the self-learning optimization controller for optimal energy-efficient control [71], as depicted in Fig. 1.4.
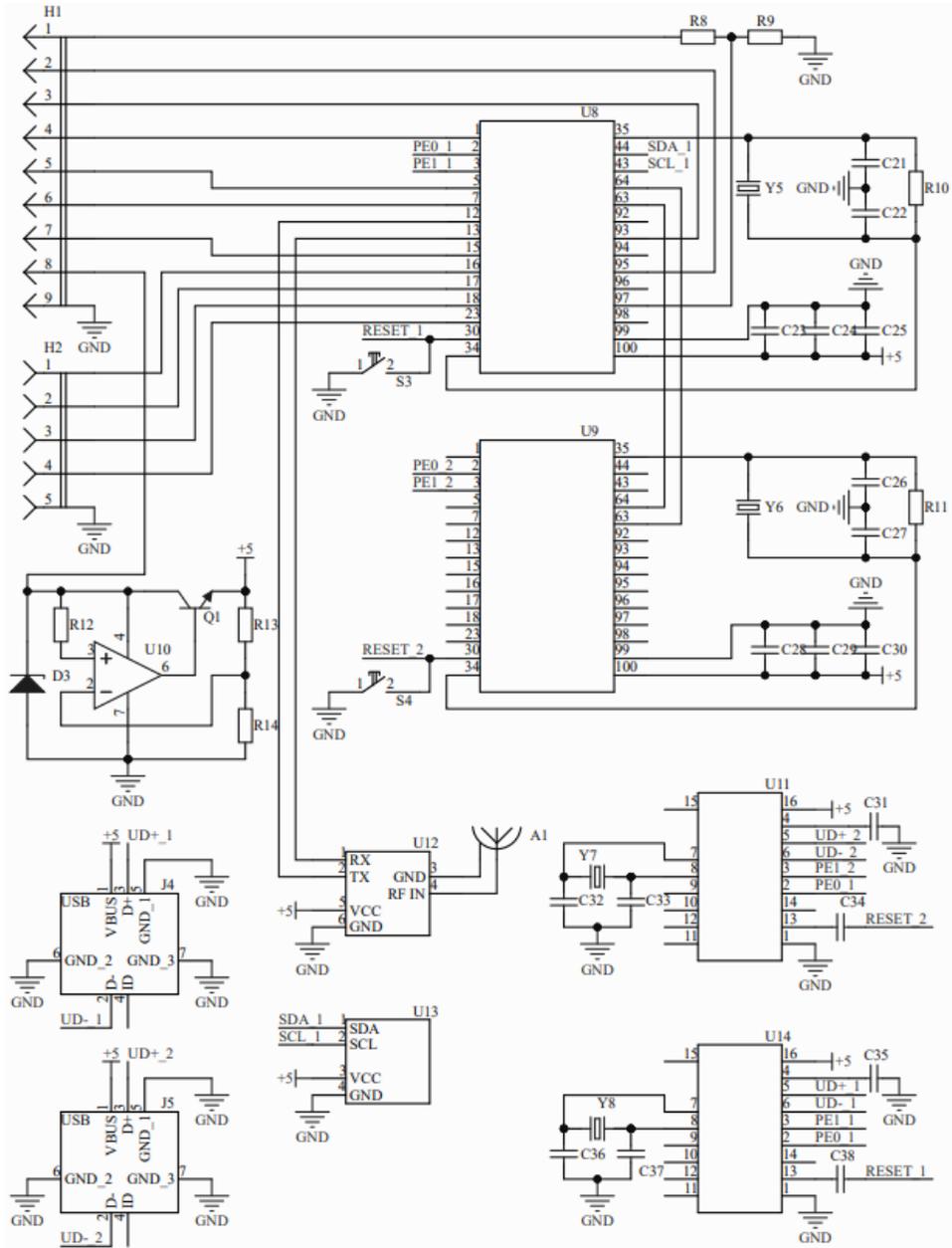
Fig. 1.4. Electrical scheme of the self-learning optimization controller.

In the electrical scheme of a self-learning optimization controller, contact 1 of connector H1 is connected to a voltage divider consisting of resistors R1/R2. Contact number 8 is connected to a voltage stabilizer consisting of microchip U3, diode D1, transistor Q1, and resistors R5-R7. Control signals c_1, c_2, c_3 and c_4 are connected to microcontroller U1 through contacts 2-5. Contacts 6 and 7 receive the current and voltage values of the electric drive, respectively. Outputs 1-4 represent the optimal control signal values c_{1opt}, c_{2opt}, c_{3opt} and c_{opt4}. USB connectors J1 and J2 are used for programming microcontrollers U1 and U2. U4 and U7 are UART/USB protocol converters. U5 is a satellite receiver. U6 is a barometer. S1 and S2 are reset buttons for microcontrollers. Y1, Y2, Y3, and Y4 are quartz crystals for frequency stabilization of the microchips. Capacitors C8, C9, and C10 represent a frequency filter that smoothens power fluctuations.

1.9. Electric motors used in UV's

Brushless DC Motors (BLDC) [42]: Brushless DC motors are commonly used in electric UAV's. They offer high power-to-weight ratios, efficiency, and reliability. These motors use electronic commutation instead of brushes, resulting in less maintenance and longer lifespan. BLDC motors are available in various sizes and can be customized for different UAV applications. Used in electric Unmanned Aerial Vehicle (UAV's), Electric Unmanned Surface Vehicles (USV's), Unmanned Underwater Vehicles (UUV's), Electric Unmanned Ground Vehicles (UGV's), Electric Unmanned Aerial Taxis.

Coreless Motors: Coreless motors are another type of electric motor used in small and lightweight UAV's, such as micro-drones or nano-drones. These motors have a rotor without an iron core, which reduces weight and inertia. Coreless motors are known for their compact size, high-speed capabilities, and low vibration levels. Used in UAV's.

Permanent Magnet Synchronous Motors (PMSM): PMSM motors are widely used in electric autonomous vehicles. They offer high efficiency, high torque density, and precise control. These motors use permanent magnets on the rotor and are controlled by an inverter to achieve the desired speed and torque. PMSM motors are known for their smooth operation and good power-to-weight ratio. Used in in electric autonomous cars, USV's, UUV's, UGV's, Unmanned Aerial Taxis.

Induction Motors (IM): Induction motors, also known as asynchronous motors, are another type of electric motor used in autonomous vehicles. They are relatively simple and robust, making them a popular choice. Induction motors do not require permanent magnets on the rotor and can operate with high reliability. However, they typically have slightly lower efficiency compared to PMSM motors. Used in electric autonomous cars, USV's, UUV's, UGV's and Unmanned Aerial Taxis.

Switched Reluctance Motors (SRM): Switched reluctance motors are gaining attention in the electric vehicle industry, including autonomous vehicles. SRM motors offer high torque density, good efficiency, and cost advantages. They have a simple structure and use the principle of magnetic reluctance to generate torque. SRM motors are known for their robustness and potential for improved efficiency at high speeds. Used in electric autonomous cars.

Linear Motors: Linear motors are utilized in some Electric UGV's, especially those with special locomotion requirements. Linear motors produce linear motion directly without the need for mechanical transmission systems like gears or belts. They can provide high acceleration, precise positioning, and simplified drivetrain designs.

1.9.1. Structure and control of a brushless direct current motor

A brushless motor consists of an external rotor with permanent magnets and a stator with windings [88]. The voltage from the controller is supplied to the A-B-C windings of the motor. A typical brushless motor has three windings (phases), which can be labeled as A, B, and C. The windings can be connected using either the "star" or "delta" methods (Fig. 1.5). The arrangement of the stator windings and rotor magnets is illustrated in Fig. 1.6.
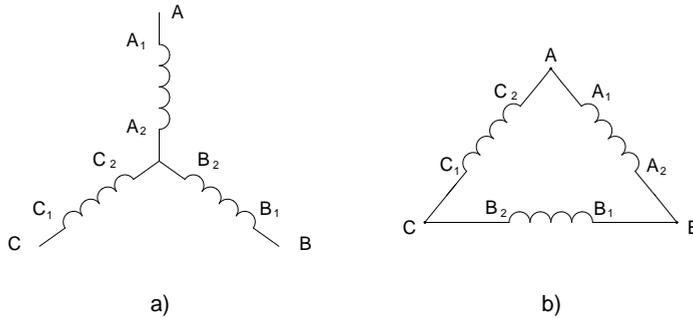
Fig. 1.5. Motor phase connections: a) Star (Y) connection, b) Delta (Δ) connection.
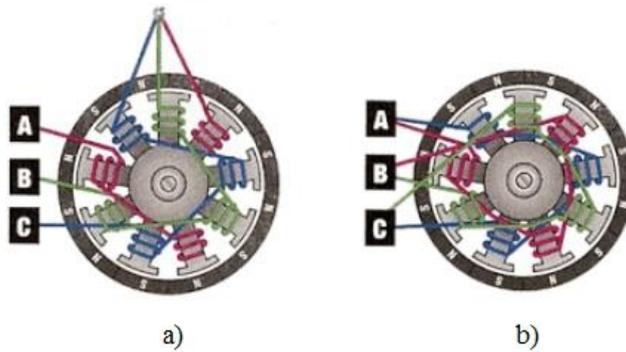
Fig. 1.6. Stator winding and rotor magnet arrangement: a) Star (Y) connection, b) Delta (Δ) connection.

When current is supplied to windings A and B, a magnetic field is created in the windings, which attracts or repels the rotor magnets and causes rotation. As long as the current flows through the winding, the rotor magnet is attracted to the winding (S pole to N pole or N pole to S pole), pulling the rotor and causing it to rotate. When the magnet passes by the winding, the controller opens other switches to repel the rotor magnet (N from N or S from S) and push the magnet further in the rotational direction.

For operation with a constant torque, which is lower than the base speed, the drive control requires information on six discrete states. These correspond to each 60 electrical degrees to deliver power to all three phases of the stator.

Parameters of the electric motor:

U_{dz} – voltage of the electric motor, V;

$I_{dz\,max}$ – maximum current, A;

$P_{dz\,max}$ – maximum power, W;

m_{dz} – mass, kg.

The flux distribution in a brushless motor has a trapezoidal shape, making the models of permanent magnet synchronous motors not applicable. Therefore, it is worth representing the mathematical model of a brushless motor in terms of phase variables, taking into account the nonsinusoidal flux distribution.

In the model development, we assume that the harmonics of the induced currents in the rotor due to the stator magnetic field are negligible, as well as magnetic and stray current losses. The motor is considered as a three-phase system, although the model can be defined for any number of phases.

Hence, the induced EMFs e_{as}, e_{bs}, and e_{cs} are assumed to have trapezoidal waveforms. The maximum value of Ep can be defined as follows:

$$E_P = (Blv)N = N(Blr\omega_m) = N\phi_a*\omega_m = \lambda_P*\omega_m \tag{1.1}$$

where N – the number of connected turns per phase in a winding sequence;

v – speed, m/s;

l – length of the winding, m;

r – rotor core diameter, m;

ω_m – angular velocity, rad/s;

ϕ – phase magnetic flux, Wb;

λ_P – maximum magnetic flux linkage between the rotor magnets, V-s;

B – flux density in the magnetic field where the windings are placed, T.

The obtained model of a PMBDC motor is derived by:

$$\begin{bmatrix} v_{as} \\ v_{bs} \\ v_{cs} \end{bmatrix} = \begin{bmatrix} R_s & 0 & 0 \\ 0 & R_s & 0 \\ 0 & 0 & R_s \end{bmatrix}\begin{bmatrix} i_{as} \\ i_{bs} \\ i_{cs} \end{bmatrix} + \begin{bmatrix} L-M & 0 & 0 \\ 0 & L-M & 0 \\ 0 & 0 & L-M \end{bmatrix} P\begin{bmatrix} i_{as} \\ i_{bs} \\ i_{cs} \end{bmatrix} + \begin{bmatrix} e_{as} \\ e_{bs} \\ e_{cs} \end{bmatrix}, \tag{1.2}$$

where $R_s = R_{as} = R_{bs} = R_{cs}$ – stator resistance for each phase, Ω;

$L = L_{aa} = L_{bb} = L_{cc}$ – self-inductance of each phase, H;

$M = L_{ab} = L_{ac} = L_{ba} = L_{ca} = L_{bc} = L_{cb}$ - mutual inductance between phases, H;

i_{as}, i_{bs}, i_{cs} – stator phase currents, A;

e_{as}, e_{bs}, e_{cs} – stator phase electromotive forces, V.

The electromagnetic torque is defined as:

$$T_e = [e_{as}i_{as} + e_{bs}i_{bs} + e_{cs}i_{cs}]\frac{1}{\omega_m}N*M, \tag{1.3}$$

The formula for the instantaneous induced electromotive force (EMF) is as follows:

$$e_{as} = f_{as}(\theta_r)\lambda_P\omega_m, \tag{1.4}$$

$$e_{bs} = f_{bs}(\theta_r)\lambda_P\omega_m, \tag{1.5}$$

$$e_{cs} = f_{cs}(\theta_r)\lambda_P\omega_m \tag{1.6}$$

Where the functions represent $f_{as}(\theta_r)$, $f_{bs}(\theta_r)$ un $f_{cs}(\theta_r)$ has the same form, as e_{as}, e_{bs} and e_{cs} with the maximum module ± 1.

The induced EMFs do not have sharp corners but have rounded edges. This is because the EMFs are derivatives of flux linkages, and the linkage lines are continuous functions that form curved curves without discontinuities.

The electromagnetic torque can be expressed as:

$$T_e = \lambda_P[f_{as}(\theta_r)i_{as} + f_{bs}(\theta_r)i_{bs} + f_{cs}(\theta_r)i_{cs}]\frac{1}{\omega_m}N*M, \tag{1.7}$$

where θ_r – is rotor position, rad.

Therefore, the rotational differential equation of the PMBDC motor is as follows:

$$J\frac{d\omega_m}{dt} = T_e - T_l - B\omega_m, \tag{1.8}$$

where J – moment of inertia, Nm;

T_l – load torque, Nm.

By combining all the relevant equations, the system in state space representation appears as follows:

$$\dot{x} = Ax + Bu \tag{1.9}$$

where

$$x = [i_{as}i_{bs}i_{cs}\omega_m\theta_r]^t \tag{1.10}$$

$$A = \begin{bmatrix} -\frac{R_s}{L_1} & 0 & 0 & \frac{\lambda_P}{L}f_{as}(\theta_r) & 0 \\ 0 & -\frac{R_s}{L_1} & 0 & \frac{\lambda_P}{L}f_{bs}(\theta_r) & 0 \\ 0 & 0 & -\frac{R_s}{L_1} & \frac{\lambda_P}{L}f_{cs}(\theta_r) & 0 \\ \frac{\lambda_P}{J}f_{as}(\theta_r) & \frac{\lambda_P}{J}f_{bs}(\theta_r) & \frac{\lambda_P}{J}f_{cs}(\theta_r) & -\frac{B}{J} & 0 \\ 0 & 0 & 0 & \frac{P}{2} & 0 \end{bmatrix} \tag{1.11}$$

$$B = \begin{bmatrix} \frac{1}{L_1} & 0 & 0 & 0 \\ 0 & \frac{1}{L_1} & 0 & 0 \\ 0 & 0 & \frac{1}{L_1} & 0 \\ 0 & 0 & 0 & -\frac{1}{J} \\ 0 & 0 & 0 & 0 \end{bmatrix} \tag{1.12}$$

$$L_1 = L - M \tag{1.13}$$

$$u = [v_{as}v_{bs}v_{cs}T_1]^t \tag{1.14}$$

The variable θ_r is necessary to define the functions $f_{as}(\theta_r)$, $f_{bs}(\theta_r)$, and $f_{cs}(\theta_r)$, which can be implemented using a lookup table [42].

Control of a brushless DC motor

One of the main reasons for using permanent magnet brushless DC motors is their simple controllability. To detect currents and communicate with the motor phases, it is necessary to track the beginning and end of the flat induced electromotive force (EMF) region. This constitutes only six discrete positions for a three-phase machine in each electrical cycle. These signals can be conveniently generated with three Hall effect sensors, each offset from the others by 120 electrical degrees. The Hall effect sensors are positioned with a small magnetic wheel attached to the rotor. The number of poles on this wheel is equal to the number of poles on the rotor and is used for rotor positioning. This configuration tracks the absolute position of the rotor magnets and thus defines the shape and state of the induced EMF in all machine phases. A simplified diagram of the control of a brushless DC motor is shown in Fig. 1.7.
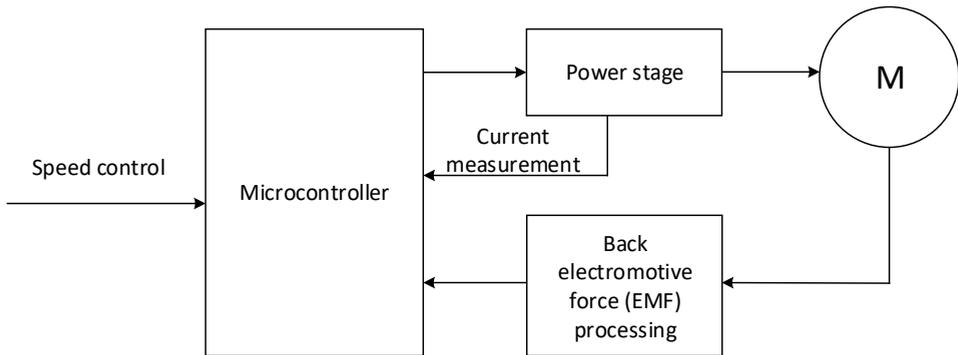
Fig. 1.7. A simplified diagram of the control of a brushless DC motor.

The power stage consists of three standard half-bridges, which are commonly used for controlling three-phase motors. The switches of the half-bridges are typically implemented using transistors or other semiconductor devices operating in a switching mode. The individual phase current commands of the stator are generated based on the current magnitude command and the absolute rotor position. These commands are amplified by the inverter and compared to the respective phase currents of the stator. In a balanced three-phase system, only two phases are necessary to calculate the current of the third phase since the sum of all three currents is zero. The current errors are amplified and utilized with pulse width modulation or hysteresis logic to generate logical switching signals for the inverter switches.

Therefore, knowing the rotor position is necessary for opening and closing the controller's switches. This can be done using Hall effect sensors, as defined earlier. However, sensorless controllers have gained widespread use, which utilizes a unique rotor position algorithm to determine the rotor position. Since the controller uses only two phases at any given time, the third phase is completely disabled. The rotating magnetic field induces an electromotive force (EMF) in the third winding. By measuring and analyzing this voltage, the position of the magnet can be determined, and the moment to close the current switch pair and open the next switch pair can be found.

The brush DC motor is a type of electric motor that utilizes a constant magnetic field to convert electrical energy into mechanical energy. The principle of operation of a brush DC motor is based on Faraday's law of electromagnetic induction and the interaction between conductors carrying current and a magnetic field (Lorentz forces).`

The main components of a brushed DC motor are:

- Stator: The stationary part of the motor that contains permanent magnets or windings to create a magnetic field.
- Rotor (armature): The rotating part of the motor with windings through which the electric current flows.
- Commutator: A cylindrical element that facilitates the current commutation between the stator and the rotor.
- Brushes: Elements that provide contact between the commutator and the external circuit.

During the operation of the engine, its rotor rotates within a magnetic field. Therefore, during rotation, an electromotive force (EMF) E_a is induced, the direction of which is determined by the right-hand rule. This EMF E_a in the engine is directed opposite to the direction of the armature current I_a, and therefore, it is often referred to as the back-EMF or counter-EMF.

Voltage drop in the circuit resistance
$$U = E_a + I_a \sum R. \tag{1.15}$$
From the expression (1.15.) we obtain
$$I_a = \frac{U - E_a}{\sum R}. \tag{1.16}$$

Than
$$E_a * I_a = M\omega = P_{em}, \tag{1.17}$$
where $\omega = 2\pi n/60$ – armature angular rotational frequency;

P_{em} – engine electromechanical power.
The dynamic torque M_D, which arises due to changes in the rotational frequency of the shaft, is determined by the formula:
$$M_D = J\frac{d\omega}{dt}, \tag{1.16}$$
where J – the total moment of inertia of all rotating parts.
The equation for the torque of a direct current motor [77] is as follows:
$$M = M_0 + M_2 \pm M_D. \tag{1.17}$$

Control of a brushed DC motor

The main parameter determining the mechanical characteristics of an electric motor is its rotational speed. Speed control of a brushed direct current (DC) motor can be achieved by changing the voltage across the armature windings or the current strength flowing through the windings.

When voltage control is used, the motor's speed can be altered by changing the voltage across the armature windings. When current control is employed, the strength of the current flowing through the windings is regulated to change the motor's rotational speed.

Both methods have their advantages and disadvantages. Voltage control provides higher efficiency and simpler implementation, but it has the drawback of a reduction in torque when speed is lowered. Current control provides higher torque at low speeds, but it involves a more complex circuitry and lower efficiency.

1.10. Conclusions on the first chapter

The first part of the doctoral thesis describes the control structures and elements as follows:

- An overview is provided of existing types of unmanned vehicles.
- The existing types of unmanned vehicles with the distribution of electric motors commonly used in these vehicles are described.
- The structure of the existing control system for unmanned vehicles is explained.
- A control structure for optimizing energy consumption in unmanned vehicles is developed, incorporating the proposed optimization controller.
- A structure for a self-learning optimization controller with a neural network is designed for achieving optimal energy consumption in electric unmanned vehicles.
- The types of electric motors used in unmanned vehicles are described, highlighting their distribution across different types of vehicles.

To optimize the energy consumption of electric unmanned vehicles, a self-learning optimization controller is integrated into their existing control system.

The minimum number of control signals for a vehicle with one degree of freedom is one, while for a vehicle with six degrees of freedom, it is four.

For controlling any unmanned vehicle, four control signals for motion are sufficient.

2. MATHEMATICAL MODELS FOR THE SELF-LEARNING OPTIMAL CONTROL SYSTEM

2.1. Description of the situation

In the second chapter of the doctoral thesis, mathematical models are developed for the described control structure of unmanned vehicles. A target function is defined for formulating the problem of optimal energy consumption. For motion modeling and computer simulation, a spatial model of the unmanned vehicle (UV), a mathematical model for motion simulation of the UV, and a mechanical model of the UV are constructed.

A mathematical model of a neural network is presented for the self-learning optimization controller of an electric unmanned vehicle.

2.2. The spatial model of vehicles

The UV with 6 degrees of freedom moves relative to an inertial reference frame fixed to the Earth, with coordinate axes Ox, Oy, and Oz. The Oz axis is directed opposite to the gravitational force vector. The UV has its own coordinate system with the center O located at the center of mass of the vehicle, and the Oxy, Oyz, and Ozy axes are parallel and co-aligned with the axes of the fixed reference frame. The angular position of the vehicle is defined by three angles: φ (roll, rotation around the Oxz axis), θ (pitch, rotation around the Oxy axis), and ψ (yaw, rotation around the Ozy axis), which respectively determine rotations around the axes. The coordinate system of the UV position is depicted in Fig. 2.1.
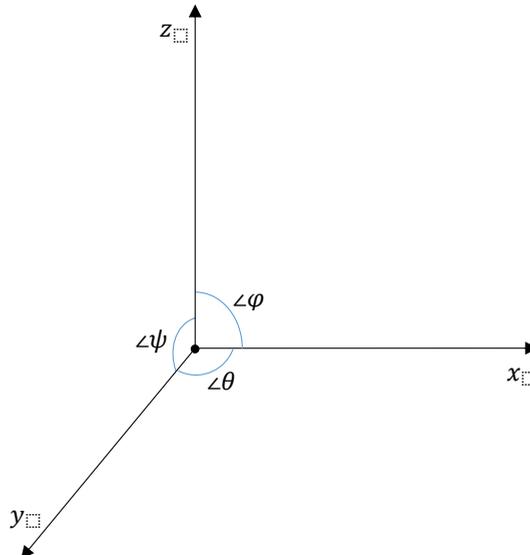
Fig. 2.1. The coordinate system of the UV position.

x , y , z – main axes direction of movement.
∠φ, ∠θ, ∠ψ – vehicle position angles relative to coordinates.

Signals of control required for movement in 3-dimensional space:

c_1 – a roll (aileron) control signal level;

c_2 – a pitch (elevator) control signal level;

c_3 – a throttle control signal level;

c_4 – a yaw (rudder) control signal level.

We assume that the motion occurs in the xy, xz, and yz planes. The angles $\angle\varphi$, $\angle\theta$, and $\angle\psi$ are formed by displacements in these planes. To control any transportation vehicle, four control signals are sufficient. Thus, the minimum number of control signals for a train is one, while the maximum number is four for a multirotor aircraft with variable-pitch propellers.

2.3. Definition of the target function

The primary criterion of the target function is UV energy consumption minimisation, which in general form is represented as the following equation:

$$E = f_1(C, Q) \to \min \tag{2.1}$$

The secondary criterion is a minimisation of the manoeuvre time that should be minimal in case when the primary criterion is satisfied, i.e., if more than one solution exists with the same minimal energy consumption, then manoeuvre with the shortest time should be selected:

$$\tau = f_2(C) \to \min, \tag{2.2}$$

where E – electrical energy consumption for the manoeuvre completion, Ws;

C – a set of adaptive control parameters, i.e., $C = (c_1, c_2, c_3, c_4)$;

Q – an uncontrollable parameter set, internal, external and environmental impacts;

τ – time spent for manoeuvre, s.

Start parameters: $c_1 = 0$, $c_2 = 0$, $c_3 = 0$, $c_4 = 0$, $az(R)\ 0°$, $targ = 0 + n°$.

$$\begin{cases} E_v = \int I \cdot U \cdot dt = f(c_1, c_2, c_3, c_4, t) \to min \\ |az(c_4) - targ| \to 0 \\ |x(c_1, c_2) - x_M| \to 0 \\ |y(c_1, c_2) - y_M| \to 0 \\ |z(c_3) - z_M| \to 0 \\ c_{1min} \leq c_1 \leq c_{1max} \\ c_{2min} \leq c_2 \leq c_{2max} \\ c_{3min} \leq c_3 \leq c_{3max} \\ c_{4min} \leq c_4 \leq c_{4max} \end{cases} \tag{2.3}$$

In the present research, the manoeuvre means the achievement of the target point M (x_M, y_M, z_M) from the current UV location S (x_0, y_0, z_0), within the condition:

$$\begin{cases} |x_M - x_0| \leq \varepsilon_X \\ |y_M - y_0| \leq \varepsilon_Y, \\ |z_M - z_0| \leq \varepsilon_Z \end{cases} \tag{2.4}$$

where $\varepsilon_X, \varepsilon_Y, \varepsilon_Z$ – an acceptable precision by O_x, O_y, O_z axes.

2.4. The definition of the power consumption function

The total electricity consumption [65] of the UV can be determined as follows:
$$E = \int_0^\tau u(t, c(t)) \cdot i(t, c(t)) \cdot dt = E_v + E_p. \tag{2.5}$$
Energy consumption of UV in continuous form is the following:
$$E_v = \int_0^\tau \sum_{j=1}^N u_j(t, c(t)) \cdot i_j(t, c(t)) \cdot dt. \tag{2.6}$$
The electricity consumption of other equipment can be determined as follows:
$$E_p = E - E_v, \tag{2.7}$$

where E – total energy consumption expenditure during maneuver, Ws;

E_v – consumed energy by traction drives for manoeuvre, Ws;

E_p – energy consumed by other electrical equipment for the maneuvere, Ws;

t – momentary time values, s;

$c(t)$ – a set of momentary control signal values, μs;

N – a number of UV traction drives (traction motor and electronic speed controllers);

j – an index of UV traction drive;

$u_j(t)$ – a momentary voltage value of j-th traction drive, V;

$i_j(t)$ – a momentary current value of j-th traction drive, A;

$u(t)$ – The battery voltage of the UV at time t, V;

$i(t)$ – The battery current of the BTS at time t, A.

In discrete [91] form, the energy consumption of UV can be determined as follows:
$$E = \sum_{t=0}^\tau P_t dt = \sum_{t=0}^\tau (u_t * i_t) dt / 3600, \tag{2.8}$$

where dt – discrete time step, in seconds, s;

P_t – instantaneous power, Wh;

u_t – measured voltage, V;

i_t – measured current, A.

When solving the problem, we assume that the design and equipment of the UV comply with the conditions of electrical equipment coordination:

– The output voltage of the battery pack and the maximum output current correspond to the current and voltage of traction motors and electronic speed controllers.

– The maximum values of peak and continuous current for electronic speed controllers correspond to the current of traction motors.

2.5. Mathematical model for simulating the motion of an UV

This part of the work is intended to create a mathematical model of the UV, which will allow calculating optimal control parameters S under uncertain conditions Q.
Therefore, it is necessary to first determine the parameters that can be obtained from the sensors of the UV.
These parameters are available, and the sensors are correctly calibrated:

– a set of parameters that need to be obtained from the accelerometer sensor
$$a = (a_x, a_y, a_z)$$

- o a_x - acceleration in the X-axis direction
- o a_y - acceleration in the Y-axis direction
- o a_z - acceleration in the Z-axis direction
- – the set of parameters obtained from a gyroscope $g = (g_x, g_y, g_z)$:
  - o g_x – angular acceleration in the X-axis direction
  - o g_y – angular acceleration in the Y-axis direction
  - o g_z – angular acceleration in the Z-axis direction
- – the set of parameters obtained from a magnetometer $m = (m_x, m_y, m_z)$
  - o m_x – the projection of the Earth's magnetic field onto the X-axis.
  - o m_y – the projection of the Earth's magnetic field onto the Y-axis.
  - o m_z – The projection of the Earth's magnetic field onto the Z-axis.
- – The parameter obtained from a barometric altimeter:
  - o h – altitude
- – The set of parameters that need to be obtained from a satellite navigation module $SAT = (\chi, \psi, \zeta, v, L, r, \dots)$
  - o χ - geographic latitude
  - o ψ - geographic longitude
  - o ζ - altitude above sea level, calculated using the WGS84 model of the Earth's ellipsoid (geoid)
  - o v – velocity of movement
  - o L – real-time in UTC format
  - o r – direction of movement (available only while in motion)

Thrust or lift force UV can be obtained from a functional dependency:
$$F_v = f_3(\omega_1, \dots, \omega_N), \tag{2.9}$$
where ω_i – i - th rotational speed of the motor, rad/s.

In turn, the rotational speed of each i-th engine is functionally dependent on the control signals C:
$$\omega_i = f_4(C). \tag{2.10}$$

Thus, the thrust force also has a functional dependency on the control signals C:
$$F_v = f_5(C). \tag{2.11}$$

2.6. Development of a mathematical model for calculating the motion of an UV

In this section, a mathematical model for the motion of the UV is being created. It will allow simulating its movement in space and calculating the energy consumption.

The model is based on the fundamental law of classical mechanics, actually Newton's second law of motion:
$$F_{vil} - F_{gr} - F_{ga} = m * a, \tag{2.12}$$
where F_{vil} – UV resultant force, N;

F_{ga} – resistance force, N;

F_{gr} – gravity force, N;

m – UV mass, kg;

a – UV acceleration, m/s2.

Figure 2.2 shows the vectors of these forces.
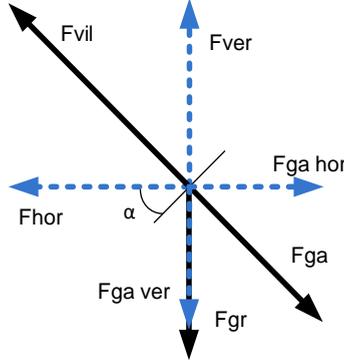
Fig. 2.2. Forces acting on the UV.

Distribution of forces into vertical and horizontal components.:

- F_{ver} – vertical lift force of the UV, N;
- F_{hor} – Horizontal lift force of the UV, N.

$$F_{ga} = \rho \cdot C_D \cdot A_{eff} \cdot v^2.$$ (2.13)

$$F_{gr} = m \cdot g_0$$ (2.14)

UV acceleration is calculated from the force equation:

$$a = \frac{F_{vil} - F_{gr} - F_{ga}}{m}.$$ (2.15)

UV velocity:

$$v = \int_0^\tau a \, dt.$$ (2.16)

UV distance:

$$s = \int_0^\tau v \, dt.$$ (2.17)

Mechanical power (instantaneous):

$$N_{(t)} = F_t \cdot v(t).$$ (2.18)

The following functional dependencies are defined for UV velocity limits:

Max vertical velocity [43]:

$$V_{ver} = \sqrt{\frac{2*m*g_0}{\rho*C_D*A_{eff}}} * \sqrt{(FR - 1)}.$$ (2.19)

Max horizontal velocity:

$$V_{hor} = \sqrt[4]{1 - \frac{1}{FR^2}} * \sqrt{\frac{2*m*g_0}{\rho*C_D*A_{eff}}}$$ (2.20)

$$FR = \frac{F}{m*g_0},$$ (2.21)

where F – motor summary traction power, N;

g_0 – gravity acceleration value 9.81 m/s^2;

C_D – aerodynamic flow factor;

A_{eff} – UV effective area, m^2;

ρ – air density, кg/m³.

Mechanical work:
$$A = \int_0^\tau \quad N \cdot dt/3600. \tag{2.22}$$

Power consumption:
$$P = U{\cdot}I. \tag{2.23}$$

Torque on the motor shaft:
$$M_{sl} = 9950\frac{P}{n}. \tag{2.24}$$

Consumed energy from source:
$$E = \int_0^\tau \quad Pdt/3600. \tag{2.25}$$

2.7. Electromechanical models of electric unmanned vehicles

Mechanical model [54], [59] of the UV defined by following parameters:
- m – mass of UV, kg;
- $A^{hor}{}_{eff}$ – area of the UV in horizontal plane, m^2;
- $A^{ver}{}_{eff}$ – area of the UV in horizontal plane, m^2;
- F_t – summarized traction force, N;
- x, y, z – translational position in the space, where z is vertical axis, m;
- φ, θ, ψ – angles of UV rotational position in the space, rad;
- a_{ver} – vertical acceleration of the UV, m/s^2
- a_{hor} – horizontal acceleration of the UV, m/s^2
- v_{ver} – vertical speed of the UV, m/s;
- v_{hor} – horizontal speed of the UV, m/s.

Battery parameters:
- C_{bat} – capacity of the battery, Ah;
- I_{bat} – relative maximal current, A;
- N_{bat} – number of battery cells;
- U_0 – battery momentary voltage without load, V.

Motor drive control parameter:
- $PW = \{PW_1 \ ... \ PW_n\}$ – set of pulse widths for each motor, μs.

Motor parameters:
- P_{nom} – nominal power, W;
- $F^j{}_t$ – traction force of each j-th motor, N;
- $I^j(U_{unload}, F^j{}_t)$ – momentary current of j-th motor with given traction force, A;
- $P^j(U_{unload}, F^j{}_t)$ – momentary power of j-th motor with given traction force, W;
- $U^j{}_{load} = P^j/I^j$ - momentary voltage of j-th motor with given traction force, V.

Approximated functions for motor current and power in a following form of second-order polynomial by obtaining empirical data:

$$I^j\left(U_0, F_t^j\right) = \alpha_i(U_0) \cdot \left(F_t^j\right)^2 + \beta_i(U_0) \cdot F_t^j + \gamma_i(U_0) \tag{2.26}$$

$$P^j\left(U_0, F_t^j\right) = \alpha_p(U_0) \cdot \left(F_t^j\right)^2 + \beta_p(U_0) \cdot F_t^j + \gamma_p(U_0). \tag{2.27}$$

where each coefficient is a linear function:

$$\alpha_i(U_0) = k \cdot U_{unload} + \delta_i^\alpha; \tag{2.28}$$

$$\beta_i(U_0) = \kappa_i^\beta \cdot U_{unload} + \delta_i^\beta \tag{2.29}$$

$$\gamma_i(U_0) = \kappa_i^\gamma \cdot U_{unload} + \delta_i^\gamma \tag{2.30}$$

$$\alpha_p(U_0) = k_p^\alpha \cdot U_{unload} + \delta_p^\alpha \tag{2.31}$$

$$\beta_p(U_0) = \kappa_p^\beta \cdot U_{unload} + \delta_p^\beta \tag{2.32}$$

$$\gamma_p(U_0) = \kappa_p^\gamma \cdot U_{unload} + \delta_p^\gamma. \tag{2.33}$$

For UV movement simulation forces are calculated by following equations:

$$F_t = \sum_{j=1}^n F_t^j \tag{2.34}$$

$$F_z = F_{ver} = F_t \cdot \cos\varphi \cos\theta \tag{2.35}$$

$$F_{hor} = \sqrt{(F_t)^2 - (F_{ver})^2} \tag{2.36}$$

$$F_x = F_{hor} \cdot \cos\psi \sin\varphi \cos\theta + \sin\psi \sin\theta \tag{2.37}$$

$$F_y = F_{hor} \cdot \sin\psi \sin\varphi \cos\theta - \cos\psi \sin\theta \tag{2.38}$$

$$F_g = m \cdot g \tag{2.39}$$

$$F_{res}^{ver} = \rho \cdot c_d \cdot A_{eff}^{ver} \cdot (v_{ver})^2 \tag{2.40}$$

$$F_{res}^{hor} = \rho \cdot c_d \cdot A_{eff}^{hor} \cdot (v_{hor})^2, \tag{2.41}$$

where $g = 9.81$ – Earth gravity constant, m/s^2;
$\rho = 1.2255$ – air density assumed as a constant, kg/m^3.

For UV hovering following condition should be satisfied:

$$F_{ver} = F_g, F_{hor} = 0. \tag{2.42}$$

For UV vertical lift up the following condition should be satisfied:

$$F_{ver} > F_g, F_{hor} = 0. \tag{2.43}$$

For UV horizontal movement on the constant altitude the following condition should be satisfied:

$$F_{ver} = F_g, F_{hor} > 0. \tag{2.44}$$

Energy consumption in Wh and battery capacity consumption in Ah is calculated by following equations:

$$E_{cons} = \int_0^\tau \left(\sum_{j=1}^n P^j\left(U_0, F_t^j\right)\right) dt \tag{2.45}$$

$$C_{cons} = \int_0^\tau \left(\sum_{j=1}^n \frac{I^j\left(U_0, F_t^j\right)}{3600}\right) dt, \tag{2.46}$$

where τ – monement time.

Mechanical power (instantaneous):

$$N_{(t)} = F_t \cdot v(t). \tag{2.47}$$

Mechanical work:

$$A = \int_0^\tau N \cdot dt / 3600. \tag{2.48}$$

Power consumption:

$$P = U \cdot I. \tag{2.49}$$

Torque on the motor shaft:

$$M_{sl} = 9950 \frac{P}{n}. \tag{2.50}$$

Efficiency of UV:

$$\eta = \frac{\sum A}{\sum E}. \tag{2.51}$$

2.8. Mathematical model of a neural network

2.8.1. Neural network notations

Let's define the following designations in neural network models [60], [92]:

t – time moments;

i,j,k – neural network indices. Neuron j is a neuron in the hidden layer and is located in the layer following layer i, while neuron k is located in the layer following neuron j;

n – iteration corresponding to the n-th training sample;

In(t) – an input signal of m dimensions at time moment t;

$In_i(n)$ – the i-th element of the input vector X(n) in the n-th iteration;

d(t) – scalar system output signal at time moment t;

y(t) – neural network output at time moment t;

e(t) – error, the deviation of the output signal y(t) from the desired signal d(t) at moment t;

$e_j(n)$ – error of neuron j in the n-th iteration;

$d_j(n)$ – target result of j-th neuron;

$y_j(n)$ – functional signal of j-th neuron;

$w_{ji}(n)$ – weight between neuron i-th in the previous layer and neuron j-th in the current layer;

$\varphi_j(y_j(n))$ - correction of the weight between neuron i-th in the previous layer and neuron j-th in the current layer;

b_j – bias of j-th neuron;

$w_{j0} = b_j$ – bias in the form of a weight, with x0 = +1;

$v_j(n)$ – induced local field (weighted sum of all weight-input and bias) of neuron j in the n-th iteration;

$\varphi_j()$ – activation or transfer function of j-th neuron;

E(n) – current sum of squared errors (error energy) in the n-th iteration;

Eav – average error for the entire training set;

∇ – gradient operator;

η – training rate parameter;

k – size of the input layer;

nq – size of the hidden layer;

m – size of the output layer.

2.8.2. Neural network models for optimal control in electric transportation tasks
General mathematical model for a neural network

Each neuron has an input data vector, weights for each input vector element, an activation function, and an output. A neural network typically consists of multiple layers. Each layer can have a defined or undefined number of neurons. Neural networks enable the analysis of an object based on the input parameter vector and determine the object's affiliation to a specific class. This means that neural networks need to be trained in order to determine the object's affiliation to predefined classes. The structure of the self-learning algorithm's neural network is shown in Fig. 2.3.
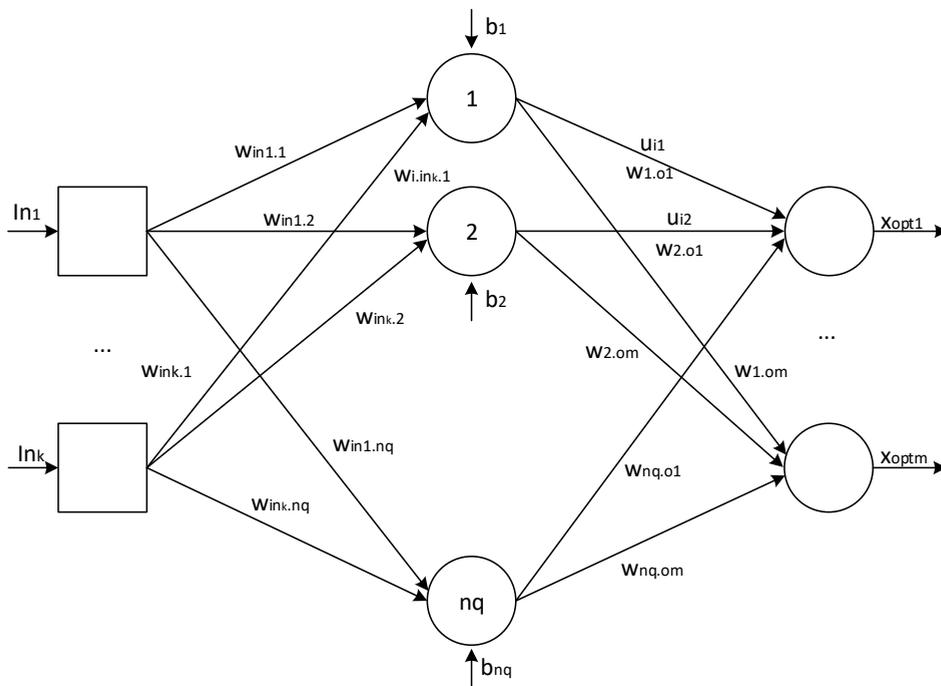
Fig. 2.3. Structure of the self-learning algorithm's neural network.

The mathematical model of a neural network can be defined as follows:
- Neural network input signal vector: $In = \{in_1, in_2, \ldots, in_k\}$;
- Set of neurons in the hidden layer: $P = \{p_1, p_2, \ldots, p_{nq}\}$;
- Neural network output vector: $c_{opt}, = \{c_{opt1}, c_{opt2}, \ldots, c_{optm}\}$;
- Set of weight vectors for each input of the i-th neuron in the j-th layer: $W_i^{\,j} = \{w_{i1}, w_{i2}, \ldots, w_{in}, w_{in}\}$;
- Bias for each i-th neuron in the j-th layer: $b_i^{\,j}$;
- Summation function for each i-th neuron in the j-th layer: $s_i^{\,j} = \sum(W_i^{\,j}*X) + b_i^{\,j}$;
- Activation function for all neurons in the j-th layer: $F^{\,j}(s^{\,j})$.

2.9. Conclusions on the second chapter

The main results and developed mathematical models in the second chapter of the doctoral thesis are as follows:

- Description of the space and motion within it for a UV with a maximum of 6 degrees of freedom.
- Definition of the target function considering two criteria - energy and time.
- Determination of the energy consumption function in continuous and discrete forms.
- Development of a mathematical model for calculating the motion of the UV, enabling the calculation of optimal control parameters under uncertain conditions.
- Development of a mathematical model for the motion of the UV.
- Mathematical model of a neural network for optimal energy-efficient control of electric vehicles, allowing for optimal control of the electric drive.

The developed mathematical models enable the control and simulation of the motion of unmanned vehicles in three-dimensional space.

The designed target function has two criteria. The first criterion is the minimum energy consumption for a given distance traveled. In case of multiple optimal values for the first criterion, the second criterion will be the time required to perform a maneuver or complete a route.

3. ALGORITHMS FOR A SELF-LEARNING OPTIMAL CONTROL SYSTEM

3.1. Description of the situation

In the third chapter of the doctoral thesis, algorithms for optimizing energy consumption based on the developed mathematical models are described.

The optimization algorithm combines existing algorithms for finding the minimum energy consumption and a neural network training algorithm, as well as an algorithm for determining the nature of the load and an algorithm for automatically creating a training set developed by the author. When the vehicle is moving, the minimum search algorithm searches for the minimum value of energy consumption, taking into account the nature of the load, and stores the value of the control signal in the training set. When a lower energy consumption value is found for a certain type of load, the value of the control signal in the training set is replaced. Using the obtained values of the training set, the neural network is trained and retrained. With each new type of load and the minimum value of energy consumption found, the neural network issues control signals that are increasingly closer to the most optimal.

3.2. UV general optimal control algorithms

All the optimal value search methods discussed in the work are based on comparing the values of two target functions and making the corresponding decisions based on the improvement (success) or deterioration (failure) of the target function value.

UV optimal control algorithm [79], [80] in general form:
Step 1. Generation of initial control signal - specify the value of the control signal.
Step 2. Measurement - measure or calculate the value of the target function.
Step 3. Optimization - apply a specific optimization method to make a decision and execute an action for the next value of the control signal.
Step 4. Check for reaching the optimal value - if the optimal value has not been reached, return to step 2 with a new control signal until the optimal control value is achieved, then proceed to step 5.
Step 5. Waiting - after reaching the optimal value, after a certain time, it is necessary to recheck the optimal value because the motion conditions may change, then repeat step 2.

Defining the algorithm in more detail, taking into account the information available from the OC controller and its sensors, the steps of the UV energy consumption minimization algorithm would look as follows:
Step 1. Specify the initial control signal c.
Step 2. Measuring the acceleration a, find the time moment when $a < eps \sim 0$, then set $v = const$. Such a transition process is not taken into account.

Step 3. Save the energy consumption value at the given moment as e_0, time as t_0, and distance as s_0.

Step 4. After a fixed time tf = const, calculate the energy consumption per meter. (Wh/m)
$$de = (e - e_0)/(s - s_0). \tag{3.1}$$

Step 5. If de_1 has not been saved yet, then save $de_1 = de$; otherwise, $de_2 = de$.

Step 6. If de_2 is defined, then proceed to step 7.

Step 7. if $de_2 < de_1$,

    Step 7.1. Then, if the current control signal is better than the previous one and movement occurs in an extreme direction, and according to the chosen optimization method, the next signal c is generated; in case of an unsuccessful attempt.

    Step 7.2. Otherwise, if the current control signal is worse than the previous one and according to the chosen optimization method, the next signal c is generated; in case of an unsuccessful attempt.

Step 8. Check the fulfillment of the condition for reaching the optimal values,

    Step 8.1. If it is completed, then the waiting mode is skipped and the next search for the optimal value will occur after time tg.

    Step 8.2. If the condition is not fulfilled, then proceed to step 2.

There are two groups of optimization methods:
– Deterministic methods: involving defined calculation formulas and parameters.
– Stochastic methods: involving the use of random numbers in the search process.

The work considers two deterministic and two stochastic methods for further testing and suitability for optimal UV control:
– Uniform Search Method (deterministic)
– Halving Method (deterministic)
– Backtracking Method (stochastic)
– Random Search Method (stochastic)

3.3. Uniform search algorithm

Uniform search algorithm [89] is defined for optimization with constraints, and its task is formulated as follows: find the minimum of a one-dimensional unimodal function $\Phi(x)$ defined on a closed interval D = [a, b], $x \epsilon$ [a, b].
$$\min \Phi(X) = \Phi(x^*). \tag{3.2}$$

This algorithm belongs to a group of methods where the main idea is to reduce the uncertainty interval of the search and exclude subintervals from the search process where the point x* does not exist, taking into account the unimodality of the function $\Phi(x)$.

The current interval with uncertainty will be denoted as TIN, and its length is represented by | TIN |. So, if TIN = [a, b], then |TIN| = b - a.

In the uniform search algorithm, attempts are made by uniformly dividing the interval = [a, b] into N equal subintervals.

Among the calculated values of the function $\Phi(x)$, the smallest value is chosen. Assume that this value is at the point x_k. Then, taking into account the unimodality of the function $\Phi(x)$,

the subintervals [a, x_{k-1}] and [x_{k+1}, b] can be excluded from consideration and the new interval chosen is [x_{k-1}, x_{k+1}], (Fig. 3.1). The algorithm refers to passive search methods

In the uniform search algorithm, attempts are made by dividing the interval [a, b] into N equal subintervals.

The minimum value is chosen from the computed values of the function $\Phi(x)$. Let's assume that this value is found at point x_k. Then, considering the unimodality of the function x_k, the subintervals [a, x_{k-1}] and [x_{k+1}, b] can be excluded from consideration, and the new interval [x_{k-1}, x_{k+1}], is selected (Fig. 3.1). The algorithm belongs to passive search methods.
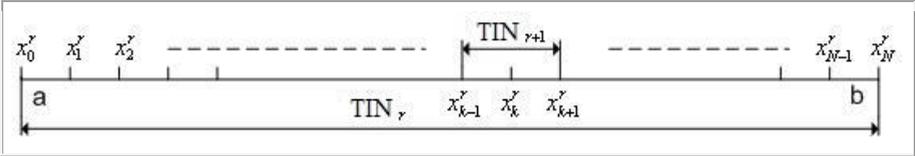
Fig. 3.1. Partitioning of the current interval of uncertainty and defining a new reduced interval.

Any point from the current interval of uncertainty found can be considered as an approximate minimum point x* with equal conditions. The first iteration is shown in Fig. 3.2 in the provided image.
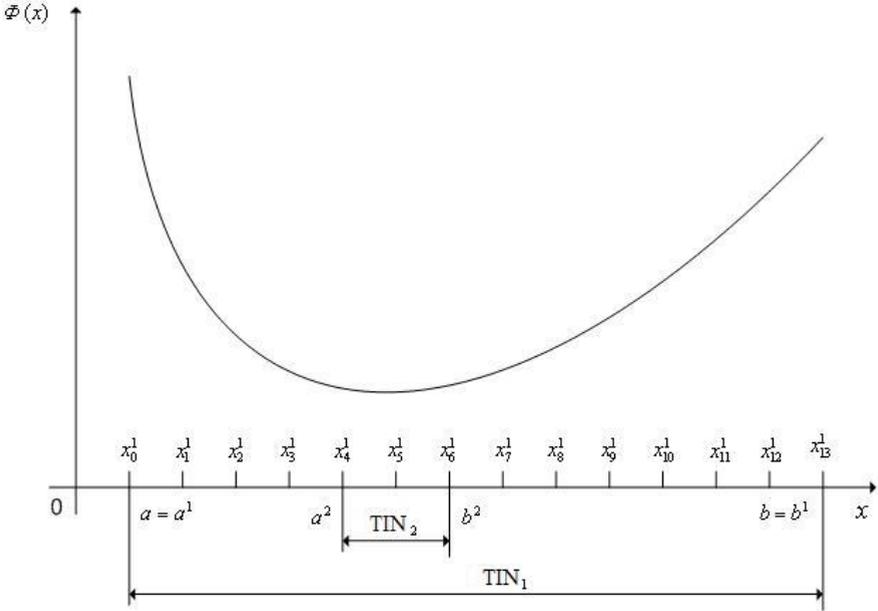
Fig. 3.2. The first iteration of the uniform search algorithm for the unimodal function $\Phi(x)$ with N = 13.

Algorithm adaptation for UV control

Taking into account that a UV needs to be controlled in real-time, it is evident that the algorithm requires real-time modifications.

If the optimized function is unimodal, it is not necessary to perform all N measurements. It is sufficient to determine the direction of finding the minimum and continue real-time measurements with a uniform step $x_k = x_{k1} + virz*dx$ until the moment when the measurement $\Phi(x_k)$ becomes larger than the previous measurement $\Phi(x_{k-1})$, indicating the departure from the minimum point. Then $TIN = [x_{k-1}; x_k]$. If necessary, the step size dx can be reduced, the direction can be changed to – direction, and the search process can be repeated.

3.4. Algorithm with halving method

The halving method [89] is also defined for optimization with conditions, and its task is formulated as follows: find the minimum of a unimodal function $\Phi(x)$ in a closed interval $D = [a, b]$.

In the halving method, also known as the uniform dichotomous search algorithm, attempts are made in pairs. The coordinates of each pair differ from the coordinates of another pair by a certain magnitude.

$$\delta_x < \varepsilon_x, \tag{3.3}$$

where ε_x − the required accuracy of the solution.

An attempt is made within the TIN. After obtaining the values of the function $\Phi(x)$ at these points, a portion of the TIN is excluded from the search due to its unimodality. The size δ_x is determined by the required solution accuracy. The algorithm belongs to the class of sequential search methods.

Mathematically, the algorithm can be described by the following scheme:

Step 1. Performs the assignment $r = 1, a^1 = a, b^1 = b, TIN_1 = [a^1, b^1]$.

Step 2. Calculates the values (Fig. 3.3)

$$x_0^r = \frac{a^r - b^r}{2}, x_1^r = x_0^r - \frac{\delta_x}{2}, x_2^r = x_0^r + \frac{\delta_x}{2}. \tag{3.4}$$

Step 3. Calculates the function $\Phi(x)$ value $\Phi(x_1^r), \Phi(x_2^r)$.

Step 4. If $\Phi(x_1^r) < \Phi(x_2^r)$,

then performs the assignments

$$a^{r+1} = a^r, b^{r+1} = x_0^r, TIN_{r+1} = [a^{r+1}, b^{r+1}] \tag{3.5}$$

otherwise, performs the assignments.

$$a^{r+1} = x_0^r, a^r, b^{r+1} = b^r, TIN_{r+1} = [a^{r+1}, b^{r+1}]. \tag{3.6}$$

Step 5. If $|TIN_{r+1}| \le \varepsilon_x$, then the algorithm ends, otherwise, it continues to execute $r = r + 1$ and go to step 2
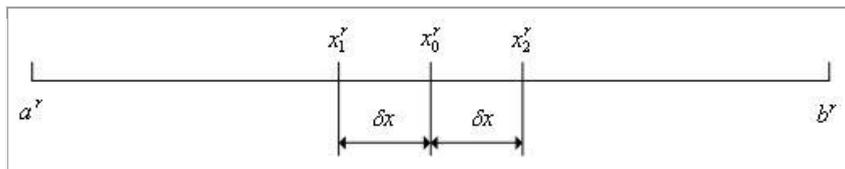
Fig. 3.3. Calculates the values of x^r_0, x^r_1, x^r_2.

Any point from the current uncertainty interval can be accepted as an approximate minimum point x* with equal conditions. The scheme of the uniform dichotomous search algorithm is described in Fig. 3.4.
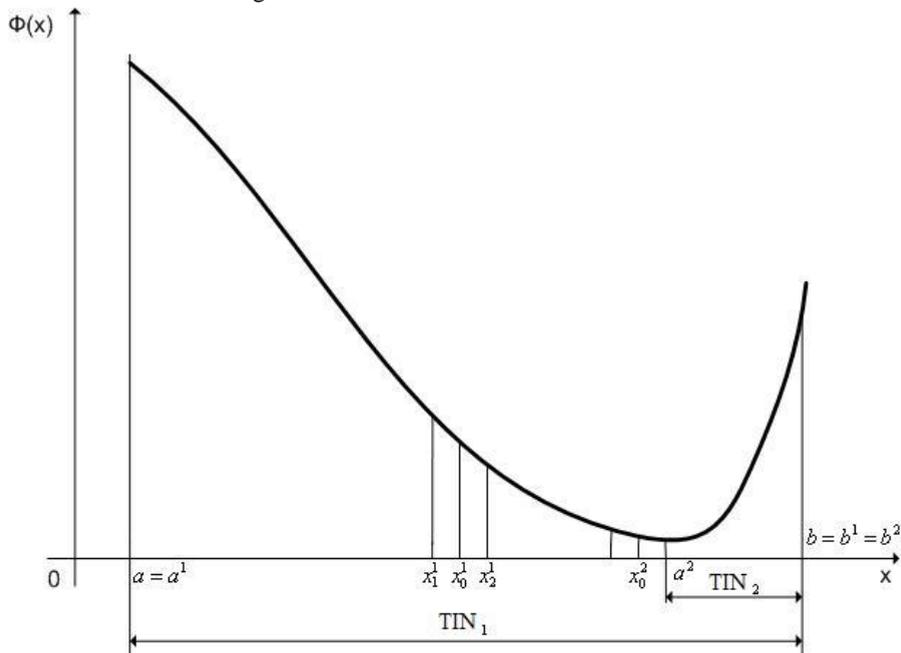
Fig. 3.4. The first two iterations of the search of the one-dimensional unimodal function $\Phi(x)$ with the smooth dichotomous search algorithm.

After each iteration, the TIN decreases twice. Considering that the algorithm requires only two measurements in each iteration, then the algorithm can be adopted as the optimal control of UV.

3.5. Algorithm with backtracking on unsuccessful step

It is useful to use stochastic search methods for multidimensional unconditional optimization: to find the minimum of the optimality criterion $\Phi(x)$, which is defined in the n-dimensional Euclidean space $\mathbb{R}^n$.

For UV control, it is necessary to enter a condition and limit the desired values in the range of allowed control signal values x = <R, P, T, Y>, $x \epsilon \mathbb{R}^4$:

$$min\ \Phi(x) = \Phi(x^*) = \Phi^* \tag{3.7}$$

$$\begin{cases} a_R \geq R \geq b_R \\ a_P \geq P \geq b_P \\ a_T \geq T \geq b_T \\ a_Y \geq Y \geq b_Y \end{cases} \tag{3.8}$$

When solving the task with a return to the failed attempt [89] (one-step optimization method), the iteration formula is used:

$$x^{r+1} = x^r + \lambda^r \frac{\psi^r}{\|\psi^r\|}, \qquad (3.9)$$

where λ^r– the step size of the r-th iteration;

$\Psi^r = (\Psi_1^r, \Psi_2^r, ..., \Psi_n^r)$ – Realization of an n-dimensional random vector;

$\|*\|$ – vector norm (numeric value of a vector).

The actions of the algorithm with return to the failed step are defined as follows:

Step 1. Set the starting point x^0, the starting step length λ^0 and set the iteration counter $r = 0$.

Step 2. Enter the number of failed attempts.

Step 3. Generates realization of random numbers $\psi_1^r, \psi_2^r, ..., \psi_n^r$ – components of the vector x, checks compliance with the constraints of the vector x, and in case of non-compliance repeats the generation, otherwise uses this value as a try point.

Step 4. Calculates the value of the function $\Phi(x)$ at this point.

Step 5. If $\Phi(x^{r+1}) < \Phi(x^r)$, then increments the iteration counter $r = r + 1$ and go to step 3. otherwise go to step 6.

Step 6. Checks the number of attempts made. If k < K, then go to step 3, otherwise go to step 7. K – is the number of failed attempts. Recommended value $K = 3n$.

Step 7. Checks the search completion condition. If it works, then accept that $X^* \approx X^{r+1}$ and completes the algorithm. Otherwise - assume r = r+1, $\lambda^r = \alpha\lambda^r$. Here, $\alpha\epsilon(0,1)$ is the search step reduction factor.

An example of the operation of the method is shown in Fig. 3.5 for the two-dimensional Himmelblau test function. Dotted lines show failed steps
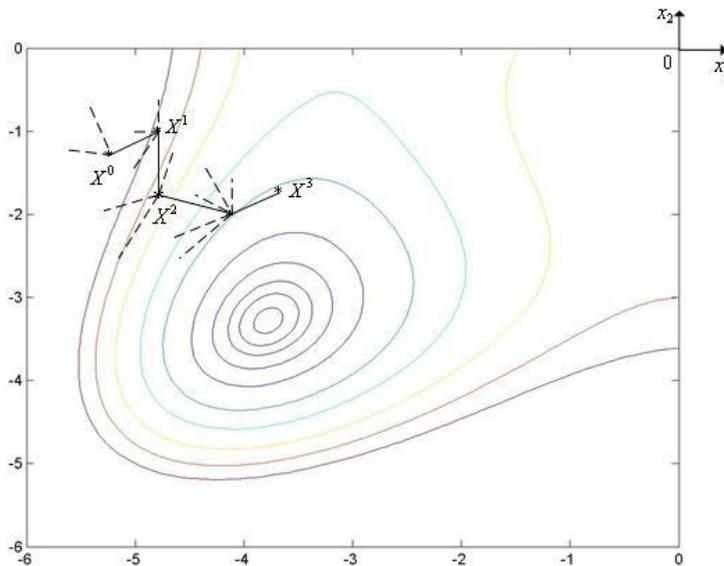
Fig. 3.5. Search trajectory with a back-to-fail search algorithm for the 2-dimensional Himmelblau function.

As a search termination condition, one of the traditional iteration termination conditions can be used:

$$\|\mathbf{X}^{r+1}\text{-}\mathbf{X}^r\|=\lambda^r \le \varepsilon_X, \tag{3.10}$$

where ε_X – required search precision by X;

$$|\Phi(\mathbf{X}^{r+1})\text{-}\Phi(\mathbf{X}^r)| \le \varepsilon_\Phi, \tag{3.11}$$

where ε_Φ – required search precision by Φ.

3.6. Repeated random search algorithm

General repeated random search algorithm

Repeated random search algorithm [89] is also commonly used for multidimensional unconditional optimization: finding the minimum of the optimality criterion $\Phi(x)$ defined in the n-dimensional Euclidean space $\mathbb{R}^n$. But for UV control, it is also necessary to enter conditions and limit the searchable values in the range of allowed control signal values x = <R, P, T, Y>, $x\epsilon\mathbb{R}^4$:

$$min\,\Phi(x) = \Phi(x^*) = \Phi^* \tag{3.12}$$

$$\begin{cases} a_R \ge R \ge b_R \\ a_P \ge P \ge b_P \\ a_T \ge T \ge b_T \\ a_Y \ge Y \ge b_Y \end{cases}. \tag{3.13}$$

This repeated random search method uses an iteration scheme

$$\mathbf{X}^{r+1}=\mathbf{X}^r+\lambda^r\mathbf{\Delta}^r, \tag{3.14}$$

where λ^r – step size in the r-th iteration;

Δ^r – (n x 1) – unit vector, where shows the search direction in the r-th iteration:

$$\mathbf{\Delta}^r=\left[\beta\frac{\mathbf{S}^r}{\|\mathbf{S}^r\|}+(1\text{-}\beta)\frac{\mathbf{P}^r}{\|\mathbf{P}^r\|}\right]. \tag{3.15}$$

where $S^r = \gamma S^{r-1} + (1-\gamma)S^{r-2}$ – the "prehistory" vector that started the average search direction from the previous two steps;

$\|*\|$ – vector norm (numeric value of a vector);

P^n – n-dimensional vector of uniformly distributed random numbers in the interval [0, 1];

$\beta\epsilon$ [0,1] – coefficient, which determined the influence of "prehistory" (determined part) for the choice of the next step;

Δ^r – random component in vector;

$\gamma\epsilon[0,1]$ – coefficient that gives the value of "prehistory" S^{r-1}, S^{r-2} in the vector S^r;

$\frac{S^r}{\|S^r\|}$ – S^r direction vector with length 1;

$\frac{P^r}{\|P^r\|}$ – P^r direction vector with length 1.
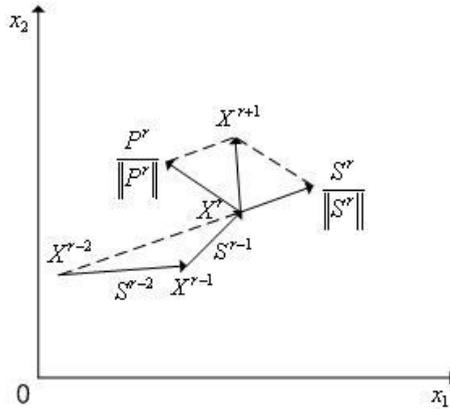
Fig. 3.6. Repeated random search algorithm iteration scheme.

Figure 3.6 show repeated random search algorithm iteration scheme.

A simplified repeated random search algorithm

Step 1. Set the starting point x^0, the starting step λ^2, the values of the coefficients β and γ and assume the iteration counter $r = 2$.

Step 2. With any method, for example, with the one-step best attempt method, the points x^1, x^2 — the acceleration stage of the method were started.

Step 3. Generates an n-dimensional random vector P^r and calculates the value of a point X^{r+1} and $\Phi(X^{r+1})$ at that point.

Step 4. If $\Phi \Phi(x^{r+1}) < \Phi(x^r)$, then the iteration completion condition is checked. If this holds, then $X^* \approx X^{r+1}$ and completes the iterations. If not, then increase the step length $X^* \approx X^{r+1}$, for example, as $\lambda^{r+1} = 2\lambda^r$, assume $r = r + 1$ and proceed to step 3. $\Phi(x^{r+1}) \geq \Phi(x^r)$, then go to step 5.

Step 5. We make attempts from the same point x^r for the specified fixed number of times, trying not to change the step length λ^r to obtain the reduction of the target $\Phi(X)$ only by the random vector P^r, and move to step 3. If these attempts were unsuccessful, then leaving this point X^r reduces the step length λ^r, according to a certain law, for example, $\lambda^r = \dfrac{\lambda^r}{2}$, and goes to the 3rd step.

An example of the operation of the method is demonstrated in Fig. 3.7 for the two-dimensional Himmelblau test function. Dotted lines show failed steps.
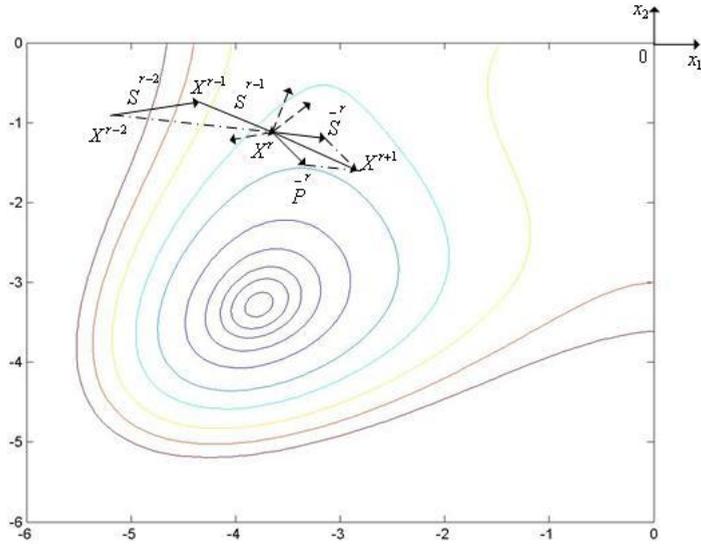
Fig. 3.7. Search trajectory with the iterative case search algorithm on an example of a 2-dimensional Himmelblau function.

As a search termination condition, one of the traditional iteration termination conditions can be used:

$$\|\mathbf{X}^{r+1}\text{-}\mathbf{X}^r\| = \lambda^r \le \varepsilon_X, \tag{3.16}$$

where ε_X – required search precision by X.

$$|\Phi(\mathbf{X}^{r+1})\text{-}\Phi(\mathbf{X}^r)| \le \varepsilon_\Phi, \tag{3.17}$$

where ε_Φ – required search precision by Φ.

3.7. Optimization algorithm for UV with neural network

An optimization algorithm for unmanned vehicles with a neural network is described here.

Algorithm description

Initialization (performed once)

Step 0.1.   Set account number n = 0

Step 0.2.   Neural network weights Wc, We, Wo are set randomly

Iterative algorithm (performed on each)

Step 1. Start

   Step 1.1. Increase starting account number n = n + 1, start = true.

   Step 1.2. Starting motors (c = 10 %).

   Step 1.3. Increase control signal c (us, %) c = c + 1.

Step 1.4. Measurement of acceleration, if a = 0, then repeat 1.2, otherwise c_{start} = c and go to step 2.

Step 2. Initial energy

Step 2.1. Waiting for the end of the transient when a < ε.

Step 2.2. During a certain period tm, we measure the energy En, with a constant signal c_n = c.

Step 3. Determining the hang point (for helicopter and multi-rotor aerial vehicles)

Step 3.1. There is a change/search for the control signal c (us, %) c = c + dc v ≈ 0 is reached (freeze).

Step 3.2. Store hover* signal: c_{hover} = c.

Step 4. Computing the c_{opt} of the neural network

Step 4.1. If the size of the training set |T| > 2, then go to step 4.2, otherwise go to step 5.

Step 4.2. En and cn are fed to the input of the neural network.

Step 4.3. Neural network performs calculations and c_{opt} = NN.

Step 4.4. If $c_{opt} \geq c_{start}$ the current control signal c = c_{opt} is set.

Step 5. Search for the minimum power consumption by the search algorithm,

Step 5.1. The algorithm for finding the minimum power consumption starts from the current value of c.

Step 5.2. The search is carried out until $c_{optn} \geq c_{hover}$ is found, at which, where E is the energy consumption for the period tc, S is the distance traveled in time tc

Step 5.3. In start mode, if start = true, then values are applied when T is found in the training sample.

Step 6. Training / retraining of the neural network.

Step 6.1. The values I = 1...n from the training sample are fed to the input of the neural network and applied.

Step 6.2. Yi is set as a target value for the training of NN.

Step 6.3. NN calculates the output and the value of Yi is compared with it and the error of the output layer is calculated.

Step 6.4. The error is propagated back to the hidden layer and the error δi is calculated.

Step 6.5. Correction of weight coefficients Wc, We, Wo.

Step 6.6. If the training termination criterion is not met, then step 5.1, otherwise, the transition to motion mode start = false, step 4.

*The hover function only applies to helicopters and multi-rotor unmanned vehicles.

Neural network weights:

Wc – input weights,

We – hidden layer weights,

Wo – output weights.

The block diagram of the algorithm with the function of minimum search of energy consumption and self-learning of the neural network is shown in Fig. 3.8.
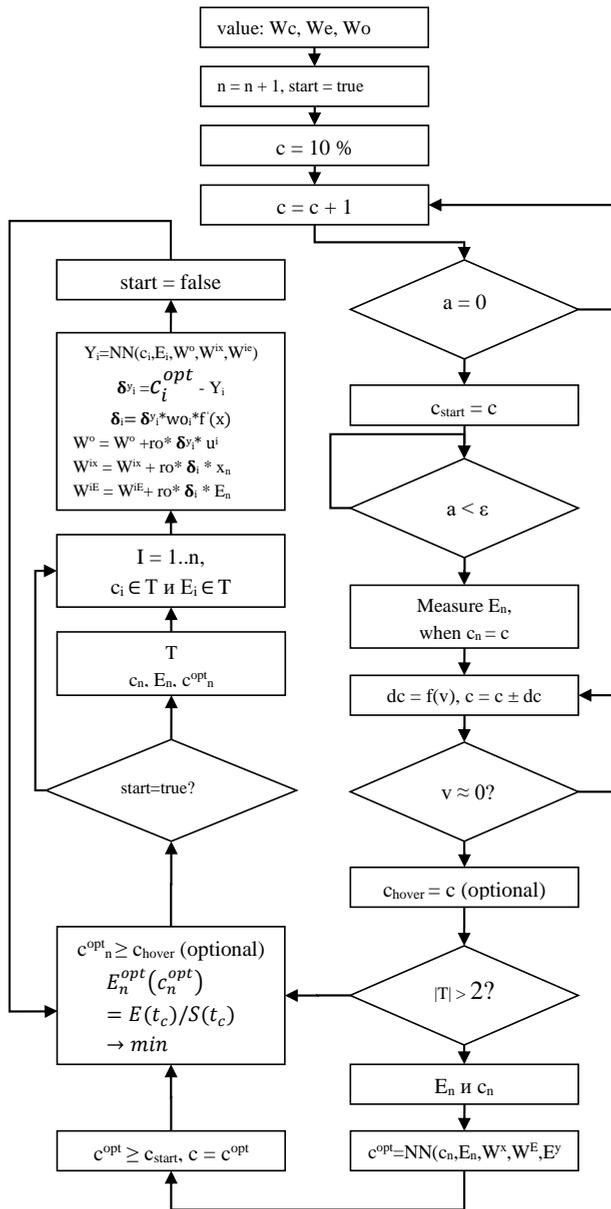
Fig. 3.8. Optimization algorithm for UV with one control signal.

3.8. A neural network learning algorithms

3.8.1. A neural adaptive filtering algorithm in general form

The algorithm is intended for a dynamic system whose mathematical characteristics are unknown [24].

Initialization.

Assume that given sets of labeled input and output data are generated by the system at discrete time intervals.

$x(t)$ – input m-dimensional signal

$d(t)$ – scalar system output signal

where $t = 1, 2, ..., n$;

In this way, the external behavior of the system can be described by the following set of data:

$$T : \{x(t), d(t); \quad t = 1, 2, ..., n\},$$ (3.18)

where

$$x(t) = \{x_1(t), x_2(t), ..., x_m(t)\}.$$ (3.19)

Step 1. Filtration procedure

The output of the neural network is

$$S = \{y(t), e(t)\},$$ (3.20)

where $y(t)$ – neural network output;

$e(t)$ – offset of the output signal $y(t)$ from $d(t)$.

Step 2. Adaptation procedure

Given the linearity of the neuron, the output signal $y(t)$ coincides with the induced local field $v(t)$:

$$y(t) = v(t) = \sum_{i=1}^{m} w_i(t) x_i(t).$$ (3.21)

In the form of matrices:

$$y(t) = X^T(t) \cdot W(t),$$ (3.22)

where

$$W(t) = \{w_1(t), w_2(t), ..., w_m(t)\}^T$$ (3.23)

$$e(t) = y(t) - d(t).$$ (3.24)

Step 3. Evaluation procedure.

Let us consider the continuously differentiable function E(w) that depends on the vector w. The function E(w) represents the elements of the vector w to the set of real views and is the optimality condition for a selected adaptive filtering algorithm of the vector w.

Step 3.1. We must find such a w* that

$$E(w^*) \leq E(w)$$ (3.25)

It poses an unconditional optimization problem:

$$E(w) \rightarrow \min$$ (3.26)

An optimality condition is required:

$$\nabla E(w^*) = 0.$$ (3.27)

Step 3.2. Calculate $\nabla E(w)$,

where ∇ – gradient operator;

$$\nabla = \left[\frac{\partial}{\partial w_1}, \frac{\partial}{\partial w_2}, ..., \frac{\partial}{\partial w_m}\right]^T$$ (3.28)

$$\text{bet} - \nabla E(w) = \left[\frac{\partial E}{\partial w_1}, \frac{\partial E}{\partial w_2}, ..., \frac{\partial E}{\partial w_m} \right]^T. \qquad (3.29)$$

Step 4. The correction of the weights takes place in the direction of decreasing the function of the maximum value, opposite to the gradient vector:

$$w(n+1) = w(n) - \eta g(n), \qquad (3.30)$$

where η – positive constant, training rate parameter;

$g(n)$ – gradient vector at point w(n).

Step 5. Weight correction calculation. When moving from the nth iteration to the n+1 iteration, the algorithm performs the correction of the weight coefficients:

$$\Delta w(n) = w(n+1) - w(n) = -\eta g(n). \qquad (3.31)$$

Step 6. Transition to the next iteration on the 1st steps at the condition

$$E(w(n+1)) < E(w(n)), \qquad (3.32)$$

where w(n) – is the previous value of the weight vector;

w(n+1) – the next value and with n = n +1.

3.8.2. *Backpropagation algorithm for neural network training*

If a set of training states is given, then we will define the following algorithms for training neural networks.

Algorithm [53] cycles examples from the training set $\{x(n), d(n)\}_{n=1}^{N}$.

Initialization

The weights W(0) are generated as case numbers with a uniform distribution with mean 0. The variance is chosen so that the standard deviation lies in the linear part of the sigmoid function.

Step 1. Defining the training set.

The training images from the training set – epoch – are passed to the network. Forward propagation and reverse propagation are performed sequentially for each image.

Step 2. Direct propagation of signals.

Let each training image be a pair (x(n), d(n))

where x(n) – vector of input signals;

d(n) is the target output of the neural network;

Step 3. Computation of weighted sums v(n) and functional signals φ(v(n)), say from the input layer. The weighted sum for the jth neuron in the lth layer is calculated according to the formula:

$$v_j^{(l)}(n) = \sum_{i=0}^{m_0} w_{ji}^{(l)}(n) y_i^{(l-1)}(n), \qquad (3.33)$$

where $y_i^{(l-1)}(n)$ – the output functional signal for the ith neuron located in the previous layer *l - 1* in the *n*-th iteration;

$w_{ji}^{(l)}(n)$ – weight for the connection of the j-th neuron of the l-th layer with the i-th neuron of the *l-1* layer.

Solis 4. Conditions of direct distribution. If the sigmoid activation function is used, then the output signal for the jth neuron of the lth layer is

$$y_j^{(l)}(n) = \varphi_j(v_j(n)).$$ (3.34)

If neuron j is in the first layer, at $l = 1$

$$y_j^{(0)}(n) = x_j(n).$$ (3.35)

If the neuron is in the output layer, at $l = L$

$$y_j^{(L)}(n) = o_j(n).$$ (3.36)

Step 5. The error is calculated by the formula:

$$e_j(n) = d_j(n) - o_j(n),$$ (3.37)

where $d_j(n)$ – the j-th element of the vector d(n).

Step 6. Reverse signal propagation

Step 7. The local gradients of the nodes are calculated

$$\delta_j^{(l)}(n) = \begin{bmatrix} e_j^{(L)}(n)\varphi_j{}'(v_j^{(L)}(n)) \\ \varphi_j{}'(v_j^{(l)}(n))\sum_k \delta_k^{(l+1)}(n)\delta_{kj}^{(l+1)}(n) \end{bmatrix},$$ (3.38)

where $\varphi_j{}'(n)$ – the derivative of the function by argument.

Solis 8. Therefore, the changes in the weights of the lth layer in training take place according to the delta-law

$$w_{ji}^{(l)}(n+1) = w_{ji}^{(l)}(n) + \alpha[w_{ji}^{(l)}(n-1)] + \eta\delta_j^{(l)}(n)y_j^{(l-1)}(n),$$ (3.39)

where η - training rate parameter;

α - moment constant.

Step 9. Iterations. The algorithm repeats, returning to step 2, successively applying forward and reverse propagation, cyclically using examples from the epoch, until the stopping criterion is reached.

3.9. Developed self-learning algorithm for optimal energy efficient control

The developed algorithm for optimal energy consumption combines an algorithm for determining path segments with different loads, an algorithm of searching for minimum energy consumption, an algorithm for creating of a training set and an algorithm for training a neural network.

The algorithm described in this chapter is generalized to fit different types of unmanned vehicles and consists of the following steps:

Step 1. Set the intial values of control signals C. For normal motion without specific maneuvering cases there is only one main control signal $c \in C$ that related to the the traction force in movement direction.

Step 2. The parameters v and E are measured in discrete moments in time dt or distance dS, thus dividing the motion into multiple segments, obtain sets of data for analysis:

$E_c = (dE_1, dE_2, \ldots, dE_n)$, $v_c = (dv_1, dv_2, \ldots, dv_n)$,

where,

n – number of motion segments;

dv_i – speed change for i-th segment

dE_i – consumed energy for i-th segment;

c – value of the control signal

Step 3. Assuming that the mass of the vehicle is constant, for the sequential segments i and j with the same control signal $c_i = c_j$, the character of load LC is decribed by the change of speed dv_j/dv_i, i.e. $LC_j = dv_j/dv_i$, that depends on different motion resistance forces – road profile, air density, frictions etc.

IF $c_i \neq c_i$ THEN repeat Step 2, since the changes of load may be caused by change of control signals.

NB: the number of sequential segments may greater than two and depends on the selected minimal search algorithm

Step 4. For the optimization controller the training set LQ is created or updated. The maximal size of the LQ set depends on the memory size of the controller. The set consists of the following records, where record lq_k is following for a segment measured by dS:

$$lq_k = \ <LC^k, \frac{dE^k}{dS}, v_k, C^k, C_{opt}^k> \ \in LQ \ ,$$

where C_{opt}^k is a target value for further training

Step 4.1. Create an empty set $LQS = \emptyset$. Measured $\frac{dv_j}{dv_i}$ is compared with all $\forall lq \in LQ$.

IF $\left| LC^k - \frac{dv_j}{dv_i} \right| < \varepsilon$, THEN record lq_k is included in LQS, i.e $lq_k \in LQS$

Step 4.2. IF $LQS = \emptyset$, THEN create new record lq_{new} in training set,

ELSE IF $C_j = C^k$, THEN

IF $\frac{dE_j}{dS} < \frac{dE^k}{dS}$ THEN $C_{opt}^k = C$, $\forall lq_k \in LQS$

This updates value of optimal control signal for all records of subset $LQS \subseteq LQ$, with the similar load characteritics LC.

NB: the conditions of choosing the optimal value may differ depend on the selected minimal search algorithm

Step 5. The neural network device work in parallel to the control device, processing learning algorithms described in 3.8. and continuously retraining the neural network using updated training set TS, calculates Mean Square Error (MSE) as a readiness value for the control device.

Step 6. The control device checks if MSE < $MSE_{threshold}$ and requests the response from neural network device, by input values $X = <\frac{dv_j}{dv_i}, \frac{dE^j}{dS}, v_j, C_j>$ expecting for C_{opt} as an output and applies it as a control value C, i.e.

$$C = C_{opt} = NN \left(\frac{dv_j}{dv_i}, \frac{dE^j}{dS}, v_j, C_j \right), if \ MSE_{NN} < MSE_{threshold}$$

Step 7. Repeat the algorithm from Step 2.

3.10. Conclusions on the third chapter

The main results of the third chapter of the doctoral thesis are as follows:

- An overall minimum search algorithm for energy optimization problems is described.
- Four minimum search algorithms are considered, two of which are deterministic and two are stochastic:
    - Uniform search algorithm
    - Algorithm with halving method
    - Algorithm with backtracking on unsuccessful step
    - Repeated random search algorithm
- An algorithm for training a neural network is described, which includes adaptation, filtering, evaluation, and weight adjustment procedures for unconditional energy-efficient control optimization.
- A new algorithm for optimal energy-efficient control of UV is developed. The algorithm involves the interaction of the minimum search algorithm, automatic generation of a training dataset, neural network, and neural network training algorithm.

The discussed minimum search algorithms allow finding the minimum energy consumption of UV required to traverse a given path.

The adaptive filtering algorithm can be used for neural network training and unconditional weight optimization for optimal UV control.

4. RESULTS OF EXPERIMENTAL RESEARCH ON DEVELOPED MODELS AND ALGORITHMS

4.1. Description of the situation

In the fourth part of the doctoral thesis, the results of the developed algorithms on physical models of unmanned vehicles using the new optimization controller and computer simulations are described.

The testing of the developed optimization method is carried out with a single control signal and is motivated by the following factors:

- The main control signal. For energy optimization, the focus can be on the main control signal that has the greatest impact on the energy consumption of the vehicle. For different types of vehicles, this can be different parameters such as speed, inclination angle, engine power, etc.
- Model simplification. Optimizing a single control signal simplifies the model and reduces the computational costs required for neural network training. This allows focusing on the key aspect of the problem and demonstrating the operation of the self-learning system.
- Practical implementation. Implementing optimization for a single control signal facilitates the integration of optimization algorithms into existing vehicle control systems. Such an approach requires minimal changes to the hardware and software infrastructure, reducing costs and simplifying the implementation process.

Thus, optimizing a single control signal is sufficient to achieve significant reduction in energy consumption in unmanned electric vehicles with different degrees of freedom. By using a self-learning neural network, this approach provides adaptability and scalability, making it effective and promising for a wide range of applications in the transportation field.

The self-learning neural network should be able to adapt to changes in vehicle operating conditions and optimize energy consumption based on training on new data. This allows the system to remain relevant and efficient in different conditions and at different stages of the vehicle's life cycle.

4.2. Experimental devices

For the research of traction motors, it is necessary to measure the parameters - current, voltage and traction force at set values of the control signal. For this purpose and for computer modeling at work, a frame was made:

- Test bench (Fig. 4.1 a).

To conduct experiments on testing the developed algorithm for optimizing energy consumption with a self-learning neural network, the following devices were made:

- UAV - unmanned aerial vehicle - quadcopter (Fig. 4.1 b).
- Model of a railroad with an unmanned electric train (Fig. 4.2).
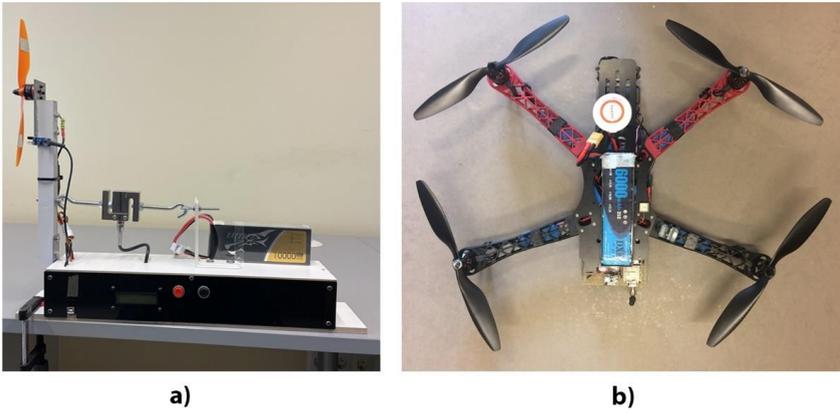
Fig. 4.1. a) Test bench b) UAV.
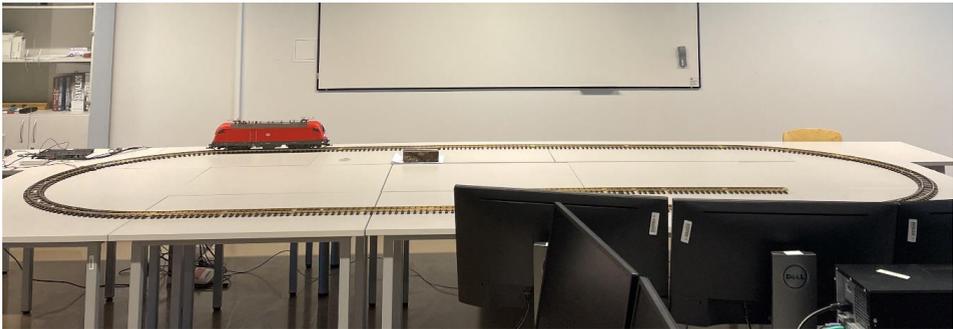
Fig. 4.2. Model of a railroad with an unmanned electric train.

Electrical boards of optimization controller (OC) of UAV is shown in Figure 4.3 a. The train control board with OC is shown in Figure 4.3 b.
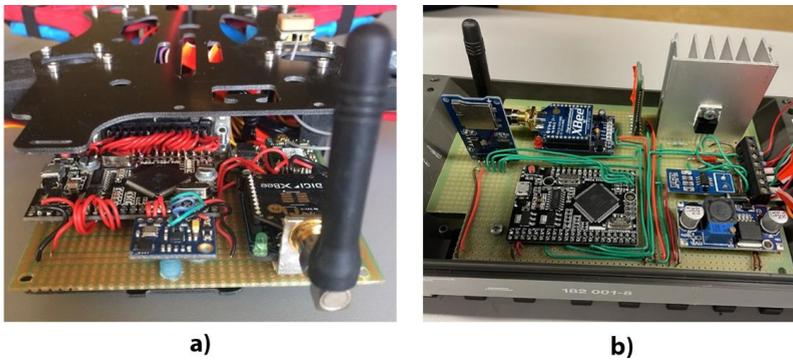
Fig. 4.3. a) Electrical boards OC UAV b) Train control electrical boards with OC.

4.2.1. Electric motors used in experimental devices

Let's take DC brushless motors BR2216-KV810, BR2212-KV920, BR2212-KV980, which are usually used in amateur quadcopters, and one DC motor without precisely known parameters, let's call it LKD-24 (Fig. 4.4).
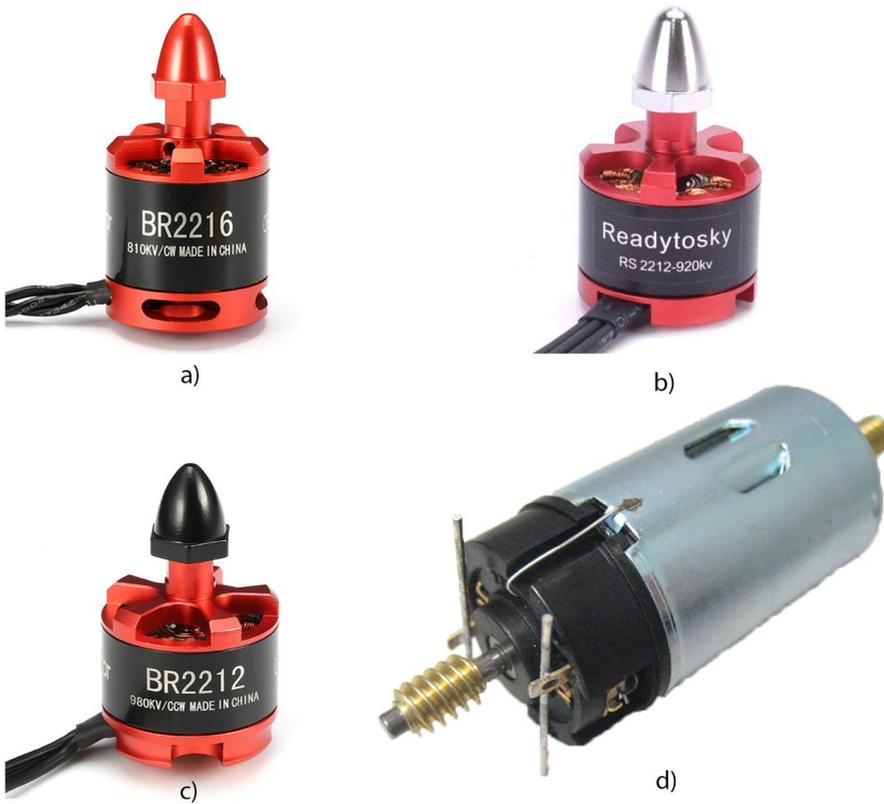
Fig. 4.4. a) BR2216-KV810 b) BR2212-KV920 c) BR2212-KV980 d) LKD-24.

Parameters of electric motors BR2216-KV810, BR2212-KV920, BR2212-KV980 are shown in Table 1.

Table 1

Parameters defined by electric motor manufacturers

Motor	KV [rpm/V]	U [V]	I [A]	F [g]	P [W]	Eff. [g/W]	LiPo Cell	m [g]
BR2216	810	14.8	15.6	1065	231	4.6	2S-4S	66
BR2212	920	11.1	9.5	642	105	6.1	2S-4S	50
BR2212	980	11.1	10.6	710	118	6	2S-4S	50

Fig. 4.4 shows the electronic speed controller [74], [75], [90] Predator 40A used in the experimental bench.

Fig. 4.4. Electronic speed controller Predator 40A.

The parameters of the ESC Predator 40A are as follows:

$Cell$ = 1S-4S;

I_{ilg} = 45A;

I_{50s} = 50A;

I_{10s} = 55A.

4.2.3. Device and calibration of an electronic odometer for measuring the distance traveled by a train model

An electronic odometer is made to measure the distance traveled. The odometer mechanism is shown in Fig. 4.5.
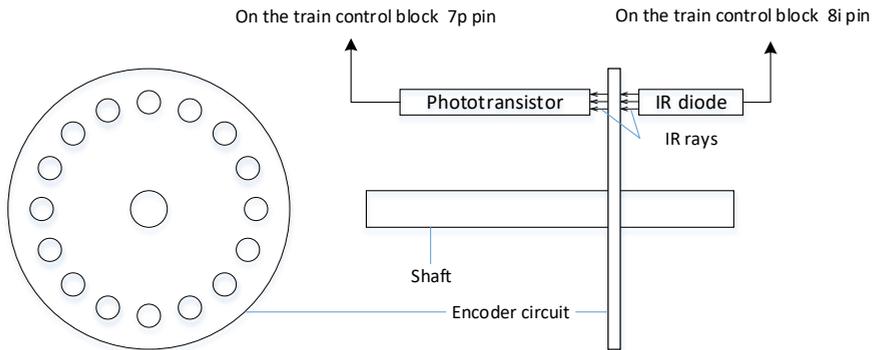
Fig. 4.5. Odometer mechanism.

The infrared diode is supplied with power and emits infrared rays. When rotating the axis on which a transparent coding disk with holes is attached. The microcontroller input is supplied with voltage from the transistor, which varies from 0 to 5 volts as the disk moves, passing through transparent and opaque areas. The 10-bit analog-digital converter (ADC) of the microcontroller converts the voltage values into discrete values from 0 to 1024. In the absence of IR radiation, the ADC value is 0, when exposed to IR radiation - 1024. The passage of one transparent and one opaque area is counted as one tact cycle. Passage of the transparent region is considered when the ADC value is greater than 900, followed by the opaque region with a ADC value less than 700. Next, we measure the number of cycles when the train travels the

route once. The length of the experimental route is 11 m. To fix one passage, a reed switch is installed on the train, and a permanent magnet is installed on the rails. When traveling 11m, 800 cycles are recorded. Thus, one odometer cycle is equal to 1.1375 cm.

4.2.4. *Control structure of experimental devices*

UAV – quadcopter

Proposed control structure of the UAV consists of the following components. The existing UAV already has flight controller, traction groups with electronic speed controllers ESC and permanent magnet brushless DC motors, accumulator, voltage regulator, radio receiver and built-in sensor components. Propose to improve the existing structure by additional optimization controller and additional sensor group containing voltmeter, current meter (hall sensor), accelerometer, barometric altimeter, satellite positioning module (fig. 4.6).
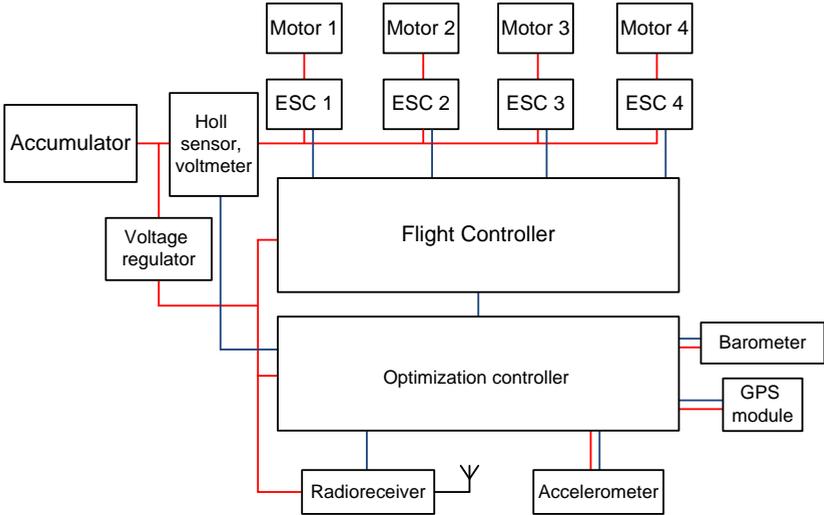
Fig. 4.6. Improved control structure of quadcopter UAV as example with optimization controller.

Flight controller of UAV has standard inputs that allows to control the UAV using the remote control module by the operator from the ground. These inputs are A – aileron, E – elevator, T – throttle, R – rudder and U – control mode.
Instead of remote control for autonomous vehicle the optimization controller is connected to ёthe flight controller and plays the role of UAV operator controlling the UAV by basic signals <A, E, T, R>, and collecting all necessary information from all available sensors.

The radio receiver in the improved structure is used to get the flight goal from the operator to the optimization controller or, in fully autonomous UAV case, the optimization controller is able to define the mission goal by itself (it requires the development of additional decision-making algorithms and is not described in this work). After the mission goal is defined the optimization controller is trying to achieve it with maximal energy efficiency, i.e. minimal energy consumption, adapting to the external conditions and environmental impacts

The NN will be trained using the values obtained by the search algorithm and stored in the memory of the optimization controller. The control system modules and the structure of the optimization controller are shown in Fig.1.

Train

To monitor the operation of the optimization controller, collect data, and control the startup, a computer [74] with the ARDUINO IDE programming environment is used [82]. The train and the computer exchange data using the Xbee radio module. The data exchange structure between the computer and the train is shown in Figure 4.7.
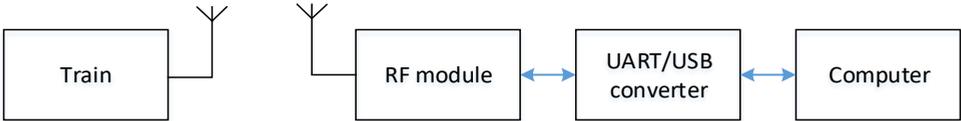
Fig. 4.7. Structure of data exchange between computer and train.

4.2.5. Electrical schemes of experimental devices for testing the developed algorithm.

Developed electrical scheme of the stand is shown in Fig. 4.8. The electrical scheme of the UAV quadrocopter is shown in Fig. 4.9. The electrical scheme of the train model is shown in Fig. 4.10.
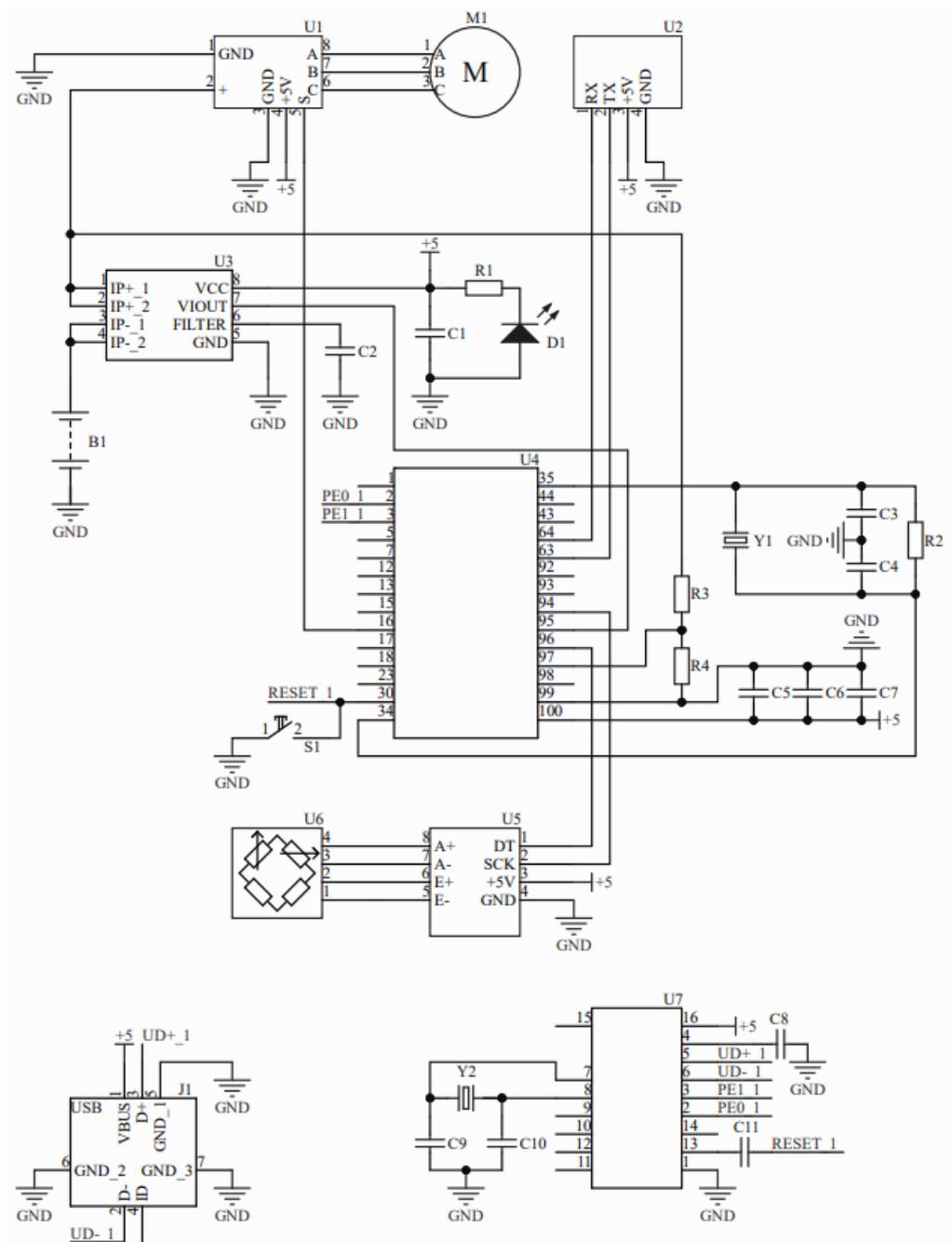
Fig. 4.1. Electric scheme of the measuring bench.
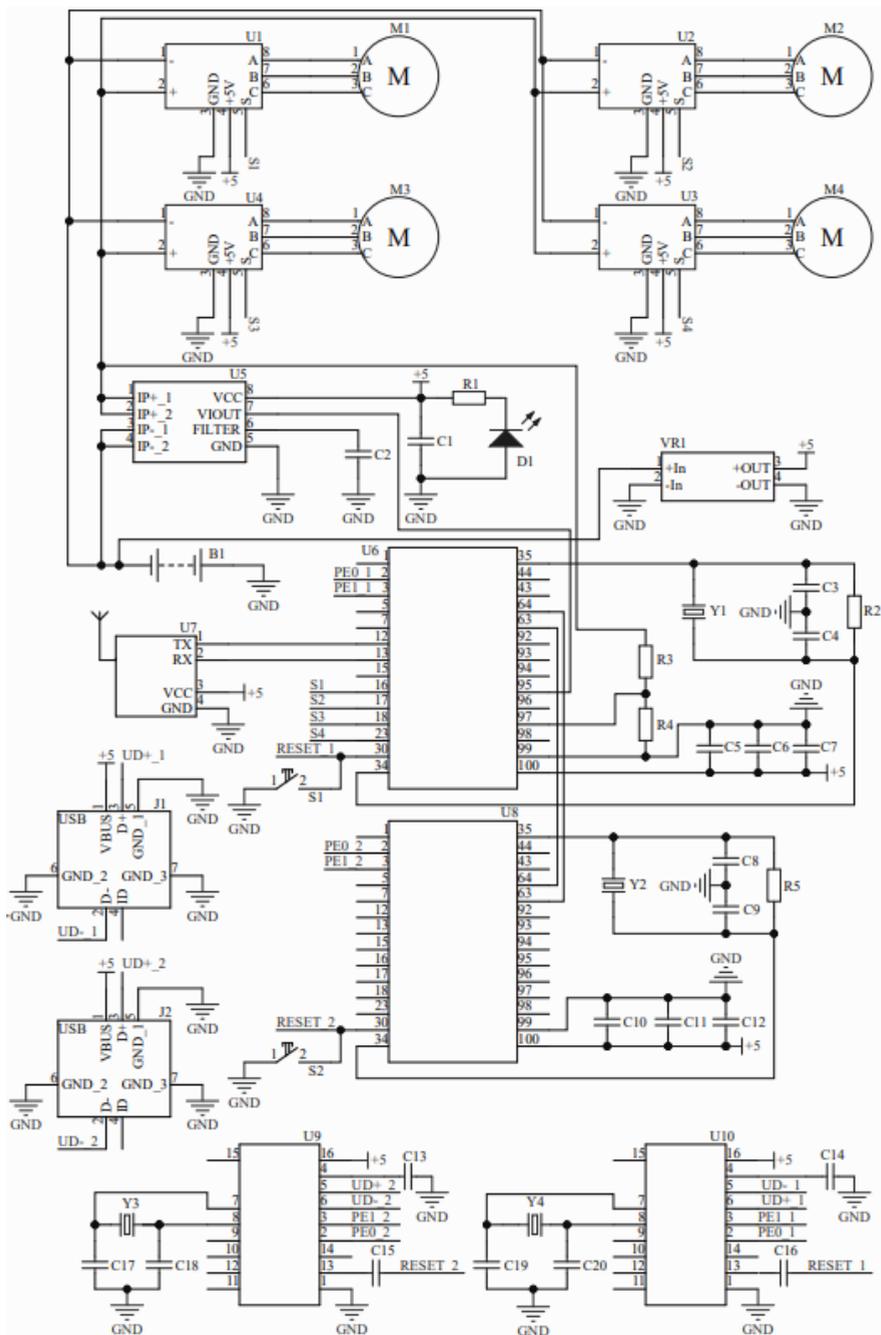
Fig. 4.9. Electric scheme of the UAV with OC.
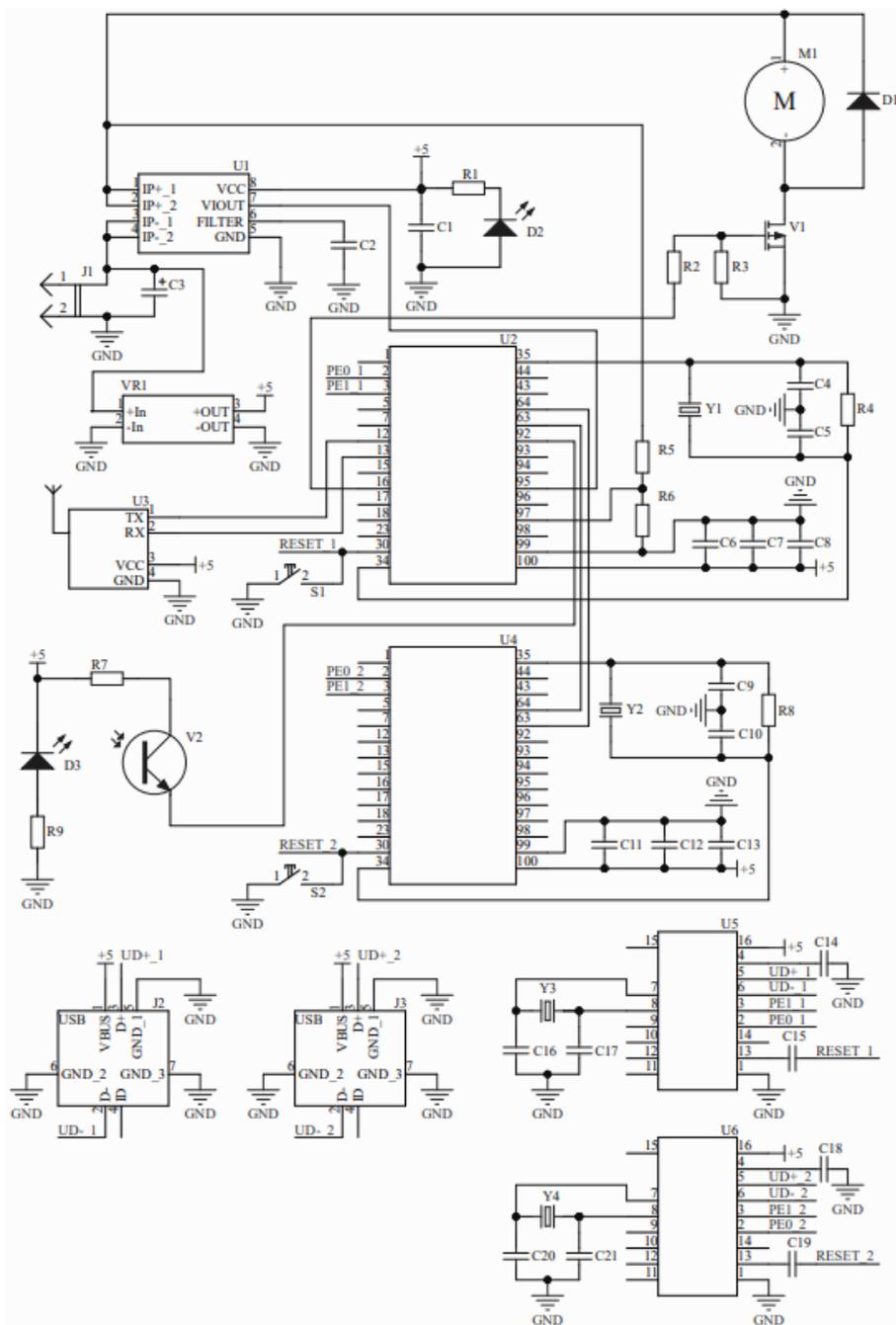
Fig. 4.10. Electric scheme of the train with OC.

Description of the test bench electrical scheme

Measurements and calculations are performed on the U4 Atmega328 microcontroller. The motor with the battery is powered by the electronic regulator U1 (ESC). The rest of the circuit is powered by 5 V from the J1 connector (USB) from the computer, where the measured

values are transmitted. The U7 microchip serves as a UART/USB converter. The built-in 10-bit ADC of the microcontroller, operating at a frequency of 77 kHz, is used to read the total voltage and current values of the motor M1 (BR2212 920 kV). The used propeller is a 10-inch 1045. The motor speed is measured using the U2 module. The Hall sensor U3 (ACS712) is used for current measurement. The force generated by the motor is measured using the U6 strain gauge, and the data is converted by the U5 24-bit DAC, controlled by the U4 microcontroller.

Description of the UAV electrical scheme

The satellite navigation module and barometer provide the optimization controller with data on the UAV's position relative to the destination and allowable deviations from the specified route trajectory. The current and voltage values of the UAV, which are input to the optimization controller, are used to calculate the power of the electric drive. The onboard voltage is stabilized by a voltage regulator to power the circuit element. The flight route is recorded in the control controller U6, which is part of the optimization controller with an optimization algorithm simulating the UAV flight controller. The motor speeds (M1, M2, M3, M4) are regulated by electronic speed controllers (U1, U2, U3, U4) that receive optimal control signals c_1 , c_2 , c_3 , c_4 .

Description of the train electrical scheme

The electrical circuit of the electric train model consists of an optimization controller implemented on microcontrollers U2 (main controller) and U4 (neural network microcontroller [62] Atmega2560). The radio module U5 (Xbee) serves as a transmitter-receiver, transmitting information about the operation of the optimization controller. The power control circuit for the electric motor M1 is assembled with resistors R2, R3, transistor V1, and diode D1. UART/USB protocol converters are built using microchips U5 and U6, and their signals are connected to USB connectors J2 and J3. The components of the electronic tachometer are placed outside the board and located inside the gearbox. The electronic tachometer is built with resistors R7, R9, infrared diode D3, and phototransistor V2. An ammeter is assembled using the Hall sensor U1 (ACS712). A voltage divider is assembled with resistors R5 and R6. VR1 is a voltage stabilizer. Contacts 1 and 2 are contact pads that make contact with the rails using springs.

4.3.   Researching the possibility of optimization

4.3.1. Removal of UAV electric drive characteristics

The thrust force of the motor was measured using a test bench, calculating the force according to the formula:

$$F_{\text{vil}} = m \cdot 9.81, \tag{4.1}$$

where   m – measured thrust, kg.

Motor power is calculated as:

$$P_{\text{electric drive}} = U * I. \tag{4.2}$$

Since in real conditions the optimisation algorithm does not consider the elements of the electric drive separately but takes into account the total energy consumption, the losses in the

wires and the losses in the speed controller are not calculated. Thus, the power consumed by the electric drive consists of

$$P_{\text{electric drive}} = \Delta P_{\text{wire}} + \Delta P_{\text{esc}} + \Delta P_{\text{motor}},$$ (4.3)

where ΔP_{wire} – power loses in wires;

ΔP_{ESC} – power loses in the speed converter;

P_{motor} – motor power (including loses).

An infrared sensor was used to detect the rotation of the motor propeller (1045 model on the test bench), whose signal was read by microcontroller contact no. 2 using interrupts. For measuring traction of electric drive the S-type load sensor and the 24-bit ADC HX711 module was used.

The following figures show the characteristics of the measured electric power of the motor as a function of the thrust force on the test bench. **A PPM signal (Pulse-Position Modulation, a specific case of Pulse Width Modulation, PWM) with a duration ranging from 1000 µs to 2000 µs is provided.**

Figure 4.11 depicts the power characteristic curve for the BR2216 KV810 motor at different thrust force values.
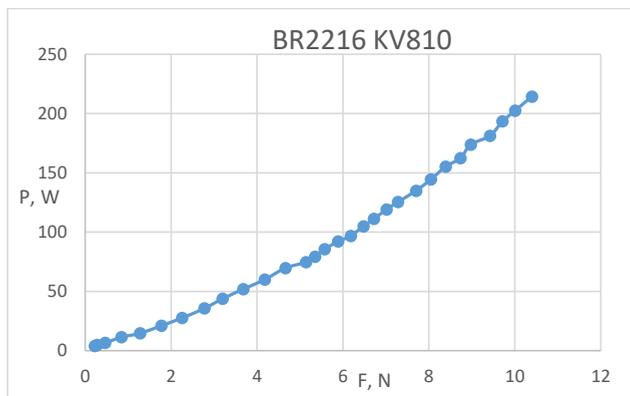
Fig. 4.11. BR2216 KV810 electric motor parameters.

The power characteristic curve for the electric motor BR2212 KV920 at different traction force values is shown in Fig. 4.12.
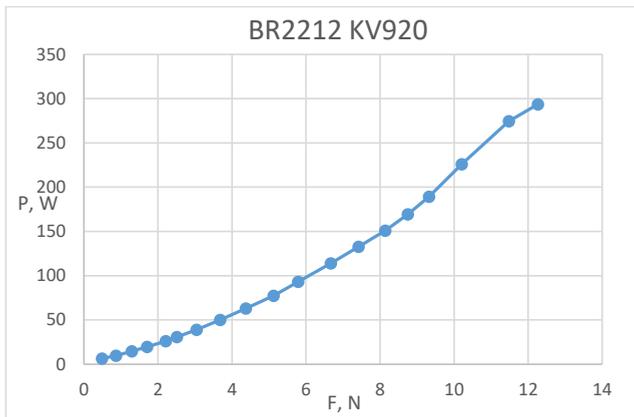
Fig. 4.12. BR2212 KV920 electric motor parameters.

The power characteristic curve for the electric motor BR2212 KV980 at different traction force values is shown in Fig. 4.13.
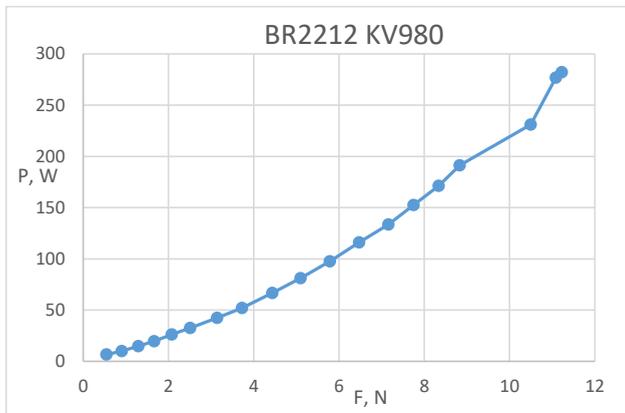
Fig. 4.2. BR2212 KV980 electric motor parameters.

From the graphs, you can see the pronounced nonlinearity, which indicates the possibility of minimizing electricity consumption.

4.3.2. *Removal of train model electric drive characteristic*

The power characteristic of the electric drive on different sections of the road with a constant control signal C = 45 with a train weight of 9.6 kg is shown in Fig. 4.14.
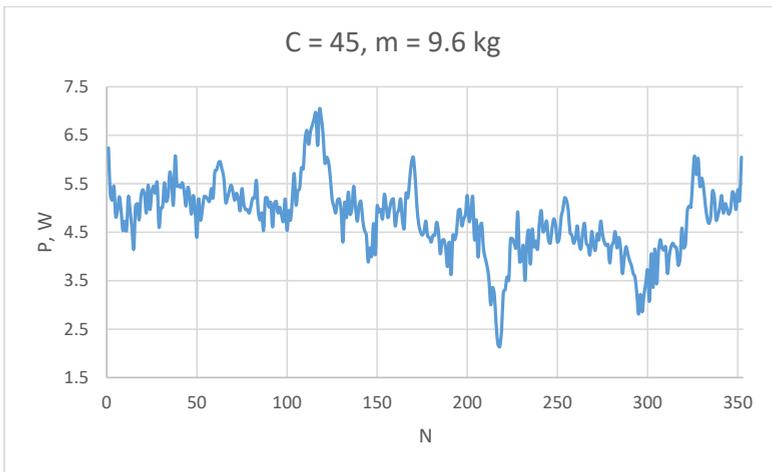
Fig. 4.14. The power characteristic of the electric drive on different sections of the road with a constant control signal C = 45 with a train weight of 9.6 kg.

The power characteristic of the electric drive on different sections of the road with a constant control signal C = 105 with a train weight of 9.6 kg is shown in Fig. 4.15.
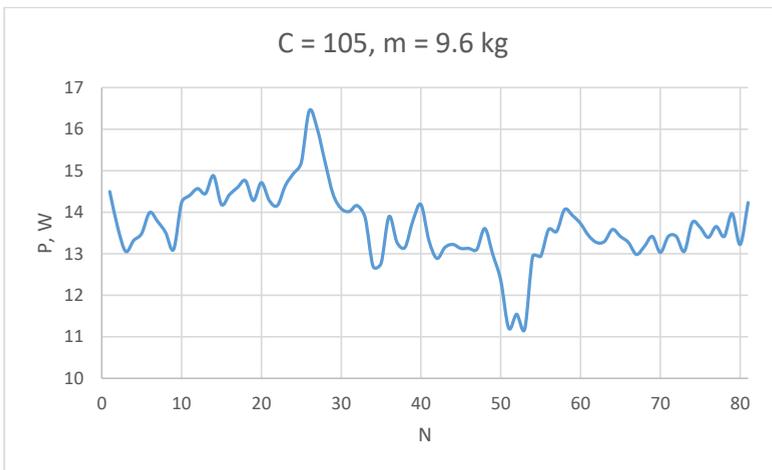
Fig. 4.15. The power characteristic of the electric drive on different sections of the road with a constant control signal C = 105 with a train weight of 9.6 kg.

The power characteristic of the electric drive on different sections of the road with a constant control signal C = 255 with a train weight of 9.6 kg is shown in Fig. 4.16.
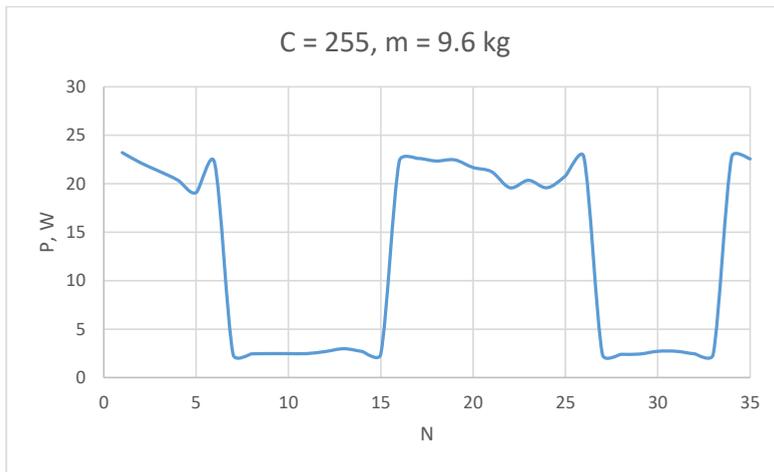
Fig. 4.16. The power characteristic of the electric drive on different sections of the road with a constant control signal C = 255 with a train weight of 9.6 kg.

The power characteristic of the electric drive on a straight section of the track under different control signals, with a train mass of 4.1 kg, is shown in Fig. 4.17.
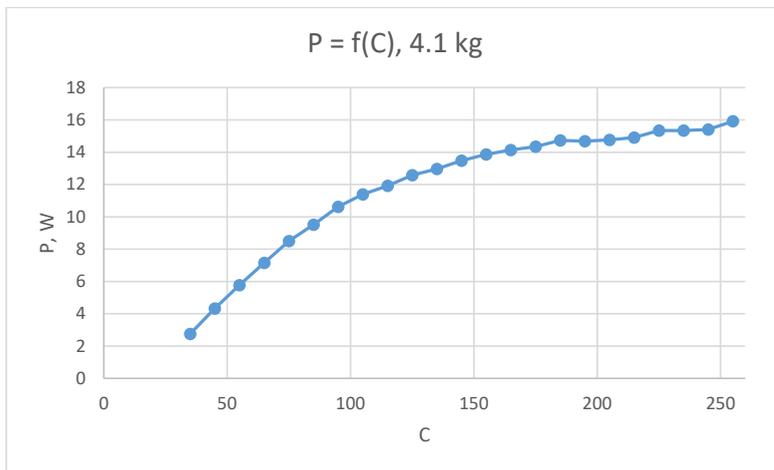
Fig. 4.17. The power characteristic of the electric drive on a straight section of the track under different control signals, with a train mass of 4.1 kg.

The power characteristic of the electric drive on a straight section of the track under different control signals, with a train mass of 9.6 kg, is shown in Fig. 4.18.
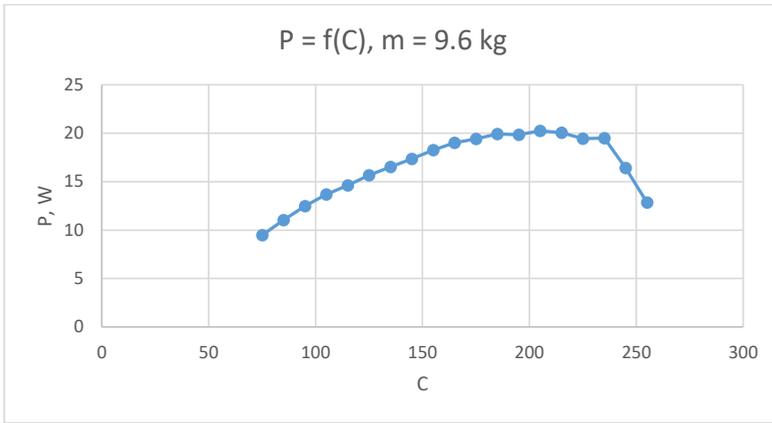
Fig. 4.18. The power characteristic of the electric drive on a straight section of the track under different control signals, with a train mass of 9.6 kg.

The non-linear nature of the power characteristics of the electric drive under different control signals and the varying power on different sections of the track indicate the potential for energy consumption optimization.

4.3.3. Research of energy consumption and battery discharge at different voltages

First of all, a series of 5 experiments were carried out after the test bench was developed, during which the stability and accuracy of the measurement results provided by the test bench was tested, which depends on both the absolute accuracy of the applied measuring equipment and the applied data processing algorithms and their working coefficients, which were selected empirically. Experiments were performed at equal power supply voltages (16.8 V) and equal control signal frequency values, which in each experiment were linearly changed from 1300 to 1700 µs in increments of 5 once per second. The average square error of electrical parameters is shown in Fig. 4.19.
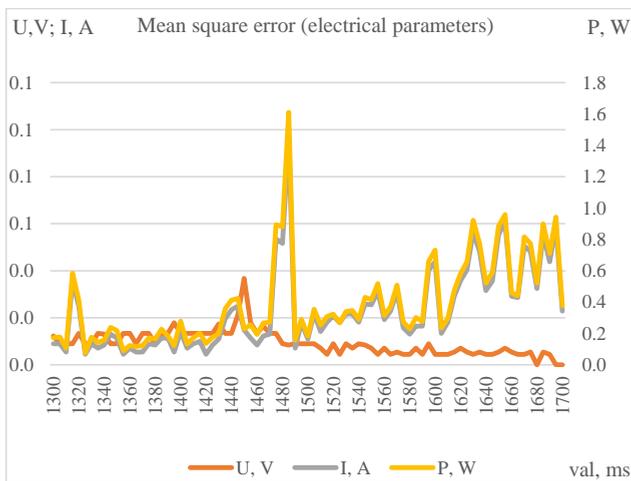
Fig. 4.19. Mean square error of electrical parameters.

Meanwhile, the average square error of the mechanical parameters is visible in Fig. 4.20.
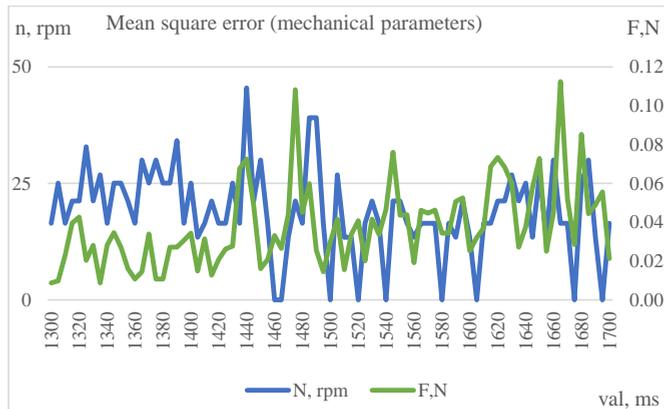
Fig. 4.20. Mean square error of mechanical parameters.

In this way it can be concluded that the average quadratic error of the parameters in the test range does not exceed:

- U – 0.037 V;
- I – 0.096 A;
- P – 1.6 W ;
- n – 46 rpm;
- F – 0.112 N.

Since the measurement of all electrical parameters is based on the average measurement result calculation, the maximum measuring frequency that can be realized on the described test bench was assessed. The main limiting parameter here is the measurement of electric drive force F, which with the above accuracy is realized by 3 measurement attempts (empirically selected number for good accuracy), which takes about 0.3 sec (about 3 sps, i.e. samples per second). Also, the optimum frequency for measuring the rotation n of the motor is about 3 sps. In turn, the individual frequency of the electrical parameters can be higher (optimally around 100 sps), which can be used for more accurate modeling of various electrical transition processes in the future.

Validating measurement results, a series of 15 experiments were performed (with 2 min intervals between each experiment, with forced motor cooling), at different U values of the supply voltage, changing it by step 0.2 V between 16.8 and 14 V. It should be noted that this is the voltage value of the power supply, while the value of the fixed power supply voltage on the test bench that was fed to the ESC was lower due to the corresponding voltage drop in the connection cables used by ΔU.
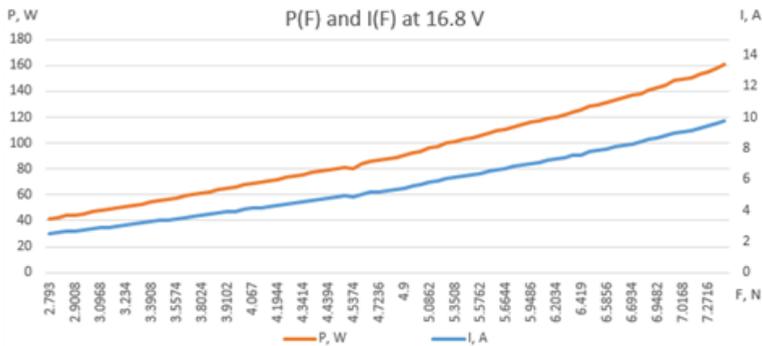
Fig. 4.21. Empirical data P(F) and I(F) at 16.8 V.
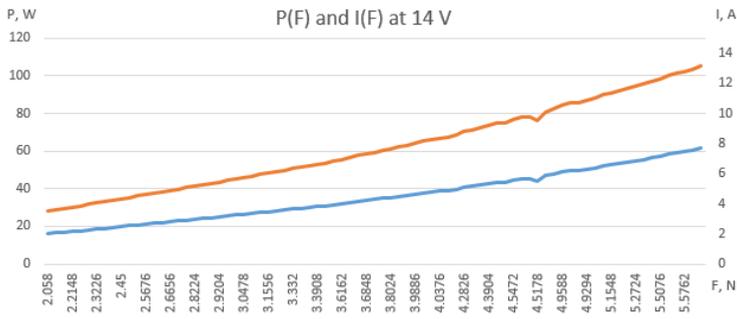
Fig. 4.22. Empirical data P(F) and I(F) at 14 V.

Figures 4.21 and 4.22 presents empirical data used for approximation of $P(U_0, F)$ and $I(U_0, F)$ at maximal and minimal voltage. It is obviously not linear, but in general may be approximated by second-order polynomial function as defined in mathematical model. However, the shape of the function at different voltages is the same and allow assuming that polynomial coefficients are changing linearly.

After the approximation all empirical data of obtained voltage, force, current and power were tested by approximated functions and the relative deviation has been calculated by

$$\varepsilon = \frac{D_e - D_a}{D_e},$$ (4.4)

where: D_e – empirical value;

D_a – approximated value.

Obtained deviations for current and power approximations are presented in Fig. 4.23. The average absolute deviation is 0.086 % for current and 0.091 % for power approximation. It is less than mean quadratic error of measurements that is 0.98 % for current and 1 % for power values.
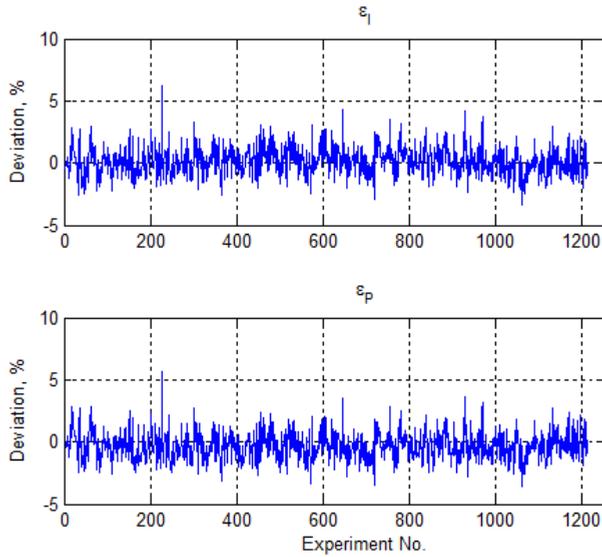
Fig. 4.23. Relative deviation of empirical and approximated data.

Thus, it proves that the approximated functions are trustworthy and usable for computer model.

Computer modelling of UAV electrical traction

The computer model is developed using the developed mathematical model and approximation functions. The model simulates 3D quadcopter flight at the predefined elevator, throttle and rudder values. The simulated flight consists of 10 seconds take-off part to the predefined altitude 150. Additional adaptive algorithm is controlling throttle to keep the quadcopter at the stable altitude Z set as 150 in horizontal flights. Elevator value sets the horizontal motion at pitch angle rotP of 32°. Additionally, rudder value is a constant to set closed circle shaped trajectory.

Mass of simulated quadcopter is 1.5 kg, vertical area 0.24 m^2, horizontal area 0.08 m^2, air density 1.2255, drag rate 1.04, battery LiPo 6000 mAh (working voltage range 16.8–14 V), 4 motors BR2212 920 kV.

Figure 4.24 presents the results of 300 seconds flight started at fully charged battery with consumption C = 0 mAh, i.e. 6000 mAh charge left, and unloaded battery voltage U0 = 16.8 V. Figure 4.25 presents the results of the same 300 seconds flight, but started at almost discharged battery with consumption C = 5000 mAh, i.e. 1000 mAh left, and unloaded battery voltage U0 = 14.47 V.

Results of simulation shows that energy consumption of the UAV is the almost the same at different voltages, at lower unloaded battery voltage it is less by 0.28 %. However, battery discharge rate is different, i.e. for voltage range 16.8–16.68 V it is 0.835 mAh/s, but for 14.47 – 14.34 V it is 0.939 mAh/s. So, battery discharge occurs faster at lower voltage values by 12.5%.
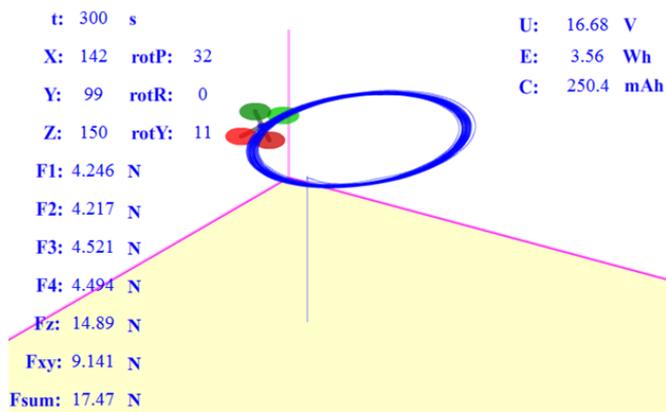
Fig. 4.24. Results of UAV simulation starting at 16.8V voltage.
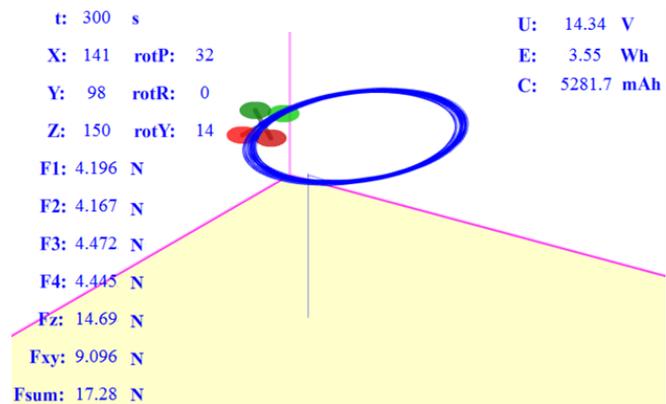
Fig. 4.25. Results of UAV simulation starting at 14.47V voltage.

The mean quadratic error of the experimentally measured electrical parameters for the development of the computer model does not exceed - 0.98 % for current, 0.22 % for voltage and 1% for power, while for mechanical parameters n = 0.64 % and F = 1.5 %. The precision of approximation is 0.086% for current and 0.091 % for power values that significantly less than mean quadratic deviation of measurements.

The frequency of measurement for the above-mentioned accuracy level separately for electrical parameters reaches 100 sps, but for mechanical parameters about 3 sps.

The obtained parameter curves at different supply voltages (16.8-14 V) in the tested range of control signals (1300-1700 μs) maintain the same parabolic character.

Computer simulation shows that the discharge rate of the battery is higher at lower battery voltage at almost the same energy consumption values. It should be taken in account also when planning the route and return of the UAV.

When evaluating the efficiency of the electric drive, it was found that higher efficiency F/W is at lower power voltages. It requires further in-depth research and further experiments

with different motors, propeller and ESC models, with the goal of discovering the cause of this fact.

4.3.4. Development of the UV computer model for studying energy consumption minimization target function

The computer model is designed for modeling the vertical motion of a quadcopter [68], [69] towards a specified target point, specifically the target altitude, which is chosen to be sufficient for calculations and further optimization.

The general steps of implementing the quadcopter computer model algorithm are as follows:

1) Initially, the calibration of the engine speed controller ESC is performed to determine the maximum and minimum values of the control signal. Typically, the control signal is a PPM signal with a pulse length ranging from 1000 v to 2000 μs. After calibration, the maximum control signal pulse length is 2000 μs, and the minimum is 1000 μs.

2) Next, the motor speed is increased gradually by incrementing the control signal starting from the minimum value to determine the control signal at which the UV takes off. This can be determined separately using a barometric altitude sensor, an accelerometer, satellite navigation, or a combination of these. The control signal is fixed so that the minimum and lower signal values are not used in the process of searching for optimal power consumption. This is necessary to avoid UV stalling or falling, as the thrust force would be less than the gravitational force.

3) Then, the algorithm for finding optimal values is executed, which searches for a control signal that minimizes the electrical energy consumption based on the specified search criteria and methodology. The measurement of search parameters occurs at stabilized motion (velocity) values where the acceleration is close to zero. A timer is activated, counting a specified time, while energy consumption and distance measurements are taken simultaneously.

4) Upon reaching the specified time (or distance) for sufficient energy consumption calculation, a decision is made to increase or decrease the control signal.

5) Steps 3 and 4 are repeated until the control signal with minimal energy consumption is found.

6) After a certain time, the algorithm checks the presence of the optimal control point, and if it is not optimal, it repeats from step 3.

Empirical data [81] obtained during the motor research time in the computer model are implemented as a four-dimensional array with the defined number of measurements n:

- Control signal array c;
- Current value array i;
- Voltage value array u;
- Thrust force array f.

To obtain parameter values between measurements, linear interpolation method is used in the computer model, which, based on the control signal c, allows finding the desired value of another parameter y (current i, voltage u, or force f):

$$y = \frac{(c-c_i)}{(c_{i+1}-c_i)}(y_{i+1} - y_i) + y_i. \qquad (4.5)$$

A code fragment of the computer model is shown in Fig. 4.26. The modeling data will be saved in the file "dati1.txt" for further analysis.

```cpp
ofstream out("dati1.txt",ios::out);
double dt=0.01, st=1000, E,F,Ft,Fr,Fg,a,v,s,h,t,x;

int main() {
    for (m=1; m<=2; m+=0.1)
     for (x=c[0]; x<=c[n-1]; x++)    {
     a=0; v=0; s=0; E=0;
     cout << "m=" << m << " x=" << x <<endl;
     int j;
     for (t=0; ;t+=dt)   {
         j=get(c,n,x);
         Ft=value(f,c,j,x)*4;
         Fr=rho*cd*Aeff*v*v;
         Fg=m*g;
         F=Ft-Fr-Fg;
         if (F<=0) break;
         a=F/m;
         v+=a*dt;
         s+=v*dt;
         E+=value(u,c,j,x)*value(i,c,j,x)*4*dt;
         if (s>=st) break;
     }
     cout << "Ssum   " << s << " m" << endl;
     cout << "time   " << t << " s" << endl;
     cout << "Energy consumed " << E/3600 << " Wh" << endl;
     out << m << "\t" << x << "\t" << E/3600 << endl;
     }
}
```

Fig. 4.26. A code snippet for a computer model of a quadcopter.

The following variables are defined in the computer model:
- Time t;
- Modeling time step dt;
- Target altitude st;
- Electrical energy consumption E;
- Total thrust of the quadcopter F;
- Thrust force Ft;
- Resistance force Fr;
- Gravitational force Fg;
- Acceleration a;
- Velocity v;
- Distance s and altitude h (in the case of vertical motion, s=h);

– Input thrust control signal c.

The core part of the model is a time cycle that calculates the energy consumption and time function to reach the specified altitude based on the thrust control signal x.

The given parameters for the quadcopter are mass m, effective area A_{eff}, drag coefficient C_d, and air density rho, which is considered constant at the altitude of the quadcopter (rho = 1.2255).

The first analysis of the target function was performed with varying mass and three different motors:
– Mass ranging from 1 kg to 1.9 kg with a step of 0.1 kg,
– Motors with 810 kV, 920 kV, and 980 kV.

The constant parameters are $C_d = 1.06$ and $A_{eff} = 0.25$ m2.
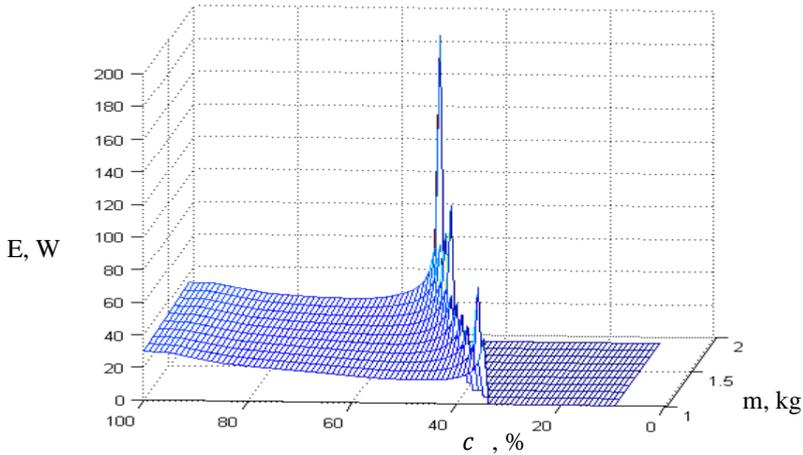
Fig. 4.27. E(c,m) analysis for motors BR2212 920 kV.
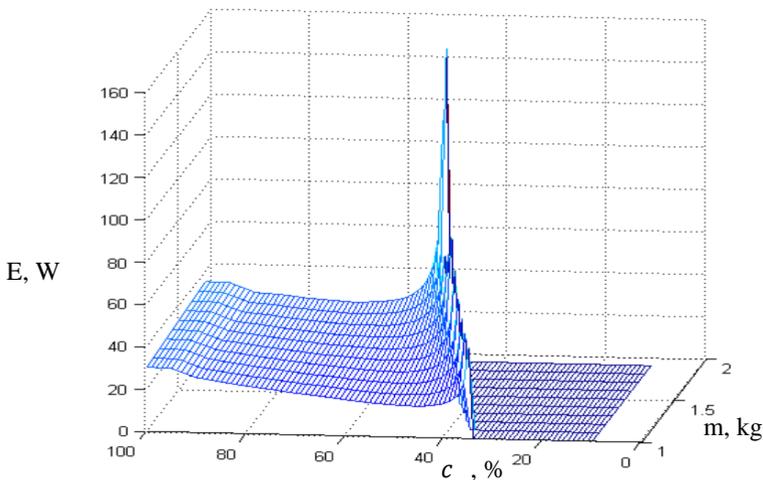
Fig. 4.28. E(c,m) analysis for motors BR2212 980 kV.
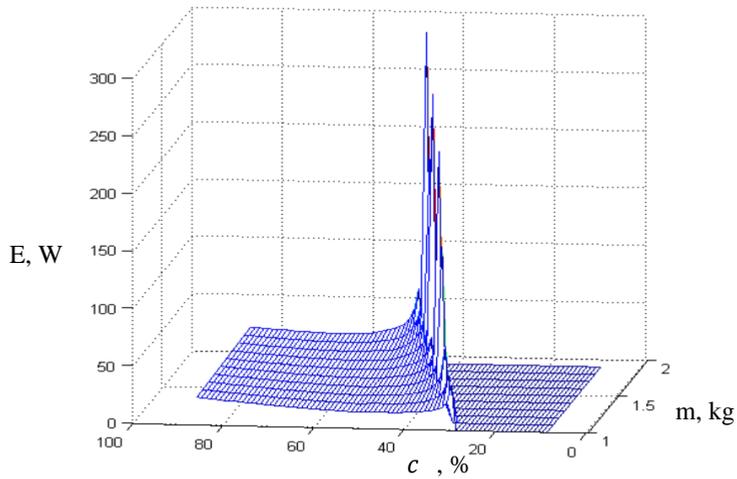
Fig. 4.29. E(c,m) analysis for motors BR2216 810 kV.

In Figures 4.27, 4.28 and 4.29, it can be observed that the energy consumption function exhibits a unimodal nature for any given mass and different motors. The only difference lies in the launch thrust control signal required to lift the quadcopter in the air and the value of consumed energy.

Analyzing the minimum function values for different masses, it can be seen that the energy consumption is higher for motors with a higher kV ratio (Fig. 4.30).

Therefore, we can conclude that in the study of the target function's dependence on the quadcopter's area and drag coefficient, it is sufficient to evaluate the function for any chosen mass, for example, m = 1.5 kg.

Figure 4.31 shows the dependency of the target function E on the effective area A_{eff}, ranging from 0.2 m^2 to 0.4 m^2 with a step of 0.01 m^2.

On the other hand, Figure 4.32 illustrates the dependency of the target function E on the drag coefficient C_D in the range from 0.8 to 1.3 with a step of 0.01.
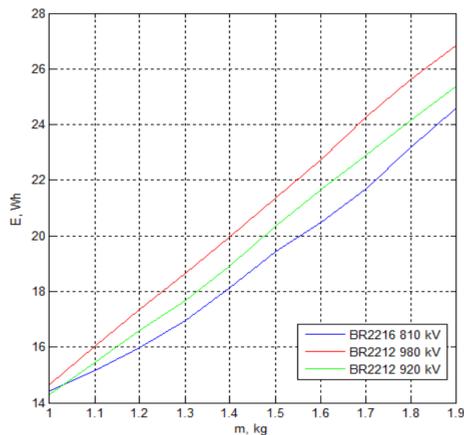
Fig. 4.30. Analysis of the minimum values of the E(m) function for different motors and different UV masses.

88
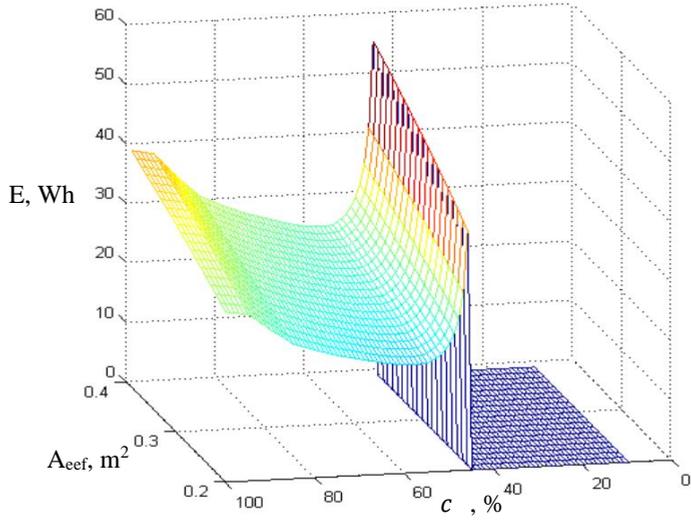
Fig. 4.31. Analysis of the values of the function E(c, A$_{eff}$).
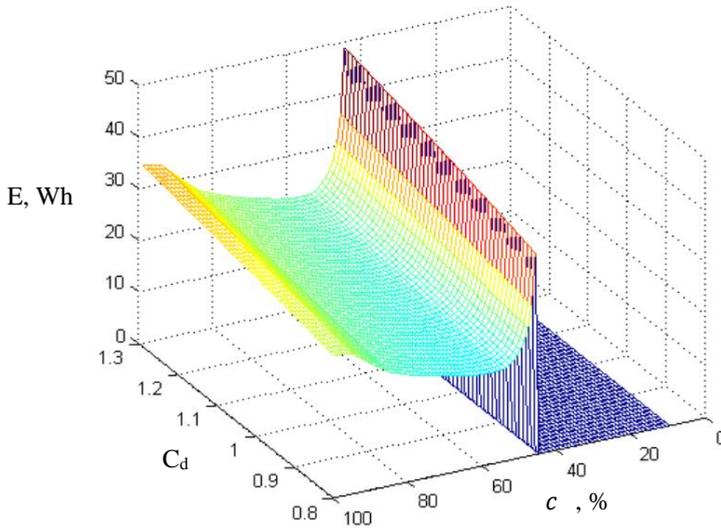
Fig. 4.32. Analysis of the values of the function E(c, C$_d$).

It can also be seen from the figures that the nature of the function is similar and unimodal and the power consumption increases with increasing effective area and streamline ratio. Quadcopter efficiency equation is the following:

$$\eta = \frac{A}{E}, \tag{4.6.}$$

where

$$A = A_{0\,sec} + A_{0,1\,sec} + \dots + A_{n\,sec} \tag{4.7}$$

$$A = E_{0\,sec} + E_{0,1\,sec} + ... + E_{n\,sec}. \tag{4.8}$$

The numerical example of mechanical work, consumed energy and efficiency calculation is presented for quadcopter following the given parameters:

- *Motor* – BR2216-KV810;
- $\rho = 1.22$ kg/m³;
- $C_d = 1.05$;
- $A_{eff} = 0.25$ m²;
- $g = 9.81$ m/s²;
- $m = 1.5$ kg;
- $dt = 0.1$ s.

Example is shown for the following values of variables assuming these values are not changing:

- $F_{t1} = 7.16$ N – traction force of one motor;
- $P_1 = 133.63$ W – power of one motor;
- $F_t = 28.6$ N – traction force of 4 motors;
- $F_{gr} = 14.7$ N, P = 534.52 W;
- $E = 0.01485$ Wh in each time interval.

The part of 100m vertical integrated take-off is shown in the Table 2.

Table 2

The part of 100m vertical integrated take-off

t [s]	0	0.1		15.5	15.6
F_{ga}, [N]	0	0.28	....	13.93	13.93
F, [N]	13.93	13.65	....	0	0
A, [m/s^2]	0	9.28	....	0	0
V, [m/s]	0	0.93	....	6.59	6.59
S, [m]	0	0.09	....	99.48	100.14
N, [W]	0	26.59	....	188.85	188.85
A, [Wh]	0	0.00074	....	0.00525	0.00525

$$\sum A = A_{0\,sec} + A_{0,1\,sec} + ... + A_{n\,sec} = 0 + 0.00074 + 0.00146 + ... + 0.00525 = 0.79669 \text{ Wh;}$$

$$\sum E = E_{0\,sec} + E_{0,1\,sec} + ... + E_{n\,sec} = 0.01485 + 0.0148 + ... + 0.01485 = 2.316253 \text{ Wh;}$$

$$\eta = \frac{\sum A}{\sum E} = \frac{0.79669}{2.316253} = 0.344.$$

4.3.5. Research of the target function of the energy consumption of the train model

To research the target function of energy consumption for the electric train model, let's take a train with different masses of 4.1 kg, 9.6 kg and 19.3 kg and measure the energy and

different control signals C in the range from 100 to 255 on a straight section. The measurement results are shown in Fig. 4.33.
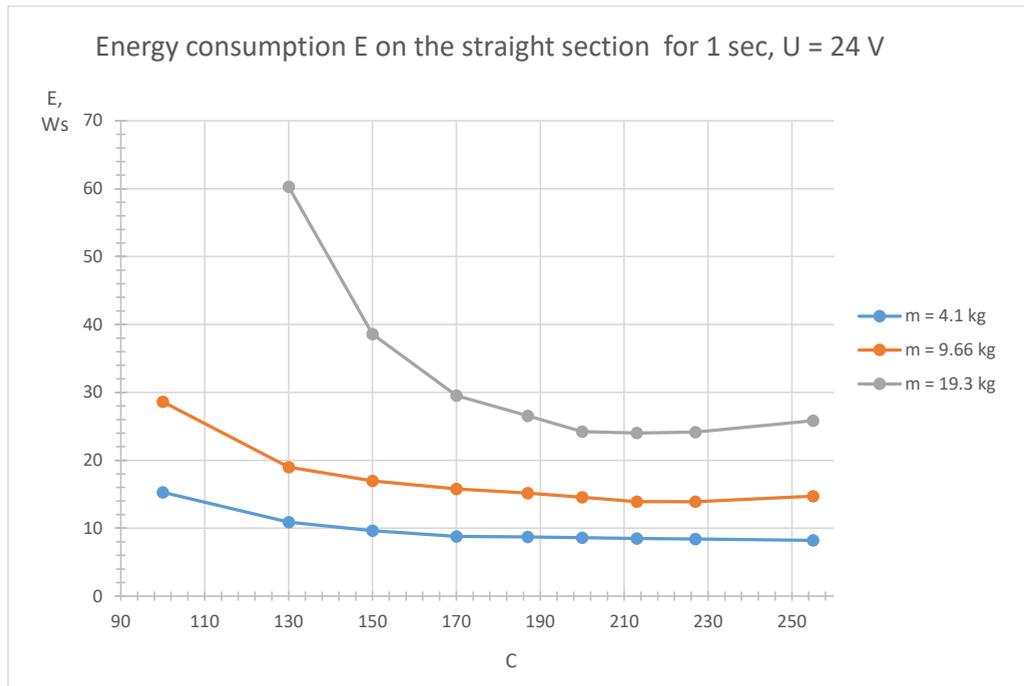
Fig. 4.33. Energy consumption of the electric drive with different control signals and with different masses of the train.

4.4. Development of computer models for verification of optimization methods

In this section, the lifting of a quadcopter with minimization of electronic energy consumption is modeled using the developed computer model [52], [53] and real-time optimization. The changes in control signal, acceleration, power, speed, and distance parameters are shown.

Experiments were conducted with two quadcopter configurations, varying in mass, wing area, aerodynamic coefficient, and different motors [25]:
– m = 1.5 kg, A_{eff} = 0.25 m^2, C_d = 1.06, and BR2212 920 kV motors
– m = 1.8 kg, A_{eff} = 0.24 m^2, C_d = 1.25, and BR2212 980 kV motors

The part of quadcopter computer model code is presented in Fig. 4.34. The part describes the computer and optimisation controller interaction to assess the ability of the microcontroller to perform the optimal control.

The microcontroller ATMEL328P is equipped with an adaptive algorithm for searching for optimal power consumption, and microcontroller output data control the propeller-motor pair of the test bench. The computer program [76] receives the signal from the sensor and simulates the flight, but only the vertical component of the flight at a given altitude S_t is used.

```
if (!ok && beg && t>=t1+1)
{
beg=0;
if (!e1) {c1=(E-e0)/(s-s1); c+=1;}
else
{
c2=(E-c0)/(s-s1);
cout << "Eprev=" << c1 << "\tEcur=" << c2 << end1;
if (c2>c1) {dc=-dc*0.5;}
if (abs(dc)<1)
{
Dc=dcmax; ok=1; t2=t;
cout << "Optimal throttle found!";
}
c+=dc;
if (ok) cout << " T = " << c << "%\n\n";
e1=e2;
}
}
```

Fig. 4.34. The part of quadcopter computer code.

Modelling of UAV take-off with adaptive algorithm

The experiment shows how the unified optimal algorithm performs the control of the UAV for the take-off motion.

Table 3 shows the parameters of the simulated quadcopter.

Table 3

Different Configuration Parameters of Quadcopters

N	Motor	m [kg]	A_{eff} [m^2]	C_d
1	BR2216KV810	1.3	0.24	1.05
2	BR2216KV810	1.6	0.25	1.1
3	BR2216KV810	1.9	0.26	1.15
4	BR2216KV810	2.2	0.27	1.2
5	BR2212KV920	1.3	0.24	1.05
6	BR2212KV920	1.6	0.25	1.1
7	BR2212KV920	1.9	0.26	1.15
8	BR2212KV920	2.2	0.27	1.2
9	BR2212KV980	1.3	0.24	1.05
10	BR2212KV980	1.6	0.25	1.1
11	BR2212KV980	1.9	0.26	1.15
12	BR2212KV980	2.2	0.27	1.2

The steps for implementing the general computer modeling algorithm of a quadcopter are as follows:

1) Initially, the calibration of the engine speed controller (ESC) is performed to determine the maximum and minimum values of the control signal. Typically, the control signal is a PPM signal with a pulse length ranging from 1000 μs to 2000 μs. After calibration, the maximum pulse length of the control signal is 2000 μs, and the minimum pulse length is 1000 μs.

2) Next, the motor speed is increased gradually by increasing the control signal starting from the minimum value to determine the control signal at which the quadcopter takes off. This can be determined using the barometric altitude sensor, acceleration sensor, satellite navigation separately or collectively. The control signal is set so that the minimum and lower signal values are not used in the process of searching for optimal energy consumption. This is necessary to avoid the quadcopter stalling or falling due to the thrust force being less than the gravitational force.

3) Subsequently, an algorithm for searching optimal values is executed, which searches for a control signal that minimizes the energy consumption according to the defined search criteria and methodology. Measurement of search parameters is performed at stabilized motion (speed) values where the acceleration is close to 0. A timer is activated to count a specified time, while energy consumption and distance measurements are taken simultaneously.

4) When the specified time (or distance) for achieving sufficient energy consumption calculation is reached, a decision is made regarding increasing or decreasing the control signal.

5) Steps 3 and 4 are repeated until the control signal with the minimum energy consumption is found.

6) After a certain time, the algorithm checks the presence of the optimal control point, and if it is not optimal, the process repeats from step 3.

4.4.1. Modeling the optimal control of the quadcopter using the uniform search method

In Figure 4.35, it can be seen that after stabilizing the speed value v, when the acceleration a is approximately equal to 0, the algorithm searches for the minimum energy consumption by increasing the control signal c.

c – electric drive control signal, varying from 0 to 100 %.
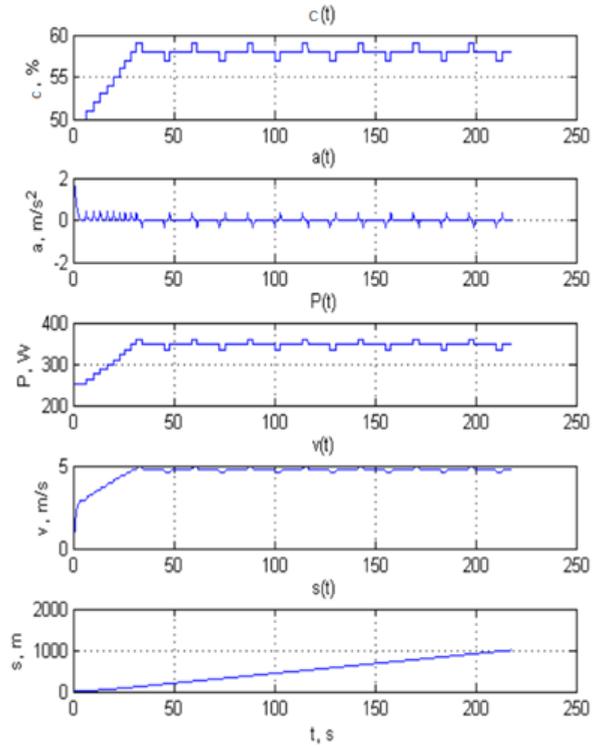
Fig. 4.3. Dynamics of control signal c, acceleration a, power P, velocity v and path s using the uniform search algorithm.

When the power consumption value becomes the worst, the algorithm stops and returns to the previous value of c, which was the best. Every 10 seconds, the algorithm rechecks to be at the optimal point. It can be seen from the graphs that the optimal speed is 5 m/s, it is maintained relatively smoothly and the path length s to the target point also varies smoothly. The power P varies in proportion to the control signal.

In Fig. 4.36 the final result of computer simulation for UAV control using the uniform search method.

Fig. 4.4. The result of the operation of the uniform search algorithm.

It took 217.34 s to reach a given target point and the electricity consumption is 20.5015 Wh.

4.4.2. *Modeling the optimal control of UV with halving algorithm*

In Figure 4.37 it can be seen that this algorithm converges to the target value faster. It can be seen from the graphs that the optimal speed is still around 5 m/s, it is also maintained relatively smoothly and the path length s to the target point also varies smoothly. The power varies in proportion to the control signal.
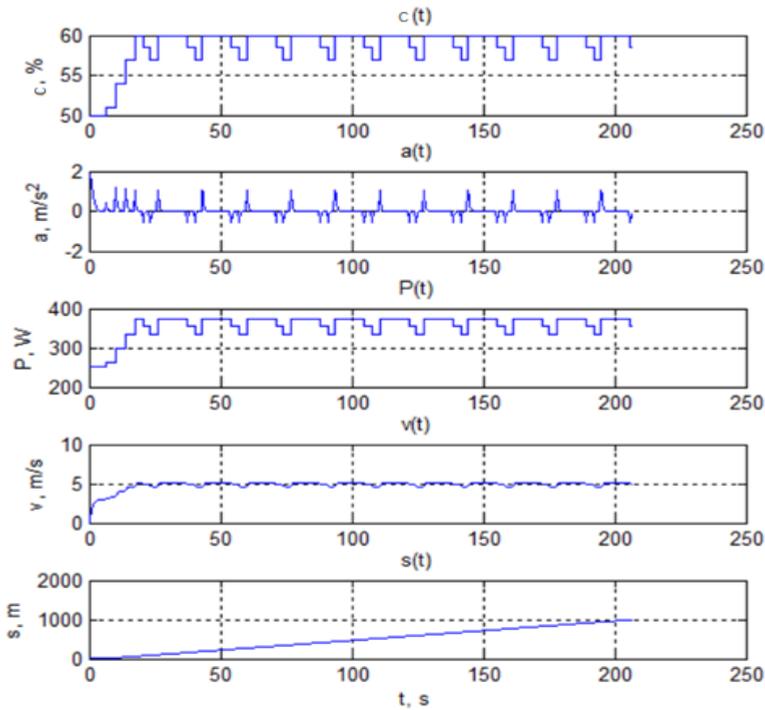
Fig. 4.5. Dynamics of control signal c, acceleration a, power P, velocity v, and path s with halving algorithm.

In Figure 4.38 shows the final result of computer modeling for UV control with halving algorithm.

Fig. 4.6. The result of the operation of the halving algorithm.

It took 207.14 s to reach a given target point and the electricity consumption is 20.502 Wh.

4.4.3. Optimal control of UV using the backtracking algorithm on unsuccessful step

In Figure 4.39, it can be observed that the changes in the control signal occur unevenly due to the random nature of the algorithm's steps. As a result, the motion speed is unstable and constantly fluctuating, although it eventually reaches 5 m/s. However, the distance s to the target point changes uniformly. The power changes proportionally to the control signal.
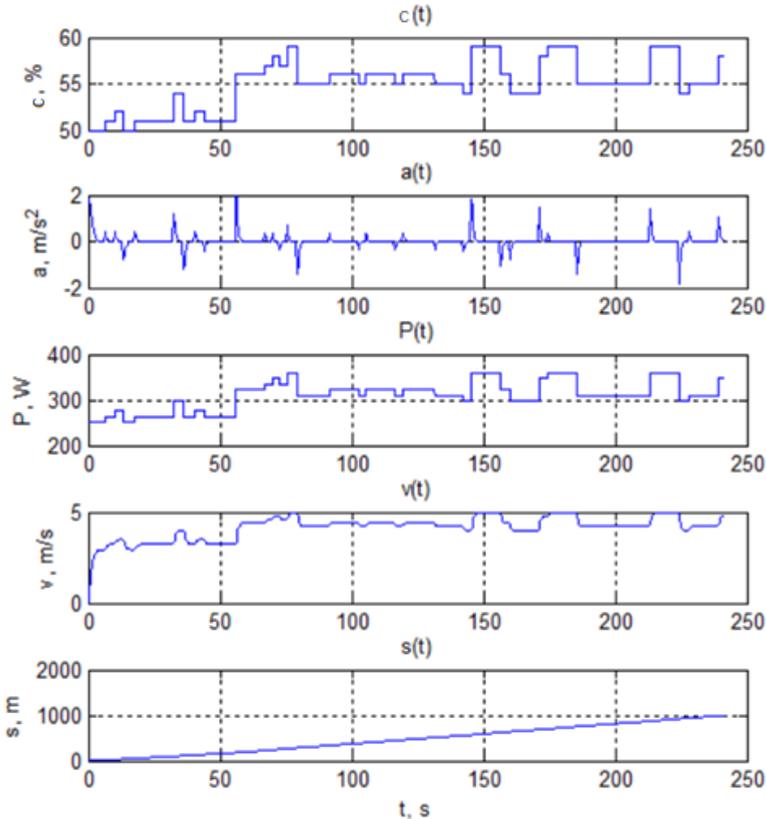
Fig. 4.39. Dynamics of control signal c, acceleration a, power P, velocity v and path s using the backtracking algorithm on unsuccessful step.

Figure 4.40 the performance results using the backtracking algorithm on unsuccessful step are shown. Considering the random nature of the algorithm, 10 repeated simulations were performed and the average energy consumption and average movement time were calculated.

Fig. 4.40. The result of the operation of the algorithm using the backtracking algorithm on unsuccessful step.

On average, it took 228.859 seconds to reach the target point, and the average energy consumption was 20.6813 Wh from 10 attempts.

4.4.4. *Optimal control of UV with repeated random search algorithm*

Figure 4.41 it can be seen that the change of the control signal is also uneven because the steps of the algorithm are random, but with the smallest range of changes because the algorithm keeps the search direction and repeats the successful attempt. Then you can see that speed maintenance is more stable than the algorithm with return. Similarly, as for the other algorithms, the path length s to the target point changes relatively evenly and the power changes proportionally to the control signal.
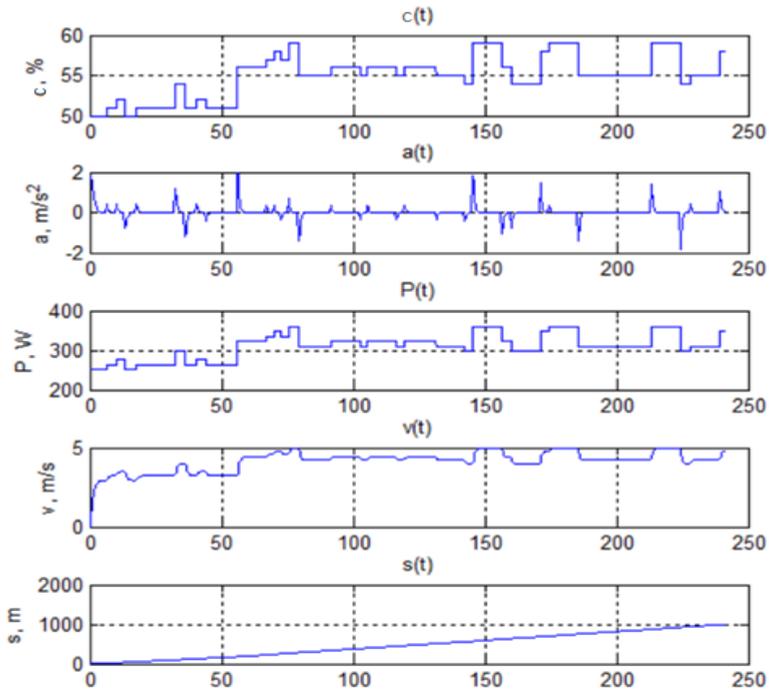
Fig. 4.41. Dynamics of the control signal x, acceleration a, power P, velocity v, and path s
with a repeated random search algorithm.

In Figure 4.42, the results of the random search repetition algorithm are shown. Considering the stochastic nature of the algorithm, 10 repeated simulations were performed, and the average energy consumption and average duration of motion were calculated.

Fig. 4.42. The result of the operation of the repeated random search algorithm.

It took an average of 218.17 s to reach a given target point, with an average electricity consumption of 20.481 Wh from 10 attempts.

Results Comparison

The algorithms in the results comparison are denoted as follows:

– Algorithm 1: Uniform search method (deterministic)
– Algorithm 2: Halving method (deterministic)
– Algorithm 3: Backtracking on unsuccessful step method (stochastic)
– Algorithm 4: Random search repetition method (stochastic)

The algorithms are compared under the condition where the optimal value of the control signal is known in advance.

For a quadcopter with the following parameters: m = 1.5 kg, A_{eff} = 0.25 m², C_d = 1.06, and BR2212 920 kV motors, the results of algorithm operations are summarized in Table 4.

Column q in the table represents the algorithm results compared to the known optimal value of energy consumption.

Table 4

Experimental results for a quadcopter with m = 1.5 kg, A_{eff} = 0.25 m², C_d = 1.06, BR2212 920 kV motors

	Energy consumption	Time	Time first solution detection distance	Deviation from optimal value
	E [Wh]	t [s]	S_{def} [m]	q [%]
Optimal value	20.344	210.59	-	0%
Algorithm 1	20.5015	217.34	128.01	-0.77%
Algorithm 2	20.502	207.14	100.83	-0.78%
Algorithm 3	20.6813	228.86	58.5	-1.66%
Algorithm 4	20.481	213.98	264.66	-0.67%

For another quadcopter with parameters: m = 1.8 kg, A_{eff} = 0.24 m², C_d =1.25 and motors BR2212 980 kV the obtained algorithm performance results are summarized in Table 5.

Table 5

Experimental results for a quadcopter with m = 1.8 kg, A_{eff} = 0.24 m^2, C_d = 1.25
BR2212 980 kV motors

	Energy consumption	Time	Time first solution detection distance	Deviation from optimal value
	E [Wh]	t [s]	S_{def} [m]	q [%]
Optimal value	27.2302	193.46	-	0%
Algorithm 1	29.3586	235.2	233.18	-7.82%
Algorithm 2	28.9652	214.32	164.35	-6.37%
Algorithm 3	30.2893	265.04	113.74	-11.23%
Algorithm 4	28.2928	211.45	165.94	-3.90%

The results show that all algorithms are capable of finding the optimal target function value of the energy minimization of control signals with different efficiency.
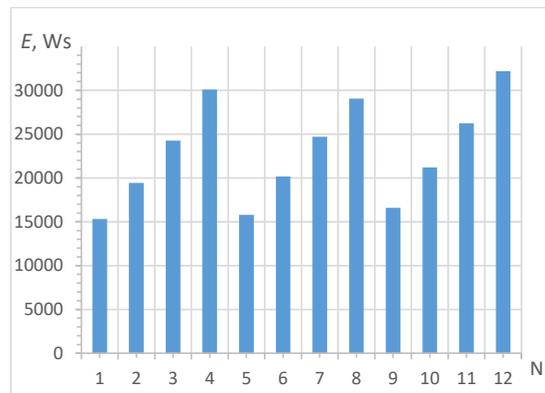
Fig. 4.43. Energy consumption for different quadcopters with an optimisation algorithm for 1000 m flight.
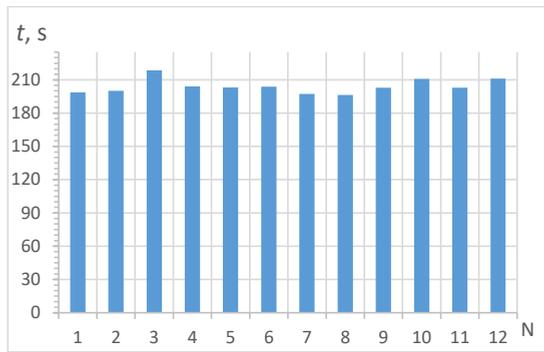
Fig. 4.44. Time spent for different quadcopters with an optimisation algorithm for 1000 m flight.
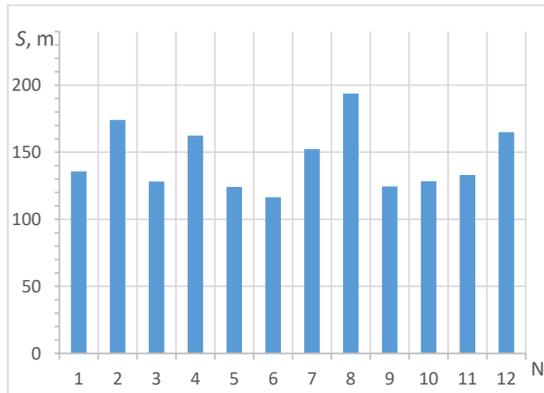
Fig. 4.45. The altitude at which the optimisation algorithm finds the optimal power consumption.
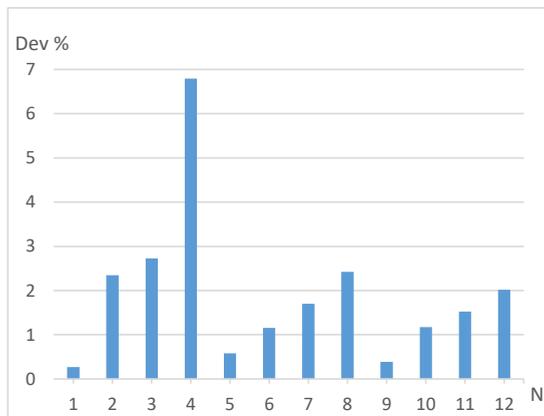
Fig. 4.46. The difference in power consumption when the optimisation algorithm is running.

Figures 4.43, 4.44, 4.45 and 4.46 show the results of experiments with different motors and quadcopter configurations.

Results show that the algorithm [45], [46], [47] is able to find an optimal solution in all cases. The search for an optimal solution needs time and it depends on the quadcopter mass. However, in practice, it is impossible to know the optimal value at the beginning of the control process due to different factors of the UAV and its environment. Therefore, it is necessary to adapt the control to these factors and minimise the energy consumption all the time during the flight.

The main tasks of research have been fully completed: UAV control system with adaptive controller has been developed; the target function of energy consumption has been defined, the optimal control algorithm has been created and successfully tested on the real traction drive testbench and the software model.

The developed optimisation algorithm generates the optimal control signals in the shortest time – 196.36 s and over the largest distance – 193.69 m with motor mass 2.2 kg, effective area 0.27 m^2 and drag rate 1.2 (configuration No. 8). The longest time 218.46 s till optimal control signals are reached is spent by the quadcopter with motor mass 1.9 kg, effective area 0.26 m^2 and drag rate 1.15 (configuration No. 3). The quadcopter with motor mass 1.6 kg, effective area 0.25 m^2 and drag rate 1.1 (configuration No. 6) travels the shortest distance until the optimal control signals are found – 116.43 m. The lowest power consumption 15317.7 Ws is provided with motor mass 1.3 kg, effective area 0.24 m^2 and drag rate 1.05 (configuration No. 1), but the highest power consumption 32178.7 Ws is provided with motor mass 2.2 kg, effective area 0.27 m^2 and drag rate 1.2 (configuration No. 12). It proves that the energy consumption to take-off at the altitude of 1000 m increases almost linearly as mass and area of the quadcopter increase independently of different motors, but the altitude when the algorithm finds the optimal control signal changes randomly. The smallest deviation of 0.26641356 % from the optimal control signal is shown by the quadcopter with motor mass 1.3 kg, effective area 0.24 m^2 and drag rate 1.05 (configuration No. 1).

The proposed adaptive algorithm can claim for versatility and be used in various types of unmanned electric vehicles – quadcopters, airplanes, trains, etc., as well as in man-driven vehicles in autopilot mode. The design feature of the optimisation controller requires minimal intervention in the vehicle control system.

The time to find the optimal energy-saving control signal using the proposed algorithm does not affect the total amount of energy consumption.

4.4.5. *Searching the optimal control signal for the railway*

The search is conducted using a uniform search algorithm with different values of the control signal – C.

C – electric drive control signal using PWM, varying from 0 to 255.

The control signal step change - from 5 to 30, and a signal change distance ranging from 0.3 to 5.5 meters. The table and graphs display the results of the energy consumption measurement experiment using the uniform search algorithm for a combination of C control signal step change of 15 and a signal change distance of 5.5 meters, which demonstrated the lowest energy consumption at a power supply voltage of 24 V.

The dynamics of the control signal of the uniform search algorithm are shown in Fig. 4.47. The dynamics of dE/dS of the uniform search algorithm are shown in Fig. 4.48. The dynamics of the energy consumption of the uniform search algorithm are shown in Fig. 4.49.

The dynamics of the train's movement speed using the uniform search algorithm are shown in Fig. 4.50.
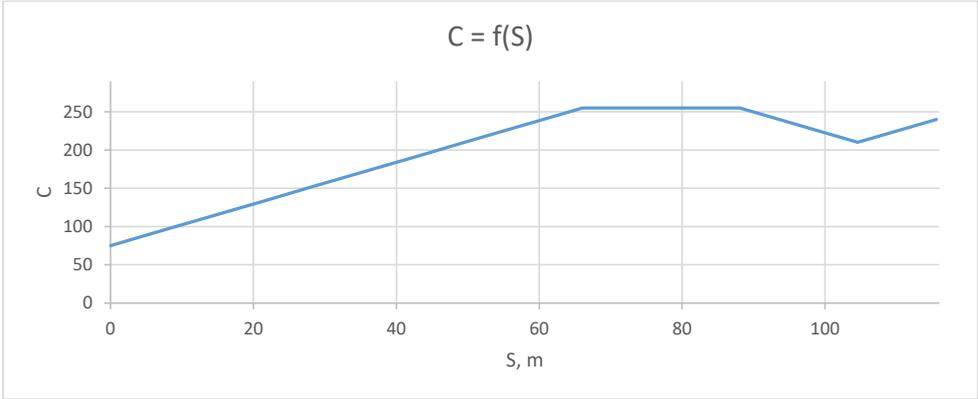
Fig. 4.47. Control signal dynamics of the uniform search algorithm.
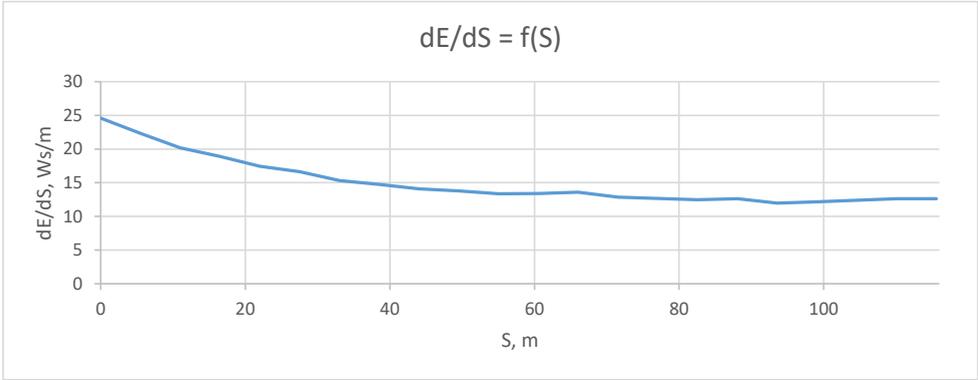
Fig. 4.48. Dynamics dE/dS of the uniform search algorithm.
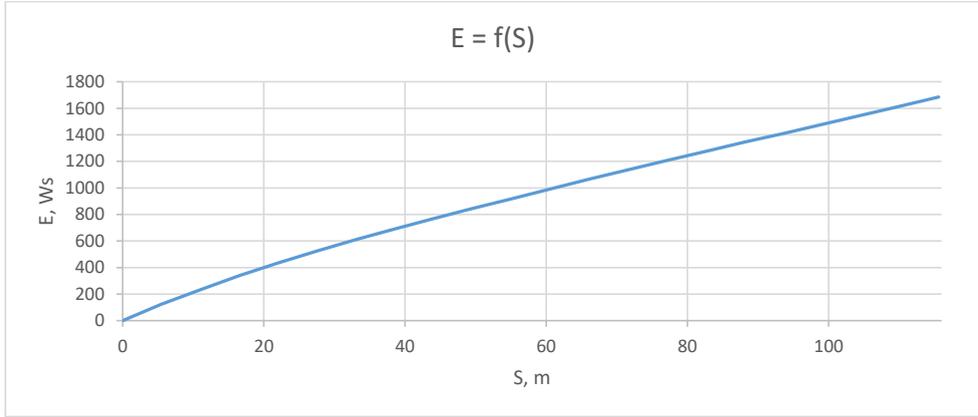
Fig. 4.49. Energy consumption dynamics of the uniform search algorithm.
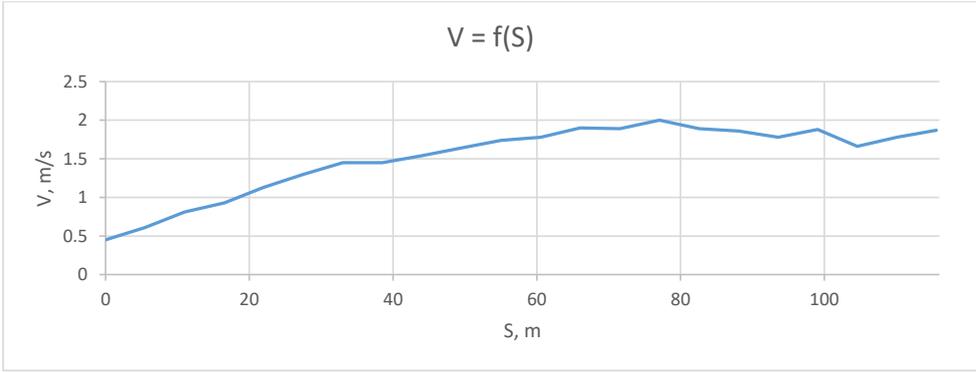
Fig. 4.50. Speed dynamics of the uniform search algorithm.

The energy consumption dynamics of an electric train with a constant control signal C = 255 and a uniform search algorithm for a distance traveled of 115 meters is shown in Fig. 4.51.
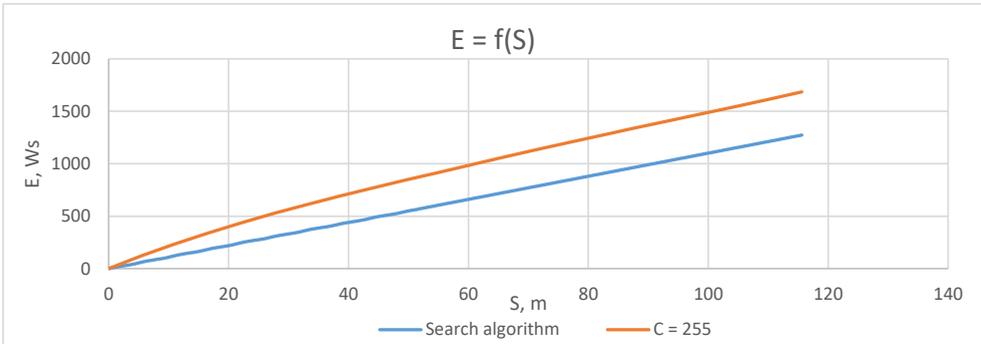
Fig. 4.51. Energy consumption dynamics of an electric train with a constant control signal and C = 255 and a uniform search algorithm.

From the dynamics of the control signal graph, it can be observed that the signal gradually increases until reaching its maximum value. However, due to the changing nature of the load, the minimum search algorithm fails to find the optimal control signal. The value of dE/dS decreases with an increase in the control signal value and approaches optimal values. Energy consumption (E) increases with the distance covered. The speed varies depending on the control signal changes and the nature of the load (straight section or turn).

From previous measurements, it is known that a train with a mass of 4.6 kg has the lowest energy consumption for a complete circuit of movement when driven with a constant signal C = 255, compared to other signals. From the graph, it can be observed that the minimum search algorithm consumes more energy than a single constant signal on all sections of the path. Therefore, the minimum search algorithm consumes more energy in the search for minimal energy consumption and cannot find the optimal control signal under such load variation.

Based on the experimental results with the train, it is evident that there is no definitive optimal signal, and the search algorithm fails to find it in time. It is necessary for the system to learn to immediately output the required control signal. The proposed solution is a neural network that requires data for training.

Due to legislative restrictions applied to aerial vehicles, experiments with quadcopters are not conducted. Further experiments will be carried out on a train model.

4.5. Analysis of data for creating a training set

Estimation of load characteristics for use in a neural network

In this experiment, the energy consumption characteristics were measured for different train masses, with different control signals, and on different sections of the track.

To do this, we measure the energy value dE measured at different sections when a train passes one circle of the experimental road. Figure 4.52 show the energy consumption characteristic dE/dS during the train's one complete circuit. The graph includes values with calculated moving averages. Moving averages are used because instantaneous values exhibit significant fluctuations.

Designations:

dS – distance for measuring consumed energy, m;

dE – energy consumed per distance traveled per dS, Ws.

Hypothesis: It is possible to assess the load characteristics at each point on the track independently of the control signal and movement speed.
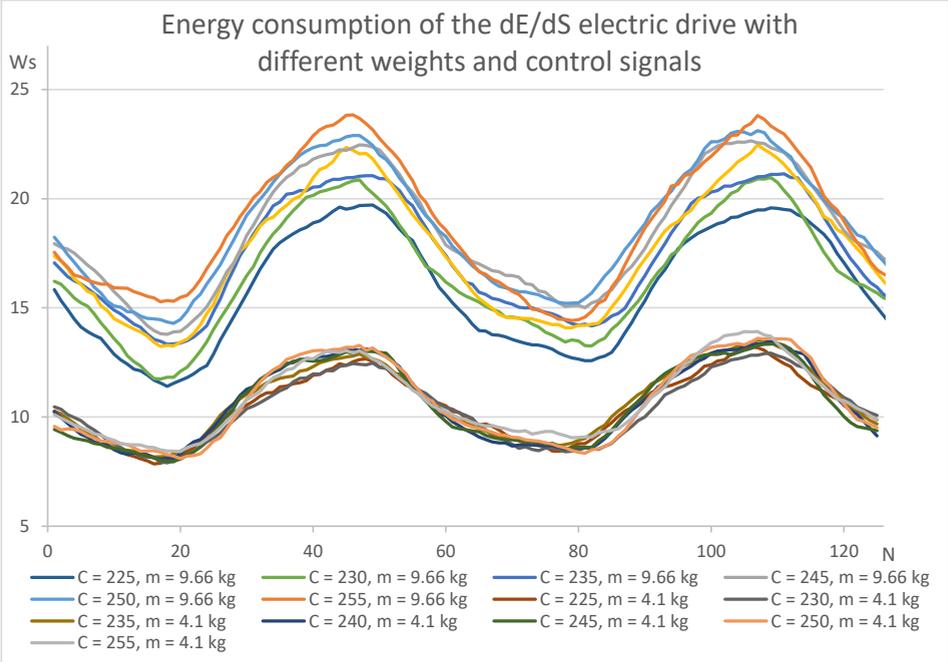
Fig. 4.52. Characteristic of energy consumption dE/dS when the train travels one circle. With train masses m = 4.1 kg and m = 9.6 kg.

It can be seen from the energy consumption graph that for different masses of a train in the same sections, energy consumption will differ.

Let's calculate a value that describes the nature of the load - LC = Summa(V2/V1). This will be the last n floating average of the ratio of the current floating average speed V2 to the previous floating average speed V1 over the last n samples. The floating average is needed for smoothing.

Let's calculate the LC values for a train with a mass of m = 4.1 kg and 9.6 kg for all sections of the road. In order to see how the nature of the load looks like on different sections of the road, we will build a graph in Fig. 4.53, from the calculated LC values for the speed values.
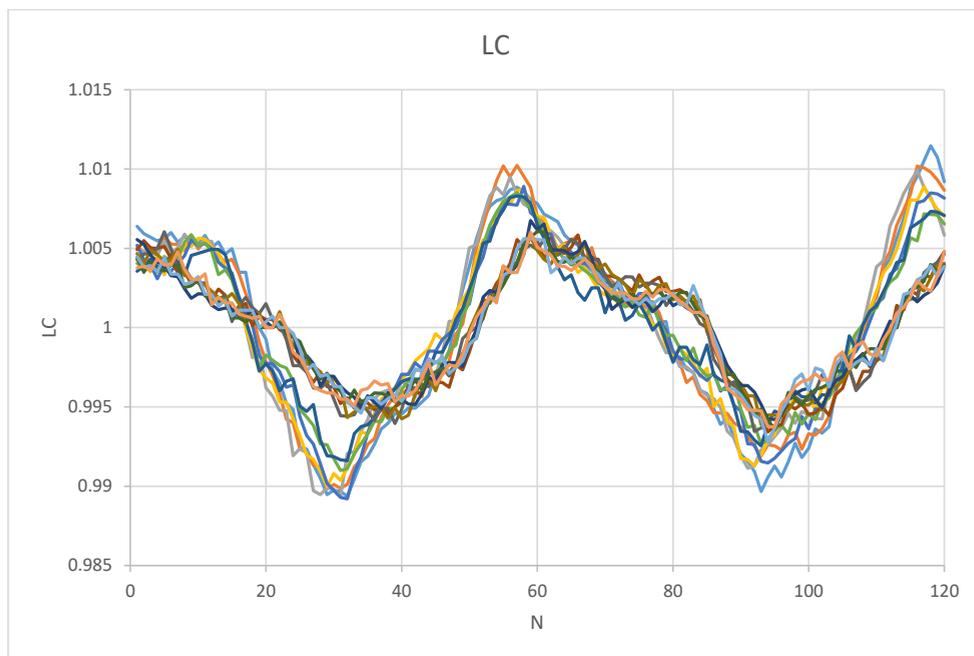
Fig. 4.53. The load characteristics (LC) for a train mass of m = 4.1 kg and m = 9.6 kg.

On the graph, it can be observed that for different masses, the LC curves intersect at certain points. During the train's movement, the track may have a negative or positive slope, thereby changing the load as if the train's mass has increased. To differentiate the nature of the effective mass, let's analyze the energy consumption and speed values at all possible sections of the track. When the speed decreases, the LC parameter is less than 1, indicating an increased load. Conversely, when the speed increases, the LC parameter is greater than 1, indicating a decreased load (with a constant control signal).

This value will serve as an auxiliary (primary) element for determining the track section.

Thus, the hypothesis that the load characteristics can be assessed at each point on the track independently of the control signal and movement speed is confirmed.

4.6. Checking the automatic training set generation algorithm

The train passes through different sections of the track using a single control signal while recording the values of LC, speed, control signal, and dE/dS for each section. This process continues until all the new sections are covered. Then, the control signal is increased, and the process described above is repeated. The energy consumption values are also compared, and this process continues until all control signals have been tested and the minimum dE/dS value is found for each section. The control signal corresponding to the minimum dE/dS becomes the optimal signal for that particular section of the track. The obtained values are recorded in the training set (TS).

The dynamics of the control signal C are shown in Fig. 4.54. The dynamics of energy consumption dE/dS are shown in Figure 4.55. The dynamics of consumed energy E are shown in Fig. 4.56. The dynamics of forming the training set LQ are shown in Fig. 4.57.
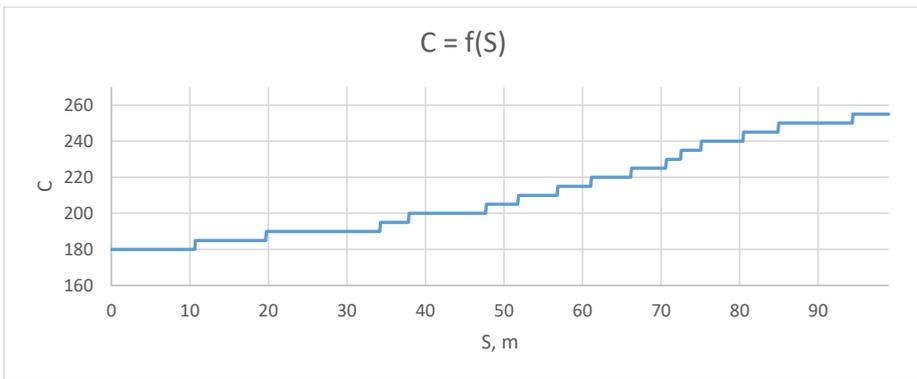
Fig. 4.54. Dynamics of control signal C.
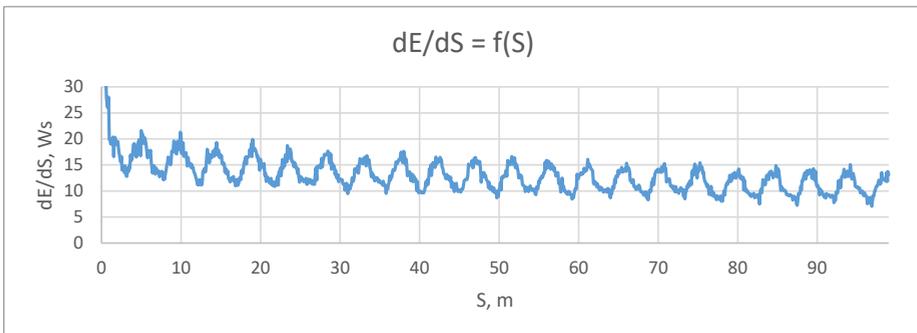
Fig. 4.55. Dynamics of energy consumption dE/dS.
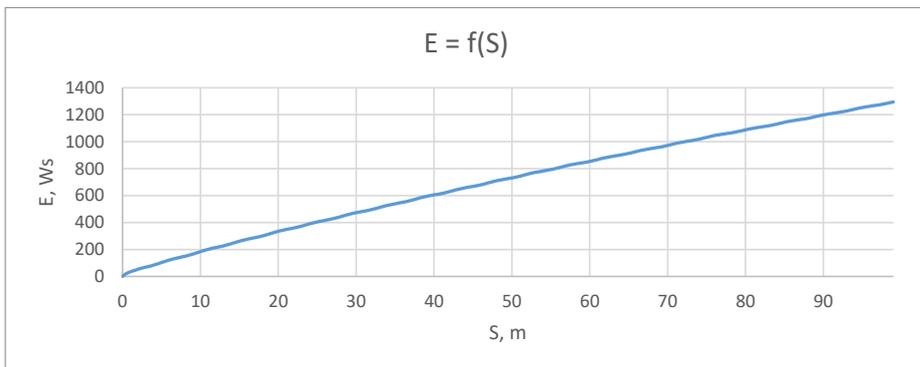
Fig. 4.56. Dynamics of consumed energy E.
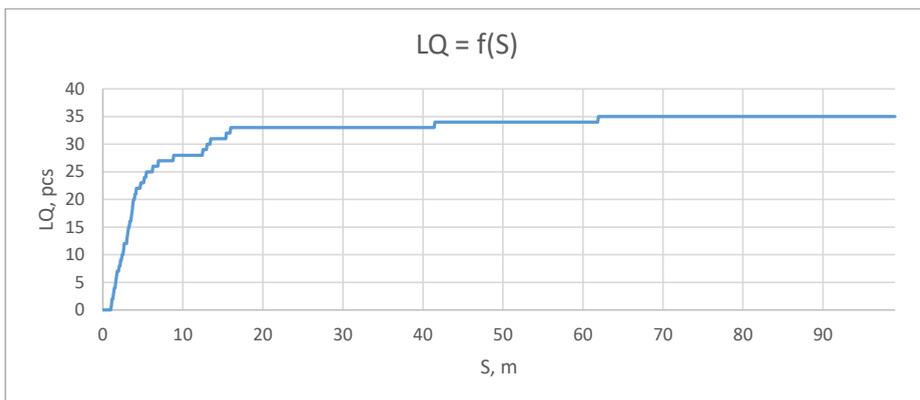
Fig. 4.57. The dynamics of the formation of the training set LQ.

The dynamics of the control signal C = f(S) and the quantity of the training set LQ = f(S) show that the train covers different distances on different control signals, i.e., the formation of the training set is not proportional to the distance traveled. Initially, the formation of the training set occurs faster and then slows down. As the control signal increases, there is a trend of decreasing instantaneous energy consumption.

4.6.1. *Training Set Data for Neural Network Training*

As a result of the experiment, the automatic training set generation algorithm created a training set for the neural network. Table 6 show the data of the training set.

Table 6

The fragment of the set created by the algorithm for automatic formation of the training set

N	LC	dE/dS [Ws]	V [m/s]	C_{opt}
1	0.978	12.163	1.0087	125
2	0.9792	13.4834	0.9797	130
3	0.9804	12.5585	1.0623	145
4	0.9817	12.5003	1.1155	145
5	0.9833	10.9373	1.4216	195
6	0.9846	9.607	1.4249	240
7	0.9857	9.4675	1.4282	195
8	0.9872	9.8068	1.5093	240
9	0.9887	9.5983	1.5093	190
10	0.9904	8.8142	1.5093	245
11	0.9924	9.4259	1.5069	180
12	0.9936	8.509	1.5081	250
13	0.9954	8.554	1.5118	200
14	0.9964	7.6106	1.6966	250
15	0.9974	7.2325	1.7044	250
16	0.9991	7.5731	1.7028	250
17	1.0003	6.7892	1.7028	240
18	1.0015	8.0456	1.717	240
19	1.0026	7.1304	1.7028	250
20	1.0037	8.0525	1.5106	250
21	1.0056	7.7383	1.7028	250
22	1.0072	8.1027	1.5381	240
23	1.0088	8.4651	1.7028	130
24	1.0108	7.9226	1.7411	240
25	1.0119	9.0005	1.7028	190
26	1.0129	9.5188	1.6369	245
27	1.0144	9.0076	1.7044	190
28	1.0157	8.838	1.5167	230
29	1.0173	9.6273	1.706	250
30	1.0196	11.4073	1.1724	135
31	1.0211	11.0061	1.278	130
32	1.0222	9.39	1.6354	245
33	1.0265	15.4454	0.8697	120
34	1.028	14.427	0.8134	120
35	1.0313	16.4004	0.8166	120
36	1.0337	18.3221	0.8117	120
37	1.0392	16.3754	0.8133	120

C_{opt} – the optimal control signal found by the minimum search algorithm for a section of track or the nature of the load LC

The algorithm for automatic creation of a training dataset for the neural network found optimal values of control signals for 35 road sections with varying load characteristics, covering a distance of 62.2 m.

4.7. Optimal structure of the neural network and training parameters

Computer simulation was conducted to select the optimal structure of the neural network [44] and training parameters for finding the optimal solution.

Computer simulation is:

- Simulation of vertical flight of a quadcopter, in order to obtain data for training a neural network
- Developed a neural network with different parameters
- Neural network calculations
- Neural network training

The parameters of the computer that performed the calculation:

- CPU- Intel Core i5 – 4460, 3.2 Ghz
- RAM – 8 Gb
- OS- Windows 7, 64 - bit.

Training NN was carried out on the data obtained during the simulation of the vertical takeoff of a quadrocopter with different masses, area, and drag coefficients. Results obtained with a neural network with 12 neurons, two inputs, one output, $\rho = 0.005$, the number of iterations – 102400, only fig.4.59 on which the number of neurons changes.
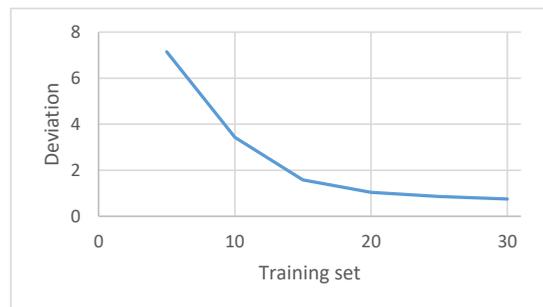
Fig. 4.58. Dependence of the accuracy of the neural network results on the number of the training set.
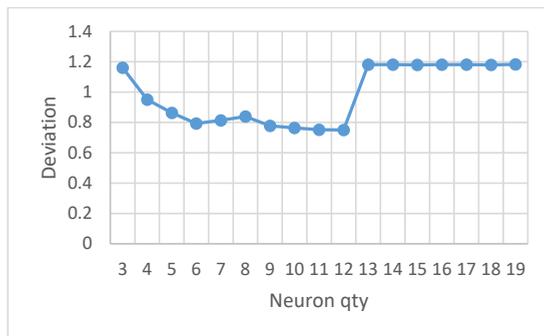
Fig. 4.59. Dependence of the error on the number of neurons.
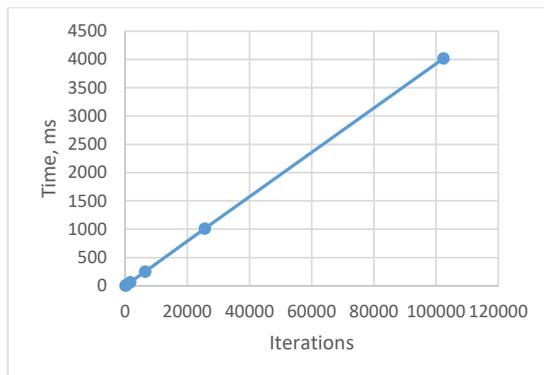
Fig. 4.60. Error depending on the number of iterations at $\rho = 0.005$.
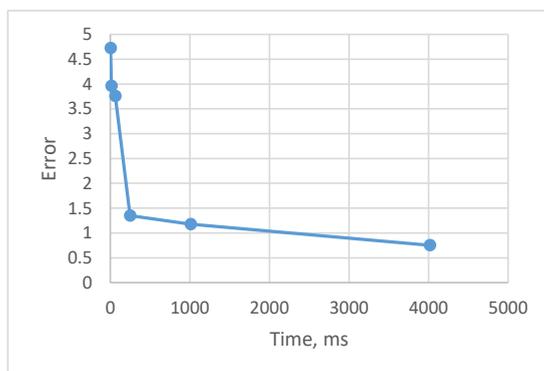
Fig. 4.61. Computation accuracy versus computation time.

When analyzing the results obtained, these parameters provided the best results of neural network calculations, excluding the time required for calculations. The obtained graphs show that the larger the training set, the number of iterations and the longer the training time, the more accurate the result obtained, the error decreases. However, there is no such dependence

for the number of neurons, and the number of neurons in the neural network will depend on the nature of the nonlinearity of the training set.

The experimental results show that the larger the training set, with the optimal parameters of the NN the calculation results are more accurate (the size of the training set is in the range from 5 to 30, Fig.4.58). The best accuracy is a deviation of 0.7503, the neural network produces with 12 neurons (Fig.4.59). With optimal parameters, an exponential dependence of the computation accuracy on the number of iterations on Fig. 4.60 is seen. The accuracy of the calculation is also affected by the time (Fig. 4.61). It takes 4017 ms to get the smallest deviation from the 0.752251 result. Based on the results obtained, we can conclude that the parameters of the NN it is necessary to choose based on priorities and tasks, finding compromises between calculation accuracy and speed.

4.8. Selection of parameter settings for the developed algorithm

Now, using the trained neural network, we will investigate and select the values of dS and the type of velocity input to be used for the neural network - instantaneous or average. To do this, we will conduct a series of experiments with different values of dS in combination with the average velocity and instantaneous velocity, with U = 28 V.

For each combination, the experiment was repeated 8 times, and the train traveled a distance of 115 m in each experiment. The measurement results are shown in Table 7.

Table 7

Energy consumption when operating different search algorithms and a constant control signal at different values of dS, average speed and instantaneous speed at voltage U = 28 V

		U = 28 V							
	C_{const}	Developed self-learning algorithm							
	-	V_{avg}	V_{mom}						
dS	-	0.25	0.25	0.5	1.0	1.5	2.5	3.5	5.5
Emax	1420.1	1389.2	1364.0	1376.3	1451.3	1484.8	1475.5	1507.2	1543.3
Emin	1410.5	1362.2	1307.2	1345.6	1344.7	1370.9	1396.2	1423.3	1407.0
Eavg	1415.3	1372.2	**1335.6**	1361.0	1398.0	1427.8	1435.8	1465.3	1475.1

Designations in the table:

Developed self-learning algorithm – developed self-learning optimal algorithm with a neural network;

dS – step of energy measurement and control signal C change, m;

V_{mom} – instantaneous value of measured speed, m/s;

V_{avg} – average speed over distance dS, m/s;

Emin – the minimum amount of energy consumed to travel 115 meters in a series of 8 experiments, Ws;

E_{max} – the maximum amount of energy consumed to travel 115 meters in a series of 8 experiments, Ws;

E_{avg} – average energy consumed to travel 115 meters in a series of 8 experiments, Ws;

$C_{const} = 255$.
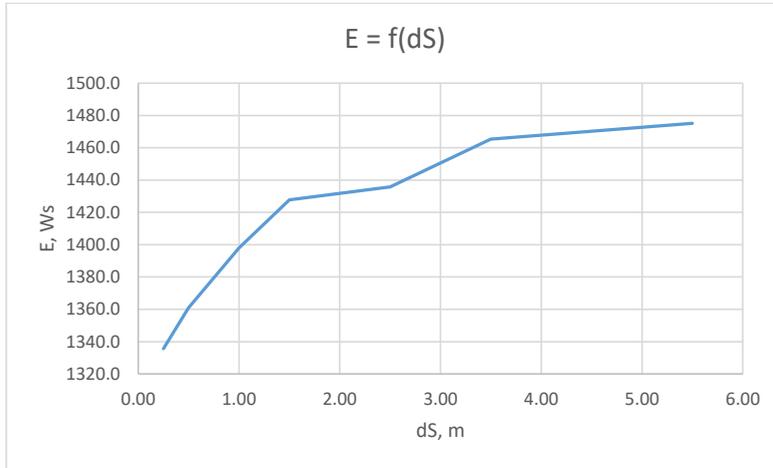
Fig. 4.62. Energy consumption of the train's electric drive depending on the measurement step and changes in the optimization algorithm.

From the graph in Fig. 4.62, it can be observed that there is a trend of increasing energy consumption with an increase in the measurement step dS. The lowest consumption using the developed algorithm is achieved at 28 volts with dS = 0.3 m and using the instantaneous velocity value. It was noticed that the overall energy consumption (relative to the work done) increases when the voltage is set to 28 V compared to 24 V. It was assumed that the motor is designed for a voltage of 24 V, and the decision was made to continue the experiments using 24 V voltage.

4.9. Analysis of developed self-learning algorithm results

The chapter presents the results of experiments for a constant control signal C with the lowest energy consumption (in the range from 60 to 255), an algorithm for finding the minimum with the best value based on the results of previous measurements, and a developed algorithm for learning optimal energy consumption using a neural network at a voltage of 24 volts.

In Fig. 4.63, the dynamics of the control signal C are displayed, while Fig. 4.64 shows the dynamics of the train speed. Figure 4.65 show the dynamics of dE/dS for the train, and Fig. 4.66 illustrates the energy consumption E per distance traveled when applying the developed algorithm for optimal energy consumption.

From the dynamics of the control signal graph, it can be observed that the signal quickly reaches the target value and changes according to the load characteristics. The speed V varies depending on changes in the control signal and the load characteristics. The energy consumption E increases with the distance traveled.
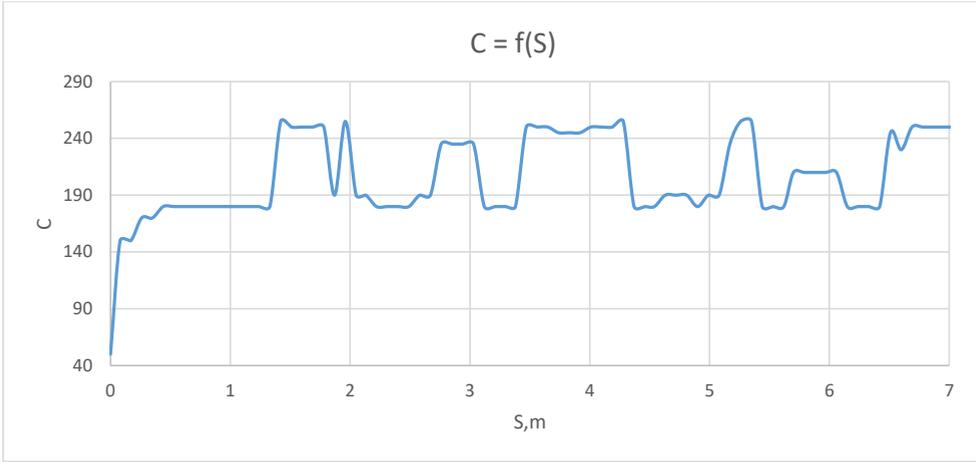
Fig. 4.63. The dynamics of the control signal of the developed algorithm can be observed in the graphs.
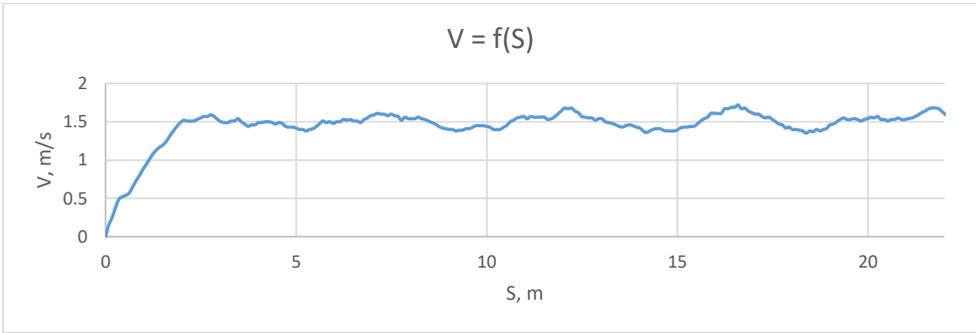
Fig. 4.64. The dynamics of the train speed when applying the developed algorithm.

115
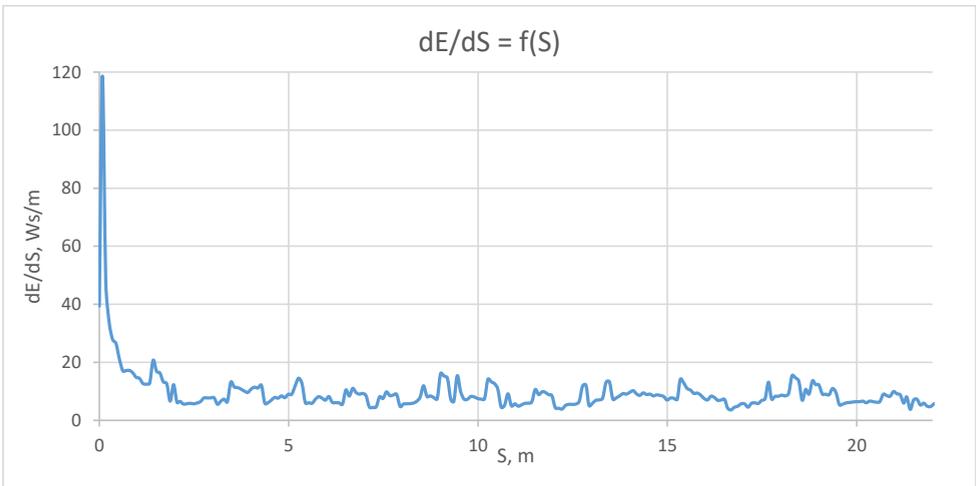
Fig. 4.65. The dynamics of dE/dS for the train electric drive when applying the developed algorithm.
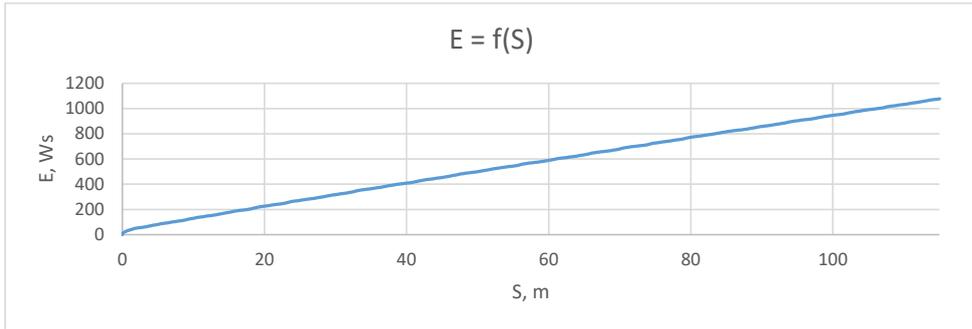
Fig. 4.66. The dynamics of energy consumption by the train's electric drive system when using the developed algorithm can be observed.

From the graph, it can be seen that the control signal quickly reaches the desired value and changes according to the load characteristics. The speed V varies depending on the changes in the control signal and the load characteristics. Energy consumption E increases with the distance traveled [83], but relative energy consumption dE/dS decreases during the self-learning process.

Table 8 shows the energy consumption values for a constant control signal C with the lowest energy consumption (in the range from 60 to 255), the algorithm for finding the minimum with the best value based on the results of previous measurements, and the developed self-learning algorithm for optimal energy consumption with a neural network. 8 series of experiments were carried out for each algorithm and in all experiments the train traveled a distance of 115 m, which is approximately 10 laps of the experimental railway.

Table 8

Energy consumption when operating different search algorithms and a constant control signal at different values of dS, average speed and instantaneous speed at voltage U = 24 V

	U = 24V					
	C_{const}	MSA	Developed self-learning algorithm			
	-	-	V_{avg}		V_{mom}	
	-	-	0.3	1	0.08	0.3
Emax	1326.3	1799.6	1276.0	1267.3	1193.95	1335.1
Emin	1198.9	1475.41	1168.4	1208.3	1028.05	1154.6
Eavg	1237.1	1685.1	1219.4	1249.3	**1077.14**	1206.3

Designations in the table:

Developed self-learning algorithm – developed self-learning optimal algorithm with a neural network;

MSA - minimum search algorithm;

dS – step of energy measurement and control signal C change, m;

V_{mom} – instantaneous value of measured speed, m/s;

V_{avg} – average speed over distance dS, m/s;

E_{min} – the minimum amount of energy consumed to travel 115 meters in a series of 8 experiments, Ws;

E_{max} – the miximum amount of energy consumed to travel 115 meters in a series of 8 experiments, Ws;

E_{avg} – average energy consumed to travel 115 meters in a series of 8 experiments, Ws;

C_{const} – constant control signal = 255, experimentally proved as the best if keeping it unchanged.

From the Table 8, it can be seen that the developed algorithm for optimal energy consumption with automatic generation of the training set for the neural network shows the best result. With a parameter measurement step of 0.08 m and using instantaneous velocity, it consumed 1077.14 Ws. The worst performing algorithm was the minimum search algorithm, which consumed 1685.1 Ws. The usage of the developed method allowed for a reduction in energy consumption of the electric train model by 159.96 Ws or 12.93 %, compared to a constant control signal of C = 255.

4.10. Conclusions on the fourth chapter

The main results of the fourth chapter of the doctoral thesis are as follows:
- Experimental devices were developed and manufactured for testing:
  - Test bench
  - Quadcopter UAV
  - Model of a railway with an electric train
- Schemes of experimental devices and their operation principles are described.
- The characteristics of UV electric drives were investigated:
  - Quadcopter
  - Electric train model
- The neural network and training methods were studied, including a new algorithm for automatic generation of the training set
- Experiments were conducted to test the developed algorithms and the energy-efficient control method

Comparing the configurations of different parameters' influence on the nature of the target function, it can be concluded that the nature remains unchanged. The optimal energy consumption point shifts in the direction of increasing control signal with an increase in the mass of the UV. The UV area and aerodynamics do not affect the optimal value of the desired control signal but increase energy consumption. This suggests that the developed target function and algorithm will work equally well, adapting adaptively to different UV configurations: different engines and mass.

The computer model developed demonstrates that the energy consumption function for vertical ascent of the quadcopter with different motors has a unimodal nature, which facilitates the application of optimization for specific maneuver types. All four optimization algorithms defined in the study are capable of finding the optimal value of the target function with a deviation of 0.6 % - 1.6 % from the optimal value at lower mass, and 6.37 % - 11.23 % at higher mass on a straight section with constant load. However, considering the unimodal nature of the o target function, in the case of one-dimensional functions, i.e., when it is necessary to find the optimal value of only one control signal, it is recommended to use deterministic search algorithms as they provide the most stable optimization results, as demonstrated by the modeling results. Among the deterministic algorithms compared, algorithm 2 - the bisection algorithm - can be considered the most suitable. This algorithm allows finding the optimal control point in the shortest time and with the smallest deviation. Regarding the results of the train experiment, it is evident that there is no single optimal signal, and the search algorithm fails to find the optimal signals. The uniform search algorithm consumes 1685 Ws, which is 36.2 % more than when using a constant control signal of 255 throughout the entire distance of 115.59 m. Therefore, the minimum uniform search algorithm consumes more energy in the search for minimum energy consumption and cannot find the optimal control signal with such a change in load characteristics.

Data analysis for creating a training dataset has shown that at each point of the path, the load characteristics can be evaluated independently of the control signal and the velocity of movement.

The algorithm for automatic creation of a training dataset for the neural network found optimal values of control signals for 35 road sections with varying load characteristics, covering a distance of 62.2 m.

The experimental results on the selection of optimal parameters for the neural network show that the larger the training set, the more accurate the computed results are, given the optimal parameters of the neural network. The best accuracy is achieved with a deviation of 0.7503 and is produced by a neural network with 12 neurons. With optimal parameters, there is an exponential dependence of the computation accuracy on the number of iterations. The accuracy of the computations also depends on time. To achieve the smallest deviation from the result of 0.752251, it takes 4017 ms.

The results of experiments on the model of an electric train demonstrate that the method developed in the doctoral thesis allows for energy savings of up to 12.93 % for electric unmanned vehicles. Using a measurement step of 0.08 m and instantaneous velocity values, the algorithm developed consumed 1077.14 Ws to cover a distance of 115 m. In contrast, when moving with a constant control signal of C = 255, the energy consumption amounted to 1237.1 Ws.

CONCLUSIONS

1) A control structure for the UV and a self-learning optimization controller with a neural network have been developed for optimal energy consumption of electric unmanned vehicles.

2) A mathematical model has been developed to calculate the movement of the UV, allowing calculating optimal control parameters under uncertain conditions and simulating the movement of unmanned vehicles in three-dimensional space.

3) A mathematical model of a neural network has been developed for optimal energy-efficient control of electric transportation, enabling optimal control of the electric drive system.

4) A new algorithm for optimal energy-efficient control of the UV has been developed, consisting of a minimum search algorithm, an algorithm for automatic creation of a training set for the neural network and a neural network training algorithm, which includes procedures for adaptation, filtering, evaluation, and weight adjustment.

5) The considered minimum search algorithms allow finding the minimum energy consumption of the UV required to travel a given path.

6) The adaptive filtering algorithm can be used for training the neural network and unconditional weight optimization for optimal control of the UV.

7) Experimental devices for testing have been developed and manufactured, including a test stand, a quadcopter, and a model of a railway with an electric train.

8) The characteristics of the electric drives of the UV quadcopter and the electric train model have been investigated.

9) Comparing the effects of different parameter configurations on the nature of the target function, it can be concluded that the nature of the function remains unchanged. The optimal energy consumption point shifts in the direction of increasing control signal when the UV mass increases. The UV area and aerodynamics do not affect the optimal value of the control signal sought but increase energy consumption. This allows concluding that the developed target function and algorithm work equally well, adapting to different UV configurations: different motors and mass.

10) A computer model has been created to demonstrate that the energy consumption function for vertical ascent of the quadcopter has a unimodal nature for different motors, which facilitates optimization for specific maneuver types. Minimum search algorithms defined in the study are capable of finding the optimal value of the target function with a deviation of 0.6 % - 1.6 % from the optimal value for a lower mass and 6.37 % - 11.23 % for a higher mass on a straight section with a constant load. However, considering the unimodal nature of the target function in the case of one-dimensional functions, i.e., when it is necessary to find only one optimal control signal value, it is recommended to use deterministic search algorithms as they provide the most stable optimization results, as demonstrated by the modeling results. Among the deterministic algorithms, algorithm 2 - the algorithm with halving method can be considered the most suitable among the compared algorithms. This algorithm allows finding the optimal control point in less time and with the smallest deviation.

11) Based on the experiments with the train, it is evident that there is no single optimal signal, and the search algorithm fails to find the optimal signals. With uniform search algorithm train consumes 1685 Ws, which is 36.2 % more than using a single constant control signal $C = 255$ throughout the path, covering a distance of 115.59 m. Therefore, the uniform search algorithm for finding the minimum energy consumption consumes more energy and cannot find the optimal control signal under such load characteristic changes.

12) Data analysis for creating a training set has shown that the load characteristic can be assessed at each point of the path independently of the control signal and velocity of movement.

13) The developed algorithm for automatic creation of a training set for the neural network has demonstrated the ability to form a training set under conditions of changing load and has found optimal control signal values for 35 road sections with different load characteristics, covering a distance of 62.2 m.

14) The results of experiments on selecting optimal parameters for the neural network show that the larger the training dataset with optimal neural network parameters, the more accurate the computed results are. The best accuracy is achieved with a deviation of 0.7503 and is produced by a neural network with 12 neurons. Under optimal parameters, there is an exponential relationship between the accuracy of computations and the number of iterations. The accuracy of computations also depends on time. To achieve the smallest deviation from the result of 0.752251, it requires 4017 ms.

15) The experimental results on the electric train model prove that the developed self-learning algorithm with neural network allows to increase energy-efficiency reducing electric energy consumption by 12.93 % in electric unmanned vehicles. With an algorithm's parameter of measurement step 0.08 m and utilizing instantaneous velocity values, the unmanned vehicle consumed 1077.14 Ws to cover a distance of 115 m. In comparison, when moving with a constant control signal $C = 255$, the energy consumption was measured at 1237.1 Ws.

The following development prospects can be highlighted:
- Research on constraint generation - defining or verifying minimum and maximum control signals.
- Checking the combination of optimized control signal proportions for compatibility with the performed maneuver or route.
- Improve the system and algorithm ensuring safe, reliable, and comfortable (in the case of passenger transportation) control criteria.
- Adaptation of control signals, their decoding and encoding for compatibility with different interfaces and control signal transmission protocols.

REFERENCE LIST

[1] Hnatov A. et al., "Development of an unified energy-efficient system for urban transport," 2020 6th IEEE International Energy Conference (ENERGYCon), 2020, pp. 248-253, doi: 10.1109/ENERGYCon48941.2020.9236606

[2] Rico J. et al., "Real time energy efficiency optimization in connected electrical vehicles," 2017 12th International Conference on Ecological Vehicles and Renewable Energies (EVER), 2017, pp. 1-6, doi: 10.1109/EVER.2017.7935950

[3] Zhang S., Luo Y., Wang J., Wang X. and Li K., "Predictive Energy Management Strategy for Fully Electric Vehicles Based on Preceding Vehicle Movement," in IEEE Transactions on Intelligent Transportation Systems, vol. 18, no. 11, pp. 3049-3060, Nov. 2017, doi: 10.1109/TITS.2017.2672542

[4] Abousleiman R. and Rawashdeh O., "Energy-efficient routing for electric vehicles using metaheuristic optimization frameworks," MELECON 2014 - 2014 17th IEEE Mediterranean Electrotechnical Conference, 2014, pp. 298-304, doi: 10.1109/MELCON.2014.6820550

[5] Abdelgadir A. A and Alsawalhi J. Y., "Energy management optimization for an extended range electric vehicle," 2017 7th International Conference on Modeling, Simulation, and Applied Optimization (ICMSAO), 2017, pp. 1-5, doi: 10.1109/ICMSAO.2017.7934911

[6] Rohkämper S., Hellwig M. and Ritschel W., "Energy optimization for electric vehicles using dynamic programming," 2017 International Conference on Research and Education in Mechatronics (REM), 2017, pp. 1-5, doi: 10.1109/REM.2017.8075252

[7] Bertram C. and Herzog H., "Optimization method for drive train topology design and control of electric vehicles," 2013 World Electric Vehicle Symposium and Exhibition (EVS27), 2013, pp. 1-8, doi: 10.1109/EVS.2013.6914933

[8] Bertram C., Buecherl D., Thanheiser A. and Herzog H., "Multi-objective optimization of a parallel hybrid electric drive train," 2011 IEEE Vehicle Power and Propulsion Conference, 2011, pp. 1-5, doi: 10.1109/VPPC.2011.6043154

[9] Qu L., Zhuang W. and Chen N., "Instantaneous Velocity Optimization Strategy of Electric Vehicle Considering Varying Road Slopes," 2019 Chinese Control And Decision Conference (CCDC), 2019, pp. 5483-5488, doi: 10.1109/CCDC.2019.8832756

[10] Allaboina V. Ramana R. "Regenerative braking system: The regenerative braking system used in the vehicles for the purpose of saving a part of the energy lost during bracking," LAP LAMBERT Academic Publishing, September 2, 2019, 64 p.

[11] Li B., Yu Z., Jin C. and Zhu Z., "Torque Allocation Algorithm of Distributed Driving Electric Vehicle Based on Energy Consumption Optimization," 2015 7th International Conference on Intelligent Human-Machine Systems and Cybernetics, 2015, pp. 319-323, doi: 10.1109/IHMSC.2015.46

[12] Guo L., Lin X., Ge P., Qiao Y., Xu L. and Li J., "Torque distribution for electric vehicle with four in-wheel motors by considering energy optimization and dynamics performance," 2017 IEEE Intelligent Vehicles Symposium (IV), 2017, pp. 1619-1624, doi: 10.1109/IVS.2017.7995941

[13] Hasan M. M., Baghdadi El M. and Hegazy O., "Energy Management Strategy in Electric Buses for Public Transport using ECO-driving," 2020 Fifteenth International Conference on Ecological Vehicles and Renewable Energies (EVER), 2020, pp. 1-8, doi: 10.1109/EVER48776.2020.9243130

[14] Fan A., Yin Q., Yan X. and Sun X., "Study of energy efficient navigation method for inland ship: A cruise ship case," 2015 International Conference on Transportation Information and Safety (ICTIS), 2015, pp. 437-441, doi: 10.1109/ICTIS.2015.7232079

[15] "LINDO User's Guide," Chicago, Illinois, USA: LINDO Systems Inc., 2008

[16] Zhong W., Xu H. and Zhang W., "Energy-efficient train reference speed profile optimization using control parameterization method," 2016 35th Chinese Control Conference (CCC), Chengdu, China, 2016, pp. 10128-10133, doi: 10.1109/ChiCC.2016.7554959

[17] Wen Y., Chenkun Y. and Zhongsheng H., "A novel energy efficient operation strategy for a train based on model-free adaptive predictive control," Proceedings of the 31st Chinese Control Conference, Hefei, China, 2012, pp. 7286-7291

[18] He Z., Yang Z. and Lv J., "An energy-efficient operation strategy for high-speed trains," 2018 Chinese Control And Decision Conference (CCDC), Shenyang, China, 2018, pp. 3771-3776, doi: 10.1109/CCDC.2018.8407778

[19] Xiao Z., Chen M., Chai Y., Liu C. and Wang Q., "Energy-Efficient Operation of High-speed Trains Based on a Multiple Phases Model," 2018 37th Chinese Control Conference (CCC), Wuhan, China, 2018, pp. 7793-7798, doi: 10.23919/ChiCC.2018.8483849

[20] Chen Y., Feng L., Zhan J. and Shang F., "Online Energy-efficient Control of Urban Rail Train Operation Based on Switching Time Optimization," 2020 Chinese Automation Congress (CAC), Shanghai, China, 2020, pp. 6094-6099, doi: 10.1109/CAC51589.2020.9327596

[21] Zhong W., Xu H. and Zhang W., "Energy-efficient train reference speed profile optimization using control parameterization method," 2016 35th Chinese Control Conference (CCC), Chengdu, China, 2016, pp. 10128-10133, doi: 10.1109/ChiCC.2016.7554959

[22] Chao G., Xinpei W., Kun H. and Qingyuan W., "Optimal energy-efficient control of high speed train with speed limit constraints," The 27th Chinese Control and Decision Conference (2015 CCDC), Qingdao, China, 2015, pp. 3076-3081, doi: 10.1109/CCDC.2015.7162449

[23] Gorobetz M., Korneyev A. and Zemite L., "Long-term Energy and Fuel Consumption Forecast in Private and Commercial Transport using Artificial Life Approach," 2022 IEEE 7th International Energy Conference (ENERGYCON), Riga, Latvia, 2022, pp. 1-7, doi: 10.1109/ENERGYCON53164.2022.9830189

[24] Gorobecs M., "ĢENĒTISKO ALGORITMU IZPĒTE ELEKTRISKĀ TRANSPORTA OPTIMĀLAI VADĪBAI," Promocijas darbs, Rīga, Latvija, 2008.

[25] Korņejevs A., "Optimizācijas algoritma realizācija un izpēte elektriskā bezpilota lidaparāta enerģijas patēriņa minimizēšanai," Maģistra darbs, Rīga, Latvija, 2018

[26] Brown H. R., Vitullo R.S., Corliss F. G., Adya M., Kaefer E. P. and Povinelli J. R. "Detrending daily natural gas consumption series to improve short-term forecasts," 2015 IEEE Power & Energy Society General Meeting, 2015, pp. 1-5

[27] Potočnik P. and Govekar E., "Applied short-term forecasting for the Slovenian natural gas market," 2016 13th International Conference on the European Energy Market (EEM), 2016, pp. 1-5

[28] Poyrazoglu G. O. and Poyrazoglu G., "Impact of Natural Gas Price on Electricity Price Forecasting in Turkish Day-Ahead Market," 2019 1st Global Power, Energy and Communication Conference (GPECOM), 2019, pp. 435-439

[29] Pradhan K. P., Dhal S. and Kamila K. N., "Artificial Neural Network Conventional Fusion Forecasting Model for Natural Gas Consumption," 2018 International Conference on Advances in Computing, Communications and Informatics (ICACCI), 2018, pp. 2200-2205

[30] Akpinar M. and Yumusak N., "Forecasting household natural gas consumption with ARIMA model: A case study of removing cycle," 2013 7th International Conference on Application of Information and Communication Technologies, 2013, pp. 1-6

[31] Wenlong H. and Yahui W., "Load Forecast of Gas Region Based on ARIMA Algorithm," 2020 Chinese Control And Decision Conference (CCDC), 2020, pp. 1960-1965

[32] Yujie L., Xiaoling Y., Jieyan X., Zheng C., Fei M. and Haoming L., "Medium-term forecasting of cold, electric and gas load in multi-energy system based on VAR model," 2018 13th IEEE Conference on Industrial Electronics and Applications (ICIEA), 2018, pp. 1676-1680

[33] Wan X., Zhang Q. and Dai G., "Research on forecasting method of natural gas demand based on GM (1, 1) model and Markov chain," 2014 IEEE 13th International Conference on Cognitive Informatics and Cognitive Computing, 2014, pp. 436-441

[34] Rui C., Jian W., Li W., Ningjie Y. and Pengyan Z., "The Forecasting of China Natural Gas Consumption Based on Genetic Algorithm," 2009 Fifth International Joint Conference on INC, IMS and IDC, 2009, pp. 1436-1439

[35] Poyrazoglu G., "Impact of Gas Price on Electricity Price Forecasting via Supervised Learning and Random Walk," 2019 16th International Conference on the European Energy Market (EEM), 2019, pp. 1-5

[36] Stana G. and Brazis V., "Predicting the Financial Yield of Mobile Energy Storage Systems for Electric Public Transport," 2021 62nd International Scientific Conference on Information Technology and Management Science of Riga Technical University (ITMS), Riga, Latvia, 2021, pp. 1-5

[37] Chen Yang, Hao Ye, Jing-Chun Wang and Ling Wang, "An Artificial Life and Genetic Algorithm based on optimization approach with new selecting methods," Proceedings. International Conference on Machine Learning and Cybernetics, 2002, pp. 684-688 vol.2

[38] Zhu X. and Li J., "Image Recognition Method Based on Artificial Life and Support Vector Machine," 2014 Sixth International Conference on Intelligent Human-Machine Systems and Cybernetics, 2014, pp. 17-19

[39] Yamashita H. and Kumano T., "Multi-objective power system planning by artificial life simulation," 2008 IEEE 2nd International Power and Energy Conference, 2008, pp. 169-174

[40] Zhang G. and Li Z., "The Emotion Mechanism of Artificial Life Fight Behavior", 2009 International Conference on Computational Intelligence and Natural Computing, 2009, pp. 15-18

[41] Ribickis L., Valeinis J., "Elektriskā piedziņa mahatronikas sistēmās," RTU tipogrāfijā, Rīga, 2008.

[42] Sitapati, K. and Krishnan, R. "Performance comparisons of radial and axial field, permanent-magnet, brushless machines," IEEE Transactions on Industry Applications, Volume: 37, Issue: 5, Sep/Oct 2001

[43] Klaus, "How fast can a quadcopter fly?" [Viewed on March 2, 2023], Available: https://klsin.bpmsg.com/how-fast-can-a-quadcopter-fly/

[44] Korneyev A., Gorobetz M., "Neural Network Based UAV Optimal Control Algorithm for Energy Efficiency Maximization," 2020 IEEE 61st International Scientific Conference on Power and Electrical Engineering of Riga Technical University (RTUCON 2020), Latvia, Riga, 5-7 November, 2020. Piscataway: IEEE, 2020, 1-5 p.

[45] Korneyev A., Gorobetz M., Levchenkov A., "Unified Energy Efficient Control Algorithm for Electric Unmanned Aerial Vehicles with Different Traction Drives and Configurations," 2018 IEEE 59th International Scientific Conference on Power and Electrical Engineering of Riga Technical University (RTUCON 2018), Latvia, Riga, 12-14 November, 2018. Piscataway: IEEE, 2018, 537-542 p.

[46] Korneyev A., Gorobetz M., Alps I., Ribickis L., "Adaptive Traction Drive Control Algorithm for Electrical Energy Consumption Minimisation of Autonomous Unmanned Aerial Vehicle," Electrical, Control and Communication Engineering, 2019, Vol. 15, No. 2, 62-70 p.

[47] Gorobetz M., Potapovs A., Korneyev A., "Analysis and Modelling of UAV Electrical Traction Drive based on Empirical Data for Energy Efficiency Tasks," 2019 IEEE 60th International Scientific Conference on Power and Electrical Engineering of Riga Technical University (RTUCON 2019), Latvia, Riga, 7-9 October, 2019. Piscataway: IEEE, 2019, 399-403 p.

[48] Pyrhonen J., Hrabovcova V., Semken R. S, "Electrical Machine Drives Control: An Introduction," Wiley, November 14, 2016, 526 p.

[49] Boldea I., Nasar A. S., "Electric Drives," Published by CRC Press, June 13, 2022, 672 p.

[50] Edited by Merabet A., "Advanced Control Systems for Electric Drives," December 2020, 342 p. ISBN 978-3-03943-699-6

[51] Haykin S., "Neural Networks. A Comprehensive Foundation," Second Edition, Prenctice Hall, 2006

[52] Karnopp C. D., "System Dynamics: Modelling and Simulation of Mechatronics Systems," 4th ed., Wiley, 2006

[53] Merkurjevs J., "Sistēmu imitācijas modelēšanas tehnoloģija," Rīga: RTU, 2008. – 120 lpp.

[54] Onwubolu G.C., "Mechatronics Principles and Applications," Elsevier Butterworth Heinemann, 2005. - 642 lpp.

[55] International Energy Agency, https://www.iea.org/data-and-statistics

[56] Valeinis J., "Elektriskās piedziņas vadība," Rīga, Rīgas Tehniskā universitāte, 1982. – 95 lpp.

[57] Valeinis J., "Ievads elektriskās piedziņas vadības sistēmās," Rīga: RTU, 2007 – 163 lpp

[58] Blumbergs E., "Elektriskās piedziņas vadība," Rīga, Rīgas Tehniskā universitāte, 1983. – 106 lpp.

[59] Bolton W., "Mechatronics," Pearson Prentice Hall, 2003, 574 p.

[60] Borisovs A., "Mākslīgā intelekta metodes," Rīgas Tehniskā universitāte. Automātikas un skaitļošanas tehnikas fakultāte, Rīga: RTU, 1993. - 75 lpp.

[61] Borisov, A. N., "Genetic algorithms, genetic programming, genetic machine learning," lecture slides. Transport and Telecommunications Inst. - Riga: TTI, 2004. - 251 lpp.

[62] Gorobetz M., Levchenkov A., "Modelling Of Artificial Neural Network Controller For Electric Drive," In Proceedings of 10th International Conference on Computer Modelling and Simulation (UKSIM), Cambridge, UK 1-3 Aprīlis 2008, 198-203p.

[63] Greivulis J., Raņķis I., "Iekārtu vadības elektroniskie elementi un mezgli," Rīga: Avots, 2005. – 288 lpp.

[64] Grundspeņķis J., "Ievads intelektuālās sistēmās," Lekciju konspekts, RTU, 1993.g. 158 lpp.

[65] Lagzdiņš Ģ., "Pamatkurss elektrotehnikā," Rīga: Jumava, 2004 – 218 lpp.

[66] Levine W., "The Control Handbook," CRC press, 1996

[67] Luger G. F., "Artificial Intelligence. Structures and Strategies for Complex Problem Solving," Williams, 2003

[68] Merkurjevs J., "Imitācijas modelēšanas tehnoloģijas," Lekciju konspekts, 2003

[69] Merkurjevs J., "Sistēmu imitācijas modelēšanas tehnoloģija," Rīga, RTU, 2008. – 120 lpp.

[70] Palm W.J., "Modeling, Analysis, and Control of Dynamic Systems," 2nd Edition, Wiley, 1999

[71] Rankis I., Gorobetz M., Levchenkov A., "Optimal Electric Vehicle Speed Control By Intelligent Devices," Rīgas Tehniskās universitātes raksti. Enerģētika un Elektrotehnika. Sērija 4, sējums 16. 2006. 127-137. lpp.

[72] Raņķis I., Zhiravetska A., "Electronics," Riga, RTU publishing House, 2005. – 106 p.

[73] Raņķis I., Bražis V., "Regulēšanas teorijas pamati," Rīga Rīgas Tehniskā universitāte, 2001. – 94 lpp.

[74] Raņķis I., Ievads specialitāte "Elektrotehnoloģiju datorvadība," - Rīga, RTU, 2003 – 41 lpp.

[75] Ribickis L., Raņķis I., "Electrical drives static characteristics and methods of speed control," Rīga, Rīgas Tehniskā universitāte, 1995. – 107 lpp.

[76] Ribickis L., Raņķis I., Ļevčenkovs A., Gorobecs M., "Programēšanas valodas industriālā elektronikā," Metodisks līdzeklis, Rīga, RTU, 2007, 70. lpp.

[77] Dirba J. Ketners K. *"Elektriskās mašīnas",* otrais izdevums, Rīga, Rīgas Tehniskā universitāte, 2009. -534 lpp.

[78] A. Korneyev, M. Gorobetz. Neural Network Based UAV Optimal Control Algorithm for Energy Efficiency Maximization //2020 IEEE 61st International Scientific Conference on Power and Electrical Engineering of Riga Technical University (RTUCON 2020), Latvia, Riga, 5-7 November, 2020. Piscataway: IEEE, 2020, 1-5 p.

[79] A. Korneyev, M. Gorobetz, A. Levchenkov. Unified Energy Efficient Control Algorithm for Electric Unmanned Aerial Vehicles with Different Traction Drives and Configurations. //2018 IEEE 59th International Scientific Conference on Power and Electrical Engineering of Riga Technical University (RTUCON 2018), Latvia, Riga, 12-14 November, 2018. Piscataway: IEEE, 2018, 537-542 p.

[80] A. Korneyev, M. Gorobetz, I. Alps, L. Ribickis. Adaptive Traction Drive Control Algorithm for Electrical Energy Consumption Minimisation of Autonomous Unmanned Aerial Vehicle //Electrical, Control and Communication Engineering, 2019, Vol. 15, No. 2, 62-70 p.

[81] M. Gorobetz, A. Potapovs, A. Korneyev. Analysis and Modelling of UAV Electrical Traction Drive based on Empirical Data for Energy Efficiency Tasks //2019 IEEE 60th International Scientific Conference on Power and Electrical Engineering of Riga Technical

University (RTUCON 2019), Latvia, Riga, 7-9 October, 2019. Piscataway: IEEE, 2019, 399-403 p.

[82] M. Gorobetz, A. Potapovs, A. Korneyev, I. Alps. Device and Algorithm for Vehicle Detection and Traffic Intensity Analysis //Electrical, Control and Communication Engineering, 2021, Vol. 17, No. 1, 83-92 p.

[83] M. Gorobetz, L. Ribickis. A. Beinarovica, A. Kornejevs. Immune Neural Network Machine Learning of Autonomous Drones for Energy Efficiency and Collision Prevention, //Drones - Various Applications, Rijeka, Published: September 18th, 2023, doi:10.5772/intechopen.1002533

[84] E. Kamolins, M. Gorobetz, K. Malnaca, A. Korneyev. Analysis of Test Results for Developed Technology of Diesel Bus Conversion into Electric Bus //Reliability and Statistics in Transportation and Communication, Cham: Springer Nature Switzerland AG 2019, 2020. 1.-10 p.

[85] M. Gorobetz, A. Korneyev, L. Zemite. Long-term Energy and Fuel Consumption Forecast in Private and Commercial Transport using Artificial Life Approach //ENERGYCON 2022: 7th IEEE International Energy Conference, Latvia, Riga, 9-12 may, 2022. Piscataway: IEEE, 2022, 1-6 p.

[86] M. Gorobetz, L. Zemite, A. Jasevics, A. Korneyev. Intelligent Algorithm for Using Overall Energy Consumption Statistics //2020 IEEE 61st International Scientific Conference on Power and Electrical Engineering of Riga Technical University (RTUCON 2020), Latvia, Riga, 5-7 November, 2020. Piscataway: IEEE, 2020, 1-13p.

[87] Malnaca, K., Gorobetz, M., Yatskiv (Jackiva), I., Korneyev A. Decision-Making Process for Choosing Technology of Diesel Bus Conversion into Electric Bus. No: Reliability and Statistics in Transportation and Communication: Selected Papers from the 18th International Conference on Reliability and Statistics in Transportation and Communication, RelStat '18. Lecture Notes in Networks and Systems. Vol.68. Cham: Springer Nature, 2019. 91.-102.lpp.

[88] Oleg, "*Контроллеры бесколлекторных моторов (Brushless ESC)"* 2010. febr. [Viewed on March 2, 2023], Available: http://onheli.blogspot.com/2010/02/brushless-esc.html

[89] Карпенко А.П. *Методы оптимизации (базовый курс),* [Viewed on March 2, 2023], Available: *http://bigor.bmstu.ru/?cnt/?doc=MO/base.cou*

[90] *Схема контроллера литий-ионного аккумулятор,* [Viewed on March 2, 2023], Available: http://go-radio.ru/sxema-kontrollera-litiy-ionnogo-akkumulatora.html

[91] Новиков Ф.А., *"Дискретная математика для программистов"*, - СПб: «Питер», 2003. - 304 с.

[92] Рутковская Д., Пилиньский М., Рутковский Л., *"Нейронные сети, генетические алгоритмы и нечеткие системы",* Телеком, 2004

Aleksandrs Korņejevs was born in 1983 in Riga. He obtained a Bachelor's degree (2016) and a Master's degree (2018) in Electrical Science from Riga Technical University (RTU). He was a board member at the company "Solar AK". Since 2019, he has been working at RTU, holding the positions of scientific assistant, senior laboratory assistant in scientific work, lecturer, and study process expert. Currently, he is a research assistant at the Institute of Industrial Electronics and Electrical Engineering (IEEI) of Faculty of Electrical and Environmental Engineering. In 2018 he was included in the RTU Golden Fund. His research interests are related to electroacoustics, radio electronics, control systems of unmanned vehicles and artificial neural networks.